Upcycling Plastic Waste to Activated Carbon for Waste Water Treatment Applications

by

Rachel Jessica Blanchard

A thesis

presented to the University of Waterloo

in fulfilment of the

thesis requirement for the degree of

Master of Applied Science

in

Chemical Engineering

Waterloo, Ontario, Canada, 2024

Author's Declaration

This thesis consists of materials all of which I authored or co-authored: see Statement of Contributions included in the thesis. This is a true copy of the thesis, including any required final revisions, as accepted by my examiners.

I understand that my thesis may be made electronically available to the public.

Statement of contributions

Chapter 2 of this thesis contains background information on plastic recycling and literature reviews on upcycling of plastic to produce activated carbon. The information used in this chapter was adapted from a published manuscript **"Valorization of plastic waste via chemical activation and carbonization into activated carbon for functional material applications", RSC Applied Polymers, 2024** in which I am the first author. Dr. Mekonnen provided guidance and reviewed the manuscript.

Chapter 3 is adapted from a published manuscript **"Synchronous pyrolysis and activation of poly (ethylene terephthalate) for the generation of activated carbon for dye contaminated wastewater treatment", Journal of Environmental Chemical Engineering, 10(6), 2022, 108810** in which I am the first author. Dr. Mekonnen initiated the project, provided guidance and supervision, and reviewed the manuscript.

Chapter 4 is also adapted from a published manuscript **"Utilization of epoxy thermoset waste to produce activated carbon for the remediation of nano-plastic contaminated wastewater", Separation and Purification Technology, 326, 2023, 124755** in which I am the first author. Dr. Mekonnen initiated the project, provided guidance and supervision, and reviewed the manuscript.

Abstract

Plastic waste disposal continues to be a widespread issue, as plastic products are discarded at high rates and do not biodegrade in the environment. Although a portion of this waste is recycled, the limitations of conventional recycling methods have prompted the need to investigate alternative disposal methods. This thesis highlights the upcycling plastic waste through carbonization and activation to produce adsorbent material for wastewater treatment applications. This conversion method involves heat treatment at high temperature under an inert atmosphere with the addition of an activating agent to produce activated carbon (AC), a carbonaceous material of high surface area. This process can yield high value material with excellent adsorption properties and can be applied to a variety of plastics including thermosets, which are notoriously difficult to recycle. The first section of this thesis focused on the synthesis of AC from poly(ethylene terephthalate) (PET) bottle waste and its application as an adsorbent for dye contaminated water. A product of high surface area (1124 m^2/g) was produced through KOH chemical activation and exhibited a high adsorption capacity (335 mg/g) for cationic methylene blue (MB) dye. The adsorption capabilities were investigated through detailed analysis of the MB adsorption mechanism in addition to the effects of solution pH and dye charge characteristic. The second section of this thesis focused on the synthesis of AC from epoxy thermoset plastic for the adsorption of nano-plastic pollution. A high surface area AC (1705 m^2/g) was obtained through KOH activation after investigation of other potassium-based activators. It was found to adsorb PET nano-plastics through multilayer physical adsorption with a substantial monolayer capacity of 325 mg/g and maximum recovery of 94%. These studies confirmed the successful conversion of a thermoplastic and thermoset into AC material with high potential for adsorption of aqueous pollutants.

Acknowledgements

I would like to thank my supervisor prof. Tizazu Mekonnen for his support and guidance during my master's degree and for all the opportunities he has given me as a co-op student. I'm not sure if I would have pursued a master's degree without the experience in his lab as an undergrad, as the research and working environment he created compelled me to keep coming back. I look up to him immensely as a professor and as a person, and I am so grateful to have worked with him for all these years. I also want to show my appreciation for the committee members prof. Alexander Penlidis and prof. Elisabeth Prince for taking the time to provide valuable feedback on my thesis. Additionally, I would like to thank my colleagues who I have worked with during my time in prof. Mekonnen's research group. Specifically, I want to thank Binh-Minh Trinh, Dylan Jubinville and Rohan Shorey for always being willing to help me and for making my time as a master's student more enjoyable. Lastly, I want to thank my beloved partner Devejya Raghuvanshi for kindly dedicating many hours to correct formatting issues in this document.

Dedication

I want to dedicate this work to my uncles Robert Shapiro and Samson Wu for funding my undergraduate education. Everything I have been able to accomplish on this academic path and in the future is all possible because of them, and I will forever be thankful to them for their unconditional love and support.

Table of contents

List of figures

List of tables

List of abbreviations

SA	Surface area
IR	Impregnation ratio
PET	Poly (ethylene terephthalate)
AC	Activated carbon
MB	Methylene blue
BG	Brilliant green
MO	Methyl Orange
BET	Brunauer–Emmett–Teller
PFO	Pseudo first order
PSO	Pseudo second order
W&M IPD	Weber & Morris Intra-Particle Diffusion
R^2	Coefficient of determination
m_{AC}	Mass of activated carbon produced
m_{PET}	Initial mass of PET feedstock
q_e	Equilibrium pollutant adsorption capacity (mg/g)
C_0	Initial pollutant concentration (mg/L)
C_e	Equilibrium pollutant concentration (mg/L)
m	Mass of activated carbon per adsorption run (g)
q_m	Langmuir monolayer adsorption capacity (mg/g)
K_L	Langmuir constant (L/mg)
K_F	Freundlich constant ($L^{1/n}mg^{1-1/n}g^{-1}$)
n_F	Freundlich exponent

K_s	Sips model parameter ($L^{\beta}mg^{1-\beta}g^{-1}$)
α	Sips model parameter ($L^{\beta}g^{-\beta}$)
β	Sips model parameter
t	elapsed adsorption time (min)
q_t	Pollutant adsorption (mg/g) at time t
C_t	Pollutant concentration (mg/L) at time t
K_1	Pseudo first order rate constant (g/mg/min)
K_2	Pseudo second order rate constant (g/mg/min)
h	Initial adsorption rate constant (mg/g/min)
K_{int}	Intra-particle diffusion rate constant ($mg/g/min^{1/2}$)
C_{int}	Intra-particle diffusion intercept (mg/g)
a	Elovich model parameter
b	Elovich model parameter
K_{ext}	Intra-particle diffusion rate constant ($mg/g/min^{1/2}$)
C_{ext}	Intra-particle diffusion intercept (mg/g)
NP	Nano-plastic
MP	Microplastic
GAC	Granular activated carbon
WWTP	Wastewater treatment plant
AD	Aranovich–Donohue
FHH	Frenkel–Halsey–Hill
m_E	Initial mass of cured epoxy feedstock (g)
q_{mBET}	BET Monolayer adsorption capacity (mg/g)
K_{BET1}	BET adsorption equilibrium parameter for the first layer (L/mg)

K_{BET2}	BET adsorption equilibrium parameter for the upper layers (L/mg)
C_A	Aranovich Constant (mg/L)
C_{sA}	Aranovich monolayer adsorbate saturation concentration (mg/L)
q_{mA}	Aranovich monolayer adsorption capacity (mg/g)
C_{sAD}	AD adsorbate saturation concentration (mg/L)
n_{AD}	AD exponent
K_{FHH}	FHH constant (mg/g)
n_{FHH}	FHH index
C_{sFHH}	FHH monolayer adsorbate saturation concentration (mg/L)
FTIR	Fourier transform infrared spectroscopy
SEM	Scanning electron microscopy
DLS	Dynamic light scattering
KOAc	Potassium Acetate

Chapter 1: Introduction

1.1. Motivation

The use of plastic products has been continuously increasing due to their lightweight, appealing cost structure, ease of processing, durability, and flexibility for various applications [1]. They are mass produced from hydrocarbons refined from petroleum, using coal powered plants resulting in large carbon footprints. Additionally, they do not biodegrade in the natural environment in a reasonable time frame. As a result, greenhouse gas (GHG) emissions from plastic production are rising in conjunction with plastic waste accumulation in landfills and spill to the environment accelerated by the quick disposal of most products after a single use consuming the global carbon budget [2]. Though plastics do not totally degrade in a short time, they can undergo fragmentation due to environmental factors causing the formation of microplastics [3] and even nano-plastics [4]. These highly mobile plastic fragments pollute marine environments, agricultural ecosystems, and other terrestrial and freshwater systems [4,5] which can affect drinking water sources. Therefore, the effective recycling of all plastics and alleviation of this pollution is a major topic of discussion.

Currently, common methods used for plastic waste management include landfilling, incineration, mechanical recycling, chemical recycling, and thermal cracking [2]. Recycling mainly refers to thermo-mechanical recycling, in which plastics are collected, sorted, cleaned, ground, extruded and pelletized to form new products. This method helps extend the lifetime of plastics, but the resulting decline of product properties limits its continued product value. Both landfilling and incineration are also widely used disposal options but cause burdens on the environment due to the negative effects on soil environments and air pollution, respectively. Finally, thermal cracking to form fuels and valuable chemicals is a type of chemical recycling,

which has received substantial interest and helps to reutilize plastics while favoring reduced emissions [2].

As a part of the efforts to divert this waste from inevitable buildup in landfills, this thesis aims to highlight an alternative method of upcycling plastic waste by carbonization to produce high value carbonaceous products. Carbonization differs from thermal cracking through pyrolysis as it focuses on the production of solid residue with high carbon content [1] as opposed to liquid or volatile fractions which are major pyrolysis products (oil and gas) [6]. It can generate valuable products such as carbon nanomaterials, carbon fibers, adsorbents and energy storage devices [1,2]. The product of interest in this work is activated carbon (AC), which is a carbonaceous material defined by a large surface area and porosity. This product is appealing because it is simply produced through the addition of an activating agent during the carbonization process and has widespread applications in waste treatment processes due to its excellent surface properties.

1.2. Research objectives

The goal of this thesis is to investigate the production of AC from plastic wastes for wastewater treatment applications. Two separate research studies were carried out, each using a different waste plastic to produce AC for adsorption of a different wastewater pollutant. In each case, key activation conditions were evaluated for their effect on AC surface properties and an optimal product was tested for adsorption of the chosen pollutant. The aim is that this work brings more understanding to both the conversion process and the adsorption behavior of aqueous solutes onto the plastic-derived AC such that the carbonization pathway of plastics to adsorbent material can be evaluated.

As will be discussed in the next chapter, there are a variety of studies which have investigated the conversion of plastics to AC and the adsorptive properties of AC. However, the research conducted in this thesis provides value through its adherence to the research objective. The goal of the first study on the conversion of PET to AC for adsorption of textile dyes, is to evaluate PET as a precursor for AC with the specific application in dye adsorption. Although PET has been converted to AC and similar products have been used for dye adsorption, this study considers the desired application during the optimization of the PET conversion process and evaluates the scope of PET-derived AC for its capabilities as a dye adsorbent.

The second study on the conversion of cured epoxy to AC for nano-plastic adsorption investigates an AC feedstock and application that are not well studied. Although some studies have used an epoxy precursor, the optimization of the activation conditions are lacking, and the AC product (or any other plastic derived product) has not been investigated for nano-plastic adsorption. Overall, these studies are meant to provide full evaluations of plastics as precursors to wastewater adsorbents using both thermoplastic (PET) and thermoset (epoxy) polymers for applications in two very impactful areas of wastewater treatment.

1.3. Thesis outline

The following sections of this thesis are organized as follows: Chapter 2 provides background information on plastic recycling techniques, the carbonization and activation of plastics, in addition to the applications of plastics-derived AC. Chapter 3 presents a research study on the production of AC from PET bottle waste for adsorption of textile dyes. In this work, the KOH chemical activation temperature and time were investigated to produce an AC with ideal surface properties, and the AC was analyzed for adsorption of methylene blue dye in detail and compared to other textile dyes. Chapter 4 presents a research study on the production of AC

from epoxy thermoset plastic for the adsorption of nano-plastics. In this work, chemical activators, activation temperature and activator levels were investigated for the conversion of epoxy to AC, and the resulting product was tested for adsorption of synthesized PET nano-plastics.

Chapter 2: Background information[1]

2.1. Plastic recycling overview

There are a variety of methods for reutilization of plastic waste, which generally can be categorized into recycling by mechanical methods, chemical methods and incineration for energy recovery. As shown in Figure 1, these can also be categorized according to ASTM D5033 definitions of primary, secondary, tertiary and quaternary recycling. Primary recycling consists of mechanical recycling of products in a closed loop system, while secondary recycling is mechanical recycling into products with different purposes, often downgraded polymeric materials. Tertiary recycling refers to the use of waste polymers for generation of lower molecular weight materials such as monomers and valuable chemicals [7]. This depolymerization can be carried out by numerous chemical methods such as hydrolysis, ammonolysis, pyrolysis etc. For the purpose of this study, chemical recycling was divided into solvolysis methods used for monomer regeneration, and pyrolysis to produce oil and gas. Furthermore, carbonization was identified separately from pyrolysis because the production of carbon materials (mainly activated carbon) will be the focus of this review. Lastly, a final resort is the quaternary recycling of plastics by combustion with recovery of energy [7].

[1] A version of this chapter is published: Blanchard, R., Mekonnen, T., RSC Applied Polymers, March 2024.

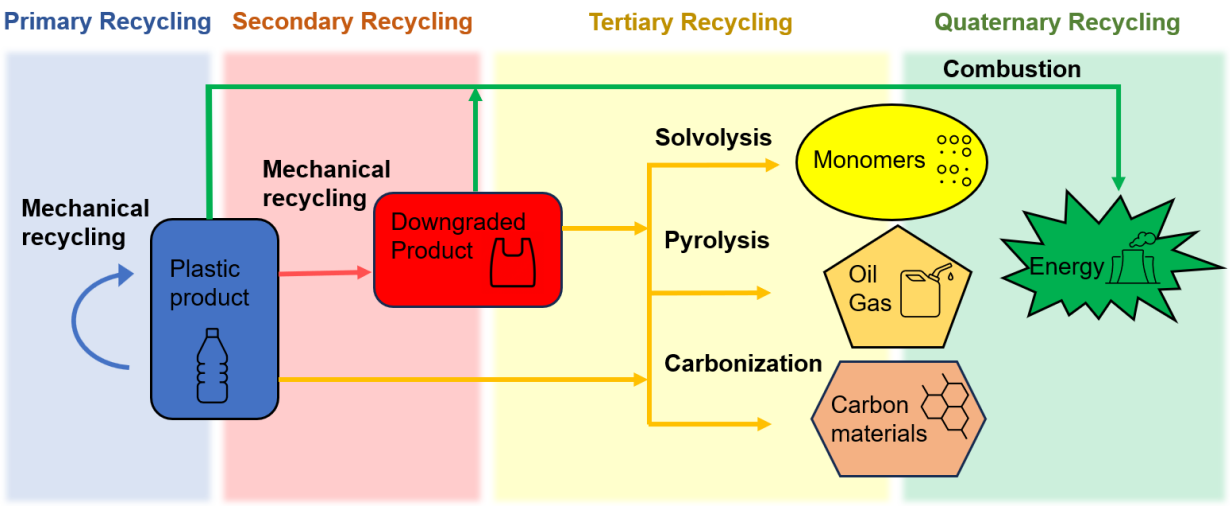

Figure 1: Schematic of the categorized plastic recycling methods.

2.1.1. Mechanical recycling

The most widely employed recycling technique is the mechanical recycling by melt processing of used plastic waste to form new products. This is conducted through sorting, washing and drying, crushing and compounding. It is a relatively simple and economical recycling technique but is limited by various shortcomings. Mainly, the effects of heat, light, oxidation, and mechanical shear lead to degradation of plastic products during their lifetime and during the mechanical reprocessing [8]. Additionally, post consumer plastics are usually laden with contaminants, co-blend partners, additives, and mixed with other plastics or non-plastics (e.g., paper), resulting in the need for additional costly washing, sorting, and separation processes. As a result, mechanical recycling can only be carried out for a few cycles. A very common example is poly(ethylene terephthalate) (PET) bottles, which are usually only recycled once into textiles. A small portion of mechanical recycling consists of primary recycling using the purest and cleanest streams while most mechanical recycling is downcycling [9]. Therefore, the other recycling techniques illustrated in **Figure 1** (tertiary and quaternary) are required as complementary recycling options.

2.1.2. Solvolysis

Because mechanical recycling can only be used for a fraction of plastic markets, chemical recycling is necessary in cases where mechanical recycling can not deliver the required mechanical performance or purity. As shown in **Figure 2a**, some plastics are more easily depolymerized into monomers while others can only be cracked through the more intense pyrolysis process to form hydrocarbon materials. In this mapping adapted from Lange (2021), the horizontal axis identifies the plastics which are easy to depolymerize based on heat of polymerization while the vertical axis indicates the incentive to recover the monomer based on the mass of resources consumed for its production [9]. As a result, the condensation polymers such as PET and polyamides (PA) in the upper left quadrant are recommended to be depolymerized into monomers through various solvent methods (solvolysis). These condensation polymers in the upper left quadrant of **Figure 2a** consist of monomers connected through bonds, such as ester, amide, urethane linkages etc., which are susceptible to chain-scission through various reactions. In **Figure 2b** select chemical approaches are illustrated for the depolymerization of PET, polyurethane (PUR), and PC.

2.1.3. Pyrolysis

As illustrated in **Figure 2a**, the chemical recycling of most polyolefins must also consider pyrolysis as a suitable alternative due to the strength of the constituent hydrocarbon bonds. Pyrolysis is a tertiary recycling method which converts high molecular weight polymers into oil, gases and char by high temperature decomposition under an inert atmosphere [10]. The oil and gas products are desirable since they are used as precursors to valuable fuels and chemicals. A recent study by Wang et al. (2023) also showed that the oil and gas products of plastic waste pyrolysis can be converted to valuable hydrogen and solid carbon products through subsequent

thermolysis [11]. The produced hydrogen fuel can generate clean electricity and the solid carbon has many applications including the investigated use as a reinforcing agent.

In the pyrolysis of polyethylene, it is understood that degradation occurs by free radical initiation, random scission, followed by recombination of various chains through termination [12,13]. The pyrolysis results in gas products consisting of C1-C4 olefins and oil products consisting of C5-C20 olefins and aromatics [14]. Das and Tiwari (2018) reported similar pyrolysis products after slow pyrolysis of PE and PP plastics, which consist of paraffins, olefins and some aromatics. However, the proportion of branched paraffins (iso-paraffin) was higher in PP compared to PE. The gaseous products consisted of light paraffins and olefins, mainly propylene, ethane, methane etc.[15].

For PS, the degradation is also known to occur through free radical reactions[16,17]. The pyrolysis results in complete conversion to oil products at 350 ºC, but as temperature is increased char production is promoted with very small proportions of gas (max 2.5 wt.%). Therefore, the products are mainly oil (toluene, ethylbenzene, benzene, and styrene) and char due to the predominant presence of aromatic degradation products leading to char formation by condensation of aromatic rings. In comparison, LDPE began degradation at 450 ºC, but increasing pyrolysis temperature promoted conversion to gases rather than char [18]. This phenomenon is shown in **Figure 2c**, in which the pyrolysis oils and following gaseous products are illustrated for the pyrolysis of PE and PP, while the aromatic oil products and following char at increased temperature are illustrated for the pyrolysis of PS.

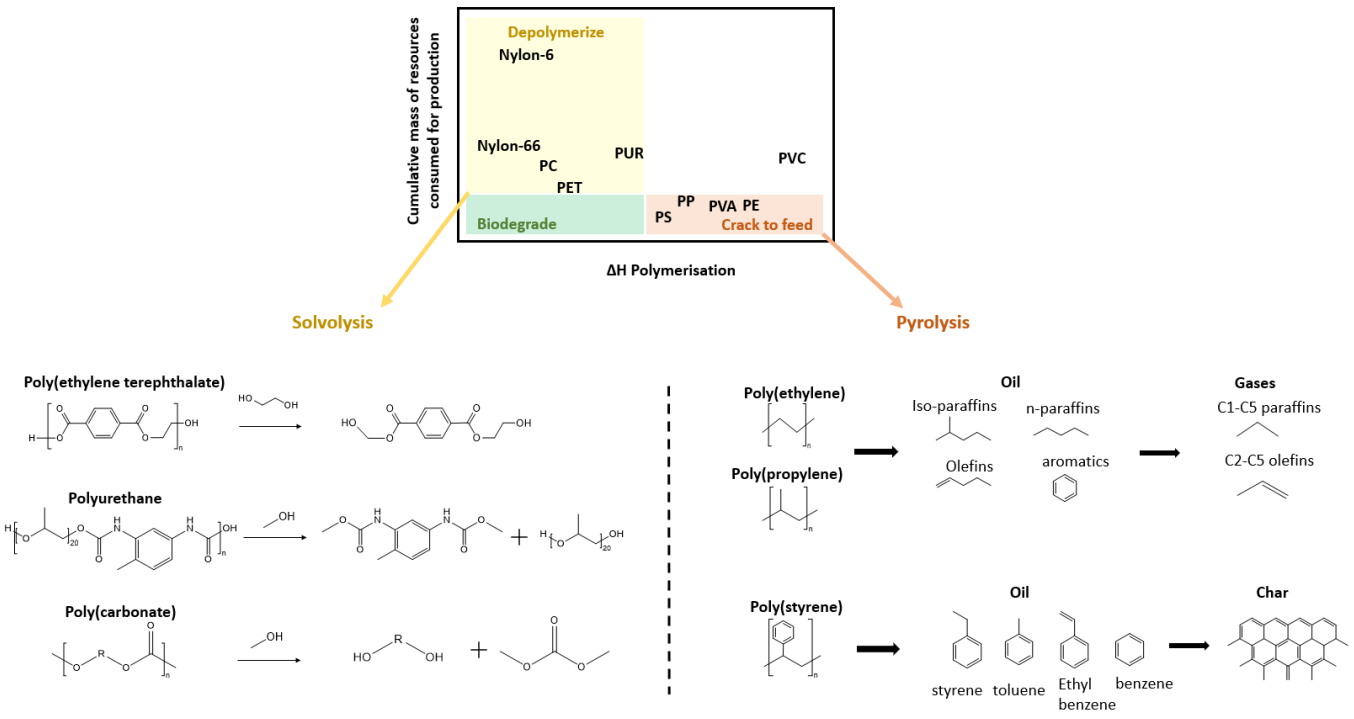

Figure 2: a) Mapping of the recommended chemical recycling technique for different plastics [8]; b) schematic of the glycolysis of PET and methanolysis of PUR and PC; c) General pyrolysis products of PE, PP and PS.

2.1.4. Carbonization

The carbonization of plastic waste is considered a distinct treatment compared with pyrolysis, because it is specific to the production of value-added carbon materials rather than fuels and chemicals. For carbonization processes, a slow heating rate is employed to promote the production of solid products containing maximum carbon content from the precursor. This slow heating rate leads to a more sequential conversion of the feedstock into a carbonized material through many reactions. Additionally, higher temperatures of 600- 1200 ºC are used in carbonization compared to pyrolysis for oil products generation, which occurs at temperatures around 500 ºC [1]. During carbonization, the plastic is heat treated at high temperature under an

inert atmosphere to produce carbon material through aromatization, while some gases (H_2O, CO_2, CH_4, NH_3 etc.) are released through decomposition of the plastic constituents [2].

Carbonization at different conditions (catalysts, templates, and pressures) can result in varying carbon products. As a result, different structures are obtained, including activated carbon, carbon fibres, carbon nanotubes, carbon spheres, and graphene [19]. In terms of the plastic precursors, polyolefins such as PP and PE are ideal for producing carbon nanotubes, carbon spheres, and graphene because they form light hydrocarbons, which are catalyzed to form these structures during the carbonization process [19,20]. This can be achieved using combined catalysts, which act as both degradation and carbonization catalysts. The degradation catalyst helps to promote the formation of the required low molecular weight compounds, while the carbonization catalyst facilitates the degradation process such that carbon materials can be formed [21]. Templates may also be employed, in which a removable mold is used to create controlled voids in the material. Some materials used as rigid templates include silica, clays, MgO and $CaCO_3$ [22].

During the carbonization of PET and PS containing benzene rings in their structure, aromatics and oil products are formed which then lead to the formation of amorphous carbon [19]. This is due the occurrence of cyclization, aromatization and crosslinking rather than degradation into small molecules [20]. As a result, polyolefins, such as PP and PE are considered non-charring while aromatic plastics such as PET and PC are considered charring plastics, as shown in **Figure 3**. Non-charring plastics are beneficial for producing ordered carbon materials (graphene, carbon nanotubes etc.) through catalysis while charring plastics can produce amorphous carbon material. Activation by chemical or physical methods can then be used to enhance the surface area and porosity of the products.

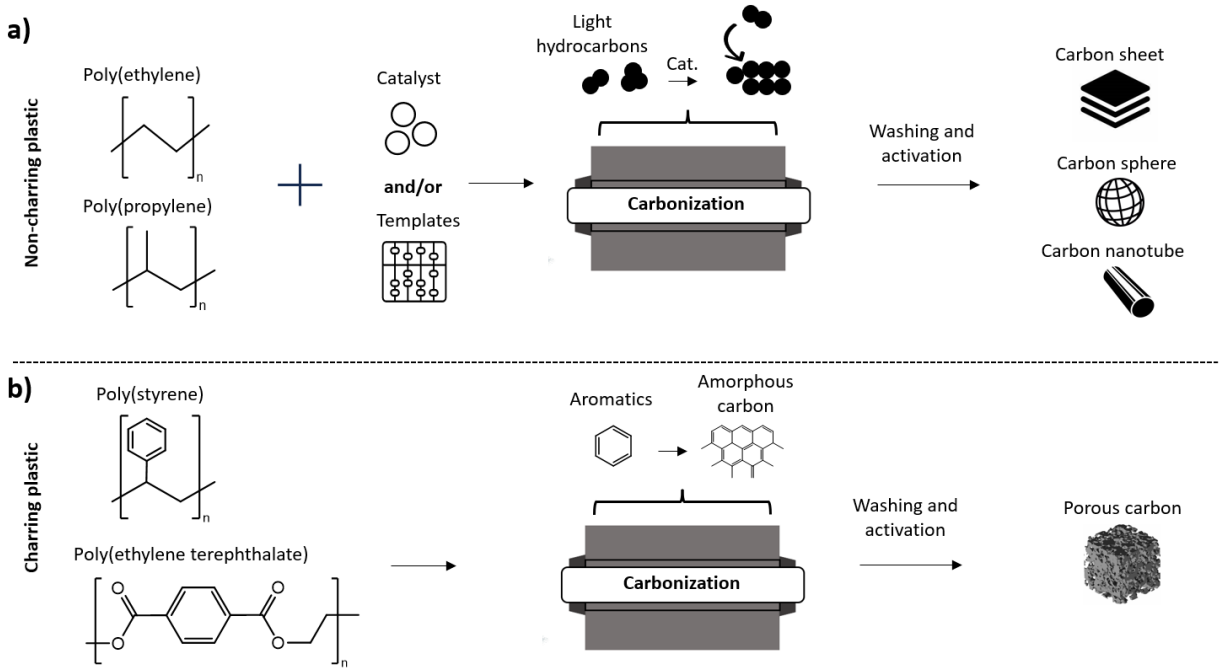

Figure 3: a) Carbonization of non-charring plastics to produce carbon sheets/carbon spheres/carbon nanotubes; b) carbonization of charring plastics to produce porous carbon.

2.2. Pre-carbonization stabilization

It is generally known that carbonization of aromatic plastics leads to the formation of oils and aromatics which enhance char formation [19]. However, the oxygen content in the polymer also plays an important role in its conversion to carbon material. Plastic which contains oxygen, such as PET and epoxy resins, are more easily carbonized through heat treatment, while non-oxygen containing plastics may require a stabilization pre-treatment. The preliminary treatment allows for an increased yield of carbon residues rather than gaseous organic molecules [2]. Therefore, polyolefins can be converted into amorphous carbons (eg. activated carbon, carbon fibres) if a stabilization through oxidation or other chemical treatment is preformed before carbonization.

In terms of stabilization treatments, sulfonation and oxidation treatments are commonly used. For LLDPE, Choi et. al. (2017) has shown that oxidation in air introduces C=O bonds and C-O bonds, which occur in the main chain and as ether bonds bridging chains. As temperature increases, the linear chains are converted to a crosslinked structure with an increasing composition of oxygen. The cyclized structure can then be carbonized at higher temperature under inert atmosphere to yield a carbonaceous product [23]. Alternatively, PE can be sulfonated using sulfuric acid to result in sulfonic acid groups among other sulfur containing groups (sultones, sulfates). Subsequently during carbonization, unsaturated polyolefin is obtained through release of sulfur and oxygen, and carbonized material can then be achieved. The sulfonation mechanism is investigated in detail by Younker et. al. (2013) [24]. The general mechanism of the oxidation and sulfonation pre-treatments are illustrated in **Figure 5a**.

Sulfonation can also be used for PS, as was reported by Hines et. al. (2004) to produce porous carbon [25]. Additionally, PS can be stabilized by the Friedel-Crafts reaction in which crosslinking occurs through carbonyl bridging using a carbon tetrachloride reagent and Lewis acid catalyst (**Figure 5b**). This leads to enhanced carbonization due to the crosslinked structure and increased oxygen content [26]. In the case of PVC, stabilization usually occurs through heat treatment in air, during which oxygen functional groups are introduced during this treatment, leading to crosslinking and aromatization [27]. A list of various carbon materials obtained from plastic precursors with or without pre-treatments is presented in **Table 1**. Evidently, the sulfonation of PE is a very common method, especially to produce carbon fibers [24,28,29]. Carbon fibres are often used in polymer composites reinforcement as alternatives to heavier construction materials like steel and are mainly produced from poly(acrylonitrile) (PAN) by melt spinning and oxidation pre-treatment [28]. Alternatives like PE are of interest due to the costs of

PAN precursor and conversion yield, which limit the applications in industries requiring lower cost products [28].

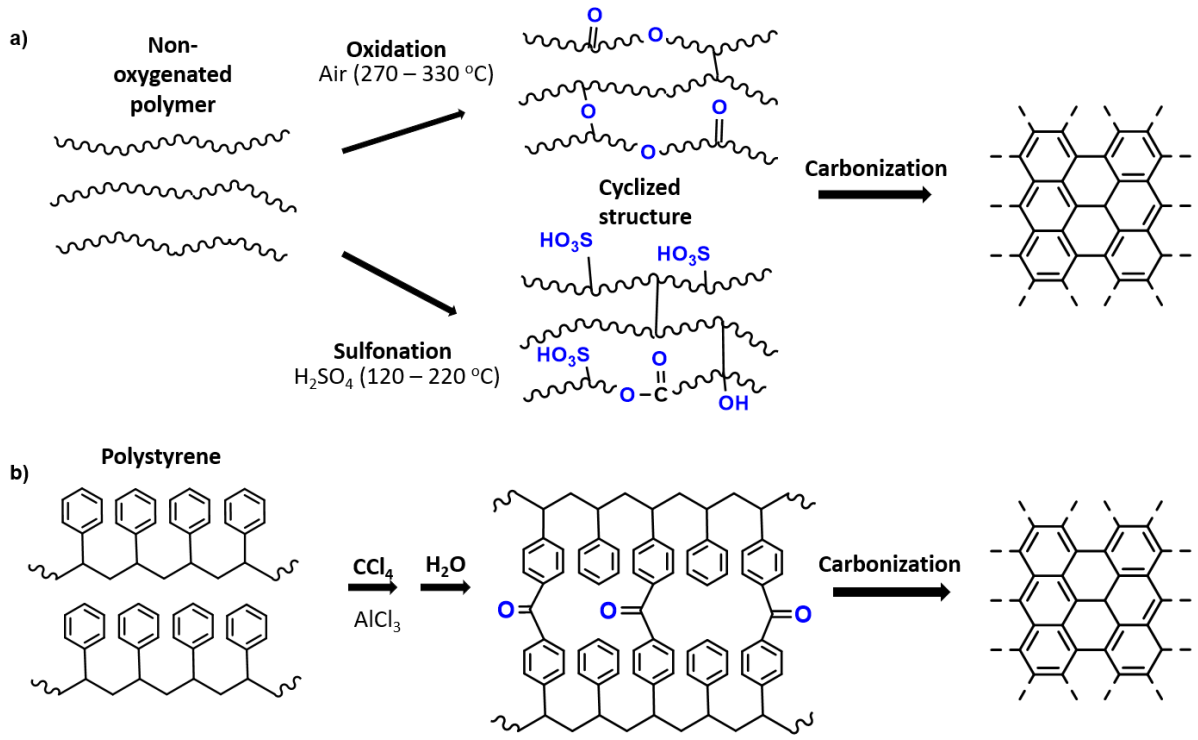

Figure 4: a) General schematic of oxidation and sulfonation pretreatments for carbonization of plastics based on the mechanisms of PE stabilizations [2]; b) Friedel-Crafts reaction as a pretreatment for polystyrene carbonization [26].

Table 1: List of carbon products obtained through anoxic pyrolysis of plastic precursors with or without stabilization pre-treatments.

Precursor	Stabilization treatment	Carbon product	Reference
LLDPE	Oxidation	Graphitic carbon	[23]
LLDPE	Chlorosulfonation	Carbon fiber	[29]
LLDPE	Sulfonation	Carbon fiber	[28]
LDPE	Sulfonation	Carbon scaffold	[30]
HDPE	Sulfonation	Porous carbon	[32]
HDPE, LDPE	Sulfonation	Amorphous carbon chips	[33]
PS	Sulfonation	Porous carbon	[25]
PS	Crosslinking (Friedel-Crafts)	Porous carbon	[26][31]
PVC	Oxidation	Porous carbon	[34]
PVC	-	Char	[35][36]

2.3. Activation methods

As seen in the previous section, porous carbons are often produced from plastic precursors (**Table 1**). These products are very valuable due to their high surface area (SA) and pore volume, which allow them to be used as high-capacity adsorbents. However, activation processes are often used to further improve the SA of the carbonized materials to produce activated carbons (ACs), which are defined by large SA, porosity, and adsorption capacity [37]. The activation process involves reactions between carbon and an activating agent to produce new pores and open existing pores in the carbon structure through physical or chemical methods. The specific SAs of commercial ACs are in the range of 500-1500 m^2/g [38], which is determined by the Brunauer-Emmett-Teller (BET) method of SA analysis through N_2 adsorption.

Physical activation involves heat treatment with an oxidizing gas such as O_2, CO_2 or steam at high temperature (800 -1200 ^oC). This takes place after carbonization of the material under an inert atmosphere, such that a two-stage process is required [39]. It can be considered a more environmentally friendly approach due to the lack of chemicals, but it has the downsides of

long activation times and high energy consumption [40]. Chemical activation on the other hand involves impregnation of the precursor with an oxidizing and dehydrating chemical, heat treatment at temperatures between 400 to 900 ºC, and subsequent washing (e.g., HCl) to remove the chemical. In this case, the carbonization and activation can occur simultaneously such that a single stage process can be employed [40]. However, many studies also employ carbonization prior to activation, using a lower temperature of around 600 ºC for carbonization where most mass loss occurs, followed by chemical activation at temperatures from 400 to 1000 ºC [37]. This two-stage chemical activation is illustrated in comparison to physical activation in **Figure 5a**.

The main parameters affecting activation include the activating agent, treatment temperature, time, and the impregnation ratio (IR), which is the mass ratio of chemical activating agent to precursor in the case of chemical activation. In general, chemical activation is preferred compared to physical activation due to the advantages of lower activation times and temperatures, generation of high specific SAs, and high carbon yield [41]. The most used chemical activating agents include alkaline chemicals, such as KOH, NaOH and K_2CO_3, acidic chemicals such as H_3PO_4 and H_2SO_4, and metal salts such as $ZnCl_2$ [40]. Of all activating agents, KOH is known to be the most effective due to its capacity to produce high SAs in AC [39]. As a result, much of the work that will be explored has focused on activation using KOH.

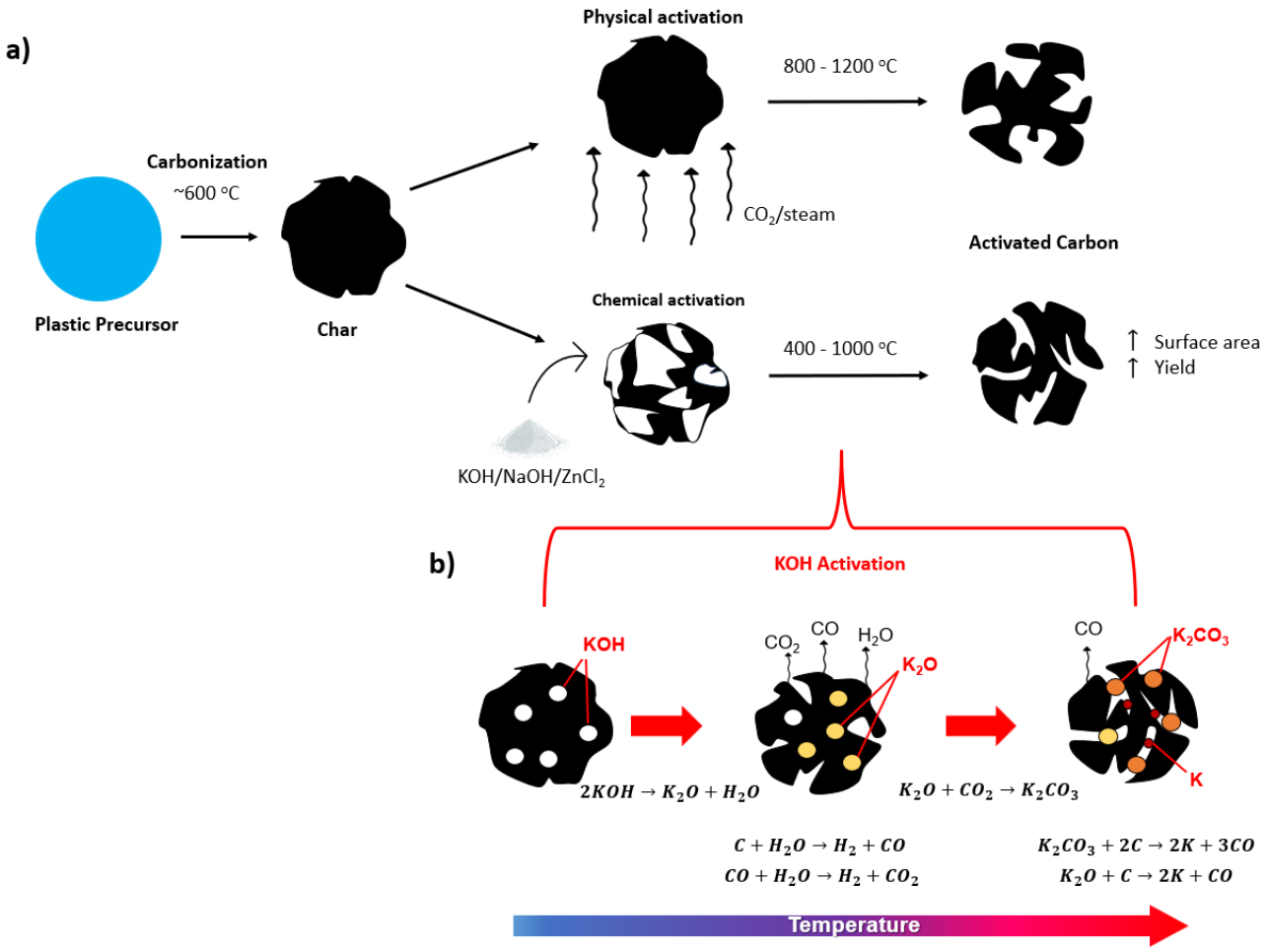

Figure 5: a) Illustration of activated carbon production through physical versus chemical activation; b) KOH activation mechanism adapted from ref. [42].

The mechanism of pore formation using KOH activation occurs through physical activation by the evolved CO_2 and H_2O, redox reactions between potassium compounds and carbon, and through the formation of potassium metal at high temperatures [43], as illustrated in **Figure 6b**. Gases such as CO and CO_2 are formed through the reaction of carbon with surface and internally bound water (**Equations (1)-(2)**), and water is released through the dehydration of KOH (**Equation (3)**). As the decomposition continues, K_2CO_3 is produced due to the transformation of K_2O (**Equation (4)**). At high temperatures exceeding 700 °C, metallic

potassium is formed through the reduction of K_2O and K_2CO_3 (**Equations (5)-(6)**) [39,43,44]. The potassium metal is important for the continued pore formation due to its ability to penetrate and expand the carbon structure. It also helps to form more active sites for reaction with carbon and improves the wettability of the surface. These effects are unique and can not be achieved through activation by acidic or neutral activating agents [39]. This is why strong alkali activating agents are very effective, especially KOH.

$$C + H_2O \rightarrow H_2 + CO \quad \textbf{(1)}$$
$$CO + H_2O \rightarrow H_2 + CO_2 \quad \textbf{(2)}$$
$$2KOH \rightarrow K_2O + H_2O \quad \textbf{(3)}$$
$$K_2O + CO_2 \rightarrow K_2CO_3 \quad \textbf{(4)}$$
$$K_2O + C \rightarrow 2K + CO \quad \textbf{(5)}$$
$$K_2CO_3 + 2C \rightarrow 2K + 3CO \quad \textbf{(6)}$$

With respect to the feedstock, commercial AC is mainly produced from charcoal, lignite, wood, peat shells and coconut, but any carbonaceous organic material are viable precursors [40]. Therefore, plastics are an enticing option for AC feedstocks since they possess high carbon content, and the utilization of plastic waste is of high concern. Currently, the production of AC from plastic waste has not been commercialized, although it is under ongoing investigation. For example, an Australian company called ByGen has reported the success in converting plastics including PET into AC [45], although they do not yet produce any AC products at full scale. Therefore, sections 2.4 and 2.5 will reflect on the current understanding of AC production from plastics based on the relevant research studies.

2.4. Conversion of plastics to AC

The conversion of plastics to AC can occur through various methods. As discussed previously, the composition of the plastic can necessitate preliminary stabilization treatments (Section 2.2) and the activation process itself can follow various paths. In this chapter, the

conversion process for common plastics will be reviewed, with a focus on chemical activation methods. The BET SAs are investigated as the main indication of AC quality due to the wide range of applications in the investigated works. The SAs achieved in ACs through activation of various thermoplastics (**Table 2**), chemical activation of PET (**Table 3**), and chemical activation of thermosets (**Table 4**) have been tabulated below. Based on these tables, it is evident that most research focuses on KOH activation of plastics in both single stage and two-stage carbonization/activation processes. The various process pathways utilized in these works have been illustrated in **Figure 6b** to showcase the combination of steps required to produce chemically activated AC from the most common types of waste plastics (PP, PE, and PET) based on **Figure 6a.**

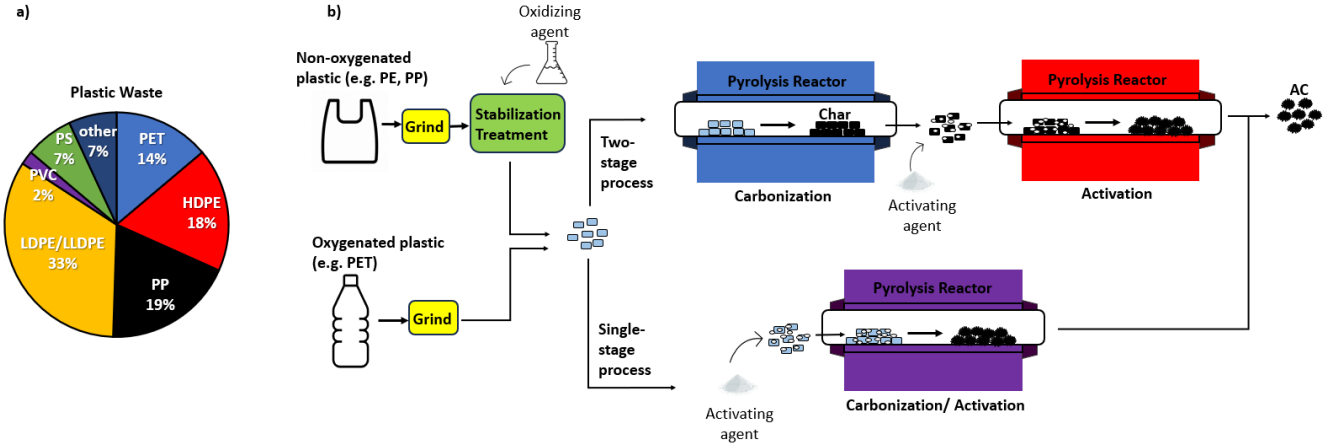

Figure 6: a) composition of plastic waste managed in the US in 2019. Data obtained from ref. [46]; b) Illustration of various pathways for the chemical activation of oxygenated and non-oxygenated plastics.

Table 2: List of activated carbon BET SAs produced from various thermoplastics with or without stabilization pre-treatments.

Precursor	Stabilization treatment	Activation type	Activating agent	AC Surface area (m^2/g)	Reference
LLDPE	Sulfonation	Chemical	KOH	156-1803	[46]
PVC	Oxidation	Physical	Steam	1096-2096	[47]
PVC	Oxidation	Physical	CO_2	528-1211	[27]
PVC	Oxidation	Chemical	KOH	4-2507	[48]
PVC	-	Chemical	KOH	2666	[49]
PS	Sulfonation	Physical	Air, Steam	567, 842	[50]
PS	-	Chemical	KOH	2109-2712	[51]
PS	-	Chemical	KOH	393-1250	[52]
PS	Crosslinking (Friedel-Crafts)	Chemical	KOH	2637	[53]
PC	-	Chemical	KOH	Max. 2098.7	[54]
PC	-	Chemical	NaOH	348-815	[55]

2.5. Conversion of PET to AC

Poly(ethylene terephthalate) (PET) plastic is a special example because it is the most researched plastic feedstock for AC production. PET is an ideal precursor to AC due to its aromatic and oxygenated structure, high carbon content (> 60 wt.%) and high char yield compared to other waste plastics [57]. Most studies have employed chemical activation for the synthesis of PET AC, which is the focus of this section. The various carbonization conditions, chemical activation conditions, and resulting AC SAs have been summarized in **Table 3**, and the trends with respect to operational conditions will be discussed.

2.5.1. Physical Activation

Despite the large number of studies and focus on chemical activation of PET (**Table 3**), it should be noted that the physical activation has also been explored using CO_2 [58–62] and steam [63–65] as activating agents. For CO_2 activation, Esfandiari et. al. (2012) found optimal conditions of 975 ºC for 240 min to produce ACs with a SA of 790 m^2/g [61]. Compared to much

of the chemical activation results presented in **Table 3**, the CO_2 activation requires a higher temperature and longer treatment time to produce a product of lesser SA. Mandoza-Carrasco et. al. (2016) compared steam activation (8.33 mL/min) of PET to KOH activation at an IR of 2 [63]. It was found that KOH activation caused an optimal SA (1002 m^2/g) at 850 ºC, while steam activation resulted in a higher SA (1235 m^2/g) at 800 ºC under the same treatment time of 1 h. Although the results are influenced by the levels of activating agent used, this showcases that steam activation can produce similar SAs as KOH at a reasonable IR of 2.

2.5.2. Alternatives to KOH activation

In terms of the chemical activation of PET, a number of studies have investigated chemical activators other than the widely used KOH activator. For example, NaOH activation was found to produce very similar SAs to that of KOH using a two-stage carbonization/ activation process [66]. Both activating agents (IR=2) produced maximum SAs of ~2000 m^2/g at 850 ºC (KOH activation) and as low as 800 ºC (NaOH activation). Castro et. al. (2018) investigated K_2CO_3 activation at 800 ºC and $ZnCl_2$ activation at 500 ºC [67]. Through analysis of the K_2CO_3 IR, it was found that an optimal SA of 1390 m^2/g was achieved at a relatively low IR of 0.5. In a separate study, a greater SA of 1439 m^2/g was achieved using a K_2CO_3 IR of 2, which was greater than that of the equivalent KOH activation (1206 m^2/g) [68]. However, $ZnCl_2$ activation at 500 ºC was not as effective as it produced an AC of 700 m^2/g using an IR of 1 [67]. Adibfar et al. also achieved a similar SA (682 m^2/g) by $ZnCl_2$ activation up to a temperature of 800 ºC [69], indicating that an increased activation temperature did not improve the SA development. This study also emphasized the significance of KOH activation, because it reported that KOH produced the highest SA compared to H_3PO_4, H_2SO_4 and $ZnCl_2$ activators under the same conditions.

2.5.3. Single stage KOH activation

The operational conditions during KOH activation can be analyzed in more detail than other activators due to the increased number of studies performed. As shown in **Table 3**, the most prevalent process used is the single stage KOH activation. The activation temperature and time were investigated by Mendoza-Carrasco et. al. (2016) at an IR of 2, in which activation at 800 ºC was found to be optimal at 1h (SA=844 m^2/g) due to the decreased SA upon further increases in time [63]. Additionally, increasing temperature to 850 ºC caused the highest SA of 1002 m^2/g. Another key factor is the IR, which was investigated by Sarici-Ozdemir & Onal (2018) in the IR range of 1-5 [70]. At the standard activation conditions of 800 ºC for 1h, the SA continuously increased with IR up to 1889 m^2/g at an IR of 5. A second study employing this high IR at even higher temperatures of 900 to 1100 ºC, produced ACs with a maximum SA of 1808 m^2/g at 900 ºC [71]. Evidently, an elevated IR may be necessary to achieve SAs as high as 1800 m^2/g but increasing temperature beyond 800 ºC does not seem to be worthwhile.

2.5.4. Two-stage KOH activation

Despite the ease of implementing a single stage carbonization/activation process, it is evident from **Table 3** that the separation of carbonization and activation can result in the highest PET AC surface areas reaching greater than 2000 m^2/g. This may be attributed to the interaction of activating agent solely with carbon rather than uncarbonized precursor. Using a 600 ºC carbonization step and a KOH IR of 2, two studies have found optimal surface areas of 2006 m^2/g [66] and 1937 m^2/g [72] at an activation temperature of 800 ºC. The decrease in SA as activation temperature is increased beyond this point results from pore expansion due to excessive activation. Based on the latter study of Yuan et. al. (2020), a higher IR was necessary to further increase the SA to a superior value of 2650 m^2/g at only 700 ºC [72]. A separate study

employing a higher carbonization temperature of 700 ºC found that an IR of 3 was optimal for activation at 700 ºC. However, a comparatively lower surface area of 1690 m^2/g was achieved in this study [73]. Therefore, the carbonization conditions may also play a significant role in the final AC properties due to the differences observed in these two studies.

Table 3: List of the ranges in activated carbon BET surface areas produced through chemical activation of PET plastic.

Carbonization conditions	Activating agent	IR	Activation conditions	AC Surface area (m^2/g)	Reference
-	$ZnCl_2$	1	500 ºC 2 h	700	[66]
-	K_2CO_3	0.25-1	800 ºC 2 h	680-1390	
-	K_2CO_3	2	800 ºC	1439	[67]
	KOH			1206	
-	$ZnCl_2$	1	400 ºC 1 h then 800 ºC 1 h	682	[68]
	H_3PO_4			1223	
	H_2SO_4			583	
	KOH			1338	
-	KOH	2	700 ºC 30 min	1418	[73]
-	KOH	2	700 ºC	1334	[74]
-	KOH	2	700 - 850 ºC 1 h	566-1002	[62]
			800 ºC 0.25 - 2 h	666-844	
-	KOH	1-5	800 ºC 1 h	817-1889	[69]
-	KOH	5	900 - 1100 ºC 1 h	1092-1808	[70]
600 ºC 1 h	KOH	2	850 ºC 1.5 h	2831	[49]
600 ºC 2 h	KOH	2	700 - 1000 ºC 1 h	1689-2006	[65]
	NaOH			1926-2060	
600 ºC 1 h	KOH	2	600 - 1000 ºC 1 h	1636-1937	[71]
		1-3	700 ºC 1 h	736-2650	
700 ºC 2 h	KOH	1-4	700 ºC 2 h	591-1690	[75]

2.6. Conversion of thermosets to AC

Another important category of plastic precursors is thermoset plastics, which are often found in composite materials. Thermosetting resins are used as a matrix to hold a structural filler in place and are chemically cross-linked such that they can't be reshaped after curing. Therefore, conversion of thermoset resins to carbon is a promising treatment as they cannot be recycled

conventionally. Some examples of AC production from commonly used phenolic and epoxy resins are summarized in **Table 4**.

2.6.1. Phenolic resin

Phenolic resin (PR) is an example of thermosetting resin material which is commonly used to make fiber reinforced composites [2]. It is a good candidate for carbonization due to its complex structure of phenol and aldehydes that facilitate high carbon yield [77]. Dong et. al. investigated the production of PR derived AC for application in supercapacitors using K_2FeO_4 as both an activating and graphitization agent [77]. An activation temperature of 950 ºC was required to produce an electrode material with a SA above 1000 m^2/g; However, this was not the only parameter of importance given its application. With respect to SA development alone, KOH has been shown to be most effective compared to K_2CO_3 and $ZnCl_2$ in the activation of phenol-melamine-formaldehyde resin [78]. Within this study, the benefit of PR was also apparent due to the excellent SA of 2376 m^2/g achieved, which is superior to that of PET ACs synthesized using similar single-stage activation conditions (**Table 3**). Additionally, Zheng & Gao (2011) produced a PR derived AC of even higher SA (2653 m^2/g) using an increased IR of 5 [79]. Similar to PET, PRs do not require a stabilization step; however, the impact of an oxidative pretreatment was investigated by Teng & Wang (2000). Oxidation after impregnation was found to increase the carbon yield and enhance SA but only at high KOH levels (IR = 4) [80].

2.6.2. Epoxy resin

Epoxy resin is another very commonly used thermosetting plastic. In addition to its application in composite materials it is also a large component of electronics, specifically printed circuit boards (PCBs). The non-metallic portions of PCBs, which comprise 70% of the material, are mainly composed of epoxy resin (~60 %) [81]. Therefore, it has been of interest to convert

the non-metallic portions of waste PCBs to high SA AC using KOH activation [82] and steam activation [81]. Both studies employed carbonization prior to activation at 800 ºC. However, the KOH activation (IR = 3) produced a much higher SA (2573 m^2/g) using a shorter treatment time of 1 h compared to steam activation, which required 1.5 h to produce ACs of SA = 803 m^2/g. Epoxy ACs were also produced for application in supercapacitors using a similar two-stage process with the same proportion of KOH [83]. However, a lower SA of 1353 m^2/g was reported, likely due to the lower activation temperature of 600 ºC. Evidently, the KOH activation of epoxy resin is limited to relatively lower activation temperatures and does not investigate any single stage activation methods.

Table 4: List of the ranges in activated carbon BET SAs produced through chemical activation of various thermoset plastics.

Precursor	Stabilization treatment	Carbonization conditions	Activating agent	IR	Activation conditions	AC surface area (m^2/g)	Reference
Epoxy	-	500 ºC 1 h	KOH	3	600 ºC 3 h	1353.78	[82]
Epoxy (PCB)	-	650 ºC 2.5 h	KOH	3	800 ºC 1 h	2573	[81]
Phenolic resin	-	-	K_2FeO_4	19.8	750 – 950 ºC 1 h	416 - 1086	[76]
Phenol formaldehyde resin	-	-	KOH	5	750C 1h	2653	[78]
phenol–melamine–formaldehyde resin	-	-	KOH	2	800 ºC 1 h	2376	[77]
			K_2CO_3		800 ºC 1 h	1610	
			$ZnCl_2$		700 ºC 1 h	1296	
Phenol formaldehyde resin	Oxidation (pre-impregnation)	-	KOH	1 - 4	700 ºC 2 h	960 - 2800	[79]
	-					1200 - 2200	

2.7. Applications of AC

Activated carbon (AC) is mainly used as an adsorbent for a variety of pollutant molecules. At its origins in ancient Egypt (1500 BC) it was used for water purifications, and

during the first world war it was implemented in gas masks to remove toxic gases [84]. In recent times, AC is often applied for purification of air and color removal from industrial wastes. For many applications, the most important property of the AC adsorbent is the specific surface area, which refers to the total internal and external surface area (SA) of the material per unit mass. Other parameters affecting adsorption include the pore structure, surface functional groups and elemental composition [85]. However, it is also dependent on the treatment conditions and the specific mechanism of adsorption.

Various adsorption isotherm models are used to describe the adsorption process, specifically the relationship between adsorbate concentration (liquid phase) or pressure (gas phase) and the resulting equilibrium adsorption (mg adsorption/ g adsorbent). For example, it is generally known that the equilibrium adsorption of dyes increases with dye concentration until the binding sites are filled and the adsorbent is saturated with dye [86]. This adsorption point is called the monolayer capacity (q_m) and is a relevant parameter in many adsorption models, such as the Langmuir model, which is a very popular isotherm describing the adsorption of a single layer of solute on an adsorbent surface (**Figure 7**). It is a very simple model assuming adsorption onto homogenous surfaces but can accurately predict the adsorption behavior of a wide variety of molecules. As shown in **Table 5** and **Table 6** outlining various plastic derived AC adsorption capacities, most plastic derived ACs exhibit adsorption behaviors which have been described by the Langmuir model. However, there are other models used to describe monolayer and even multilayer adsorption, which will be discussed as necessary within the research studies of this thesis.

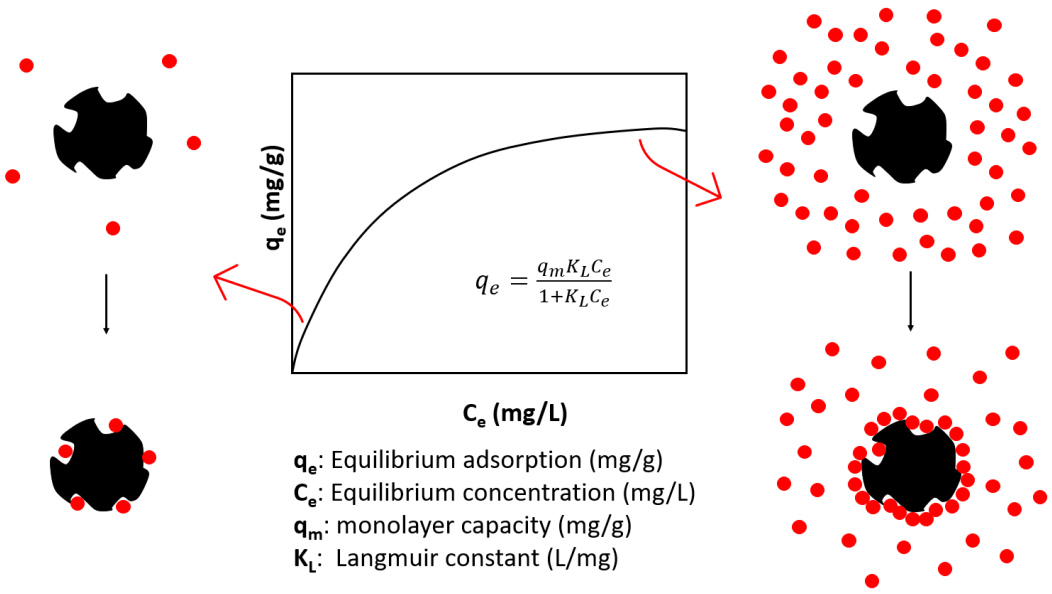

Figure 7: Langmuir adsorption isotherm and corresponding illustrations of adsorption onto AC at low and high solute concentrations [86].

2.7.1. Dye adsorption

One very large application of AC is in the treatment of dye contaminated wastewater produced from textile industries. For this application an additional process consideration is the pH due to its effect on the ionization degree of the adsorbate dye in addition to the chemical state of the AC [86]. This is important because textile dyes are often charged molecules, so electrostatic interaction with the AC plays a large role in the adsorption process. For example, the adsorption of a cationic dye such as methylene blue (MB) is enhanced by a negatively charged AC surface [57]. As shown in **Figure 8b**, a basic pH improves MB adsorption as explained by the development of negative charge on AC through deprotonation of acidic functional groups such as hydroxyls (**Figure 8a**). Therefore, not only does the pH influence the electrostatic interaction with charged dyes but also the amount and types of AC surface functional groups. Kuang et al. (2020) reported increased MB adsorption onto AC modified by anionic surfactants,

while AC modified by a cationic surfactant reduced MB adsorption (**Figure 8d**) [88]. The effect of dye type as it relates to charge is exemplified in **Figure 8c** in which PET ACs selectively adsorb cationic MB dye over anionic methyl orange (MO) dye (**Figure 8c**). The monolayer capacity (q_m) of MB dye and other aqueous pollutants by plastic derived ACs can be seen in **Table 5** alongside their corresponding AC surface areas.

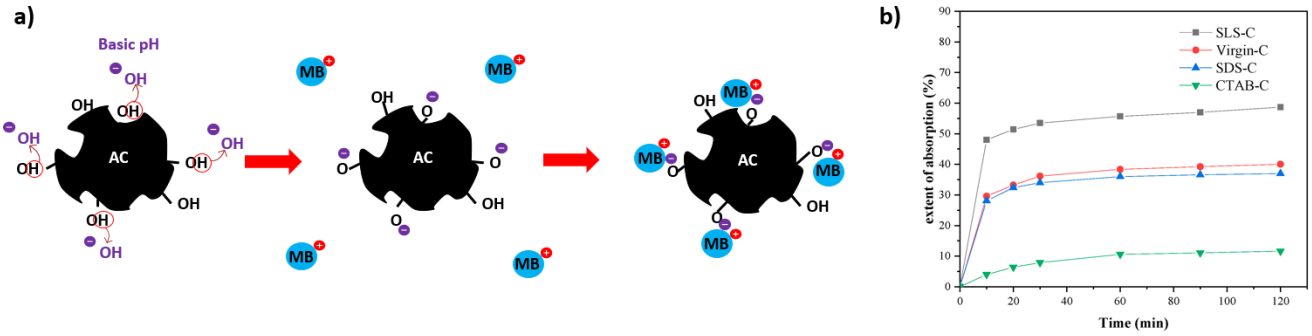

Figure 8: a) Adsorption of methylene blue (MB) by AC in basic solution with hydroxyls as representative surface functional groups facilitating electrostatic interactions; b) Adsorption isotherm of MB onto unmodified AC (Virgin-C), and AC modified with anionic sodium lauryl sulfate (SLS-C), anionic sodium dodecyl sulfonate (SDS-C), and cationic hexadecyl trimethyl ammonium bromide (CTAB-C). Adapted from ref. [88].

Table 5: Tabulated BET surface areas and monolayer adsorption capacities (q_m) exhibited by plastic derived ACs during the adsorption of various pollutants in liquid phase.

Precursor	Activating agent	Adsorbate	AC surface area (m^2/g)	q_m (mg/g)	Isotherm model	Reference
PVC	KOH	Trichloroethylene	2666	1418.9	Polanyi-Dubinin-Manes	[49]
		Dichlorobenzene		1308.3		
		Dinitrobenzene		1193.6		
		Hexachlorocyclohexane		2326.5		
PET		Trichloroethylene	2831	1510.9		
		Dichlorobenzene		1381.8		
		Dinitrobenzene		1277.6		
		Hexachlorocyclohexane		2471.9		
PS	Steam	Ni(II)	842	40.82	Langmuir	[50]
PET	KOH	Methylene blue	1334	326.2	Langmuir	[74]
		Chloromethylphenoxyacetic acid		298.9		
PET	K_2CO_3	Methylene blue	1390	625	Langmuir	[66]
		Victoria blue		137		
	$ZnCl_2$	Methylene Blue	700	333		
		Victoria blue		196		
PET	KOH	Phenol	1418	207	Langmuir	[73]
		nitrophenol		278		
Epoxy	KOH	Methylene blue	2572	737.19	Langmuir	[81]
Commercial AC		**Methylene blue**	**900**	**303**	**Langmuir**	[66]

2.7.2. Nano-plastic adsorption

Another noteworthy application of AC is in the adsorption of micro- and nano-plastic (NP) pollution from wastewater. This waste is caused by human activities such as laundering and exfoliant products which introduce small plastic particles into wastewater effluents [4]. These particles breakdown into microplastics (MPs) and further into nano-plastics (NPs), which can escape wastewater treatment operations much more easily [89]. With respect to MPs, various studies have investigated biochar within columns [90–92] and AC filters [93]. Similarly, the adsorption of the more difficult to treat NPs using biochar [94,95] and commercial AC [96] have

been studied using batch mixing experiments. All these studies were limited to testing charged polystyrene (PS) NPs, which followed monolayer adsorption described well by the Langmuir model (**Figure 9 a and b**).

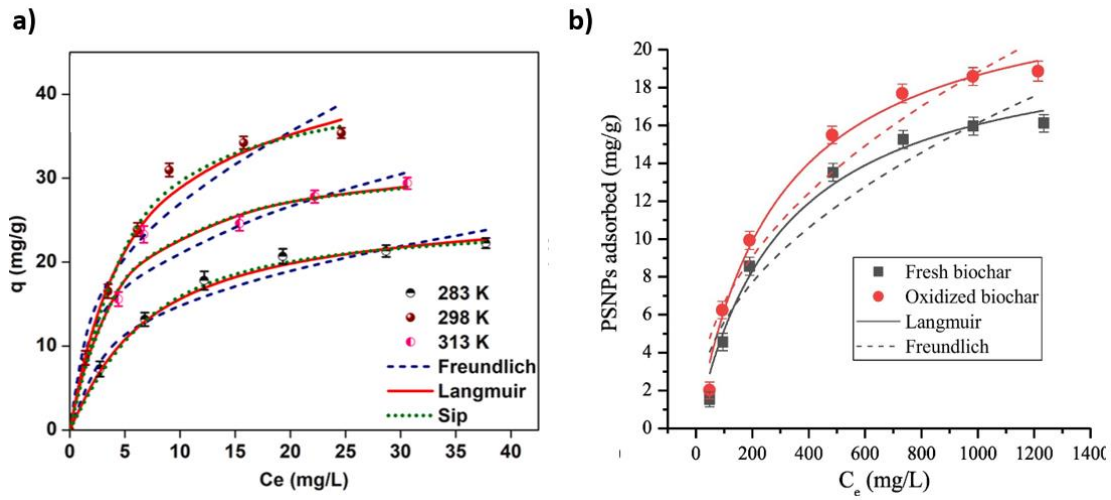

Figure 9: Adsorption isotherm curves of a) PS NPs onto sugarcane Bagasse biochar at varying adsorption temperatures. Adapted from [94] with permission from Elsevier. Copyright ©2021; and b) PS NPs onto oxidized and non-oxidized corncob biochar. Adapted from ref. [95] with permission from Elsevier. Copyright ©2021.

The NP adsorption capacity of the various carbonaceous adsorbents and the maximum percentage recovery of NPs are reported in **Table 6**. It is evident that the adsorption capacities are quite limited but were able to achieve high NP recoveries above 95%. This may be attributed to the oppositely charged NP and adsorbent combinations in these studies (**Table 6**) which enhance the adsorption even at low solute concentrations. Although these examples show promise in the usage of carbonaceous adsorbents for NP adsorption, the data is very limited with respect to the adsorbent material and NP properties. There is a need to investigate the adsorption

of non-charged NPs due to the great influence of surface charge on the adsorption process. Additionally, it is of interest to utilize higher surface area sustainable adsorbents such as chemically activated ACs derived from plastics or biomass.

Table 6: Comparison of polystyrene nano-plastic adsorption capacities and recovery using various carbon-based adsorbents.

Adsorbent type	Adsorbent Surface area (m^2/g)	pH	NP zeta potential (mV)	AC zeta potential (mV)	Monolayer capacity (mg/g)	Isotherm model	Maximum NP recovery (%)	Reference
Bagasse biochar	540.36	5.5	-39.8	+2.85	44.9	Langmuir	>99	[92]
Corncob biochar	36.3	7	-48	-45.1	20.89	Langmuir	-	[93]
Commercial AC	1150	7.4	~(+40)	~(-28)	2.15	Langmuir	98	[94]

Chapter 3: Synchronous pyrolysis and activation of poly(ethylene terephthalate) for the generation of activated carbon for dye contaminated wastewater treatment[2]

3.1. Introduction

Poly (ethylene terephthalate) (PET) is the most popular packaging material for beverages worldwide [95], possessing many ideal properties, including transparency, lightweight, and barrier [96]. As a result, PET bottle use has continued to increase over the years, leading to a buildup of waste that takes about180 years on average to degrade [97]. Although thermo-mechanical recycling has been attempted for bottle-to-bottle recycling processes, it cannot be used successively due to the property degradation after each cycle [98]. Additionally, the challenges associated with sorting and cleaning bottles have limited the recycling rate to 29% in the US, as reported in 2018 [99]. With large amounts of plastics reaching landfills, incineration at landfill sites for heat generation has been a common approach for dealing with the waste despite the harmful emissions produced [100].

Since it is of interest to utilize this waste while avoiding the production of harmful effluents, the carbonization of PET under an inert atmosphere appears to be a promising way to create valuable carbonaceous products. PET is an excellent candidate for carbonization processes due to its large carbon composition of over 60 wt.% and low inorganic content [101]. Additionally, controlled PET carbonization results in high char production compared to other waste plastics [102]. This may be attributed to the thermally stable benzene rings on PET's backbone structure, which do not easily crack to form gaseous compounds upon degradation [103]. In this study, PET was investigated as a precursor to produce activated carbon, which is

[2] A version of this chapter is published: Blanchard, R., Mekonnen, T., Journal of Environmental Chemical Engineering Volume 10, Issue 6, December 2022, 108810.

currently obtained from a variety of carbonaceous synthetic and biomass feedstocks. While activated carbons are conventionally produced through the heating and activation of coal, lignite and peat, the non-renewable feedstock is a major drawback. The environmental impact of coal and hence its decreasing availability has caused biomass feedstocks to become popular [104]. For example, sources such as coconut shell [105] and lignin [107] present attractive alternatives to coal that are sustainable, inexpensive and can be regenerated easily [108]. Similarly, waste plastics such as PET are available with seemingly unlimited supply, and their utilization benefits the environment.

Production of activated carbon from PET is mainly accomplished by physical activation by steam [63,97] or CO_2 [109,110]. However, chemical activation using chemicals such as NaOH [111,112], KOH [65,73,97], H_2SO_4 [69,115] and H_3PO_4 [111,114] have also been investigated. Using chemicals to produce porous activated carbon has many advantages over physical activation such as lower processing times and temperatures in addition to higher char yield and surface areas. In terms of activating agents, potassium salts are very popular, with KOH specifically well known for its ability to produce very high surface areas [41]. A literature review by Sharifian & Asasian-Kolur (2022) reported that KOH was the most popular activating agent and was used in 70% of the studies investigating the chemical activation of PET [101]. Additionally, Adibfar et al. [69] found that KOH activation of PET waste resulted in activated carbon with the highest surface area compared to other common activators, such as H_3PO_4, H_2SO_4, and $ZnCl_2$.

The high surface area activated carbons have many useful applications, with outstanding potential as adsorbents due to their porosity [115]. The treatment of waste effluents is a very important area of research with many recent advances in the purification of hard-to-treat wastes

such as oily water streams [117][118], raw biogas streams [119], and produced water [120][121]. Activated carbons are specifically very useful in the adsorption of small contaminant molecules from wastewater by the porous surface of the carbon. For example, some recent applications of biochar derived adsorbents include their application in treatment of dye contaminated [122] and metal contaminated waters [123]. Activated carbons derived specifically from KOH activated PET have also been investigated for applications including the adsorption of carbon dioxide [114,124,125], hydrophobic organic compounds [49], phenolic compounds [73], pesticides [67], Bisphenol A [126], Iron(III) and p-Nitrophenol [97], aqueous drug components [69] and nitrogenous organic pollutants [74].

One very common organic waste compound is methylene blue dye, which is heavily produced by the textile industry in the production of jeans. In general, coloured wastewater is a major concern because 10-15% of the applied dye remains in wastewater streams after the dying process [127]. This results in an enormous amount of waste, as textile wastewater accounts for 17-20% of all industrial wastewaters [128] and is expected to grow with the increasing demand for textile products [129]. Due to this effluent, around 200,000 tonnes of dye is lost as waste yearly, which is difficult to clean using traditional wastewater treatments [130]. Activated carbon is a very appealing option for the treatment of such wastes since it is inexpensive and simple to implement. For this reason, a lot of work has focused on the use of low cost activated carbons for the recovery of methylene blue dye. Some relevant works include the study of mesoporous zeolite activated carbon from oil palm ash [131], mesoporous NaOH activated carbon from chitosan flakes [132], mesoporous NaOH activated carbon from rattan hydrochar [133], nanoporous KOH activated carbon from karanj fruit hulls [134], cross-linked composites of

chitosan and sepiolite [135], and cross-linked NaOH activated oil palm ash zeolite/chitosan composite beads [136].

The goal of this study was to convert PET into an activated carbon product for the intended adsorption of dyes from textile wastewater. Although PET has been previously investigated as a precursor for the production of activated carbon [101], AC has not been produced with intended application as an adsorbent of charged dye molecules. Therefore, the surface charge has not been considered in the optimization of the processing conditions and the effects of adsorbent-adsorbate electrostatic interactions on the adsorption process have not been studied. In this study, the activation conditions (temperature and time) were investigated to provide a preliminary optimization of the activated carbon properties (surface area and surface charge) for the prospective adsorption of textile dyes. In addition, the adsorption of methylene blue dye was studied in detail and compared to a second cationic dye (Brilliant Green) and an anionic dye (Methyl Orange) to analyze the effects of surface charge interactions on the adsorption process as they relate to dye recovery.

3.2. Materials and methods

3.2.1. Materials

Used water bottles (Real Canadian Brand) were collected and used as the source of (polyethylene terephthalate) (PET). Sodium hydroxide (NaOH) (ACS reagent grade, ≥97.0%), Potassium hydroxide (KOH) (ACS reagent grade, ≥97%), hydrochloric acid (HCl) (ACS reagent grade, 37%), methyl orange (ACS reagent grade, dye content 85%), and Brilliant Green (BG) (dye content 90%) were all purchased from Sigma-Aldrich, Canada. Methylene Blue (MB) (Baker Analyzed reagent) and Sodium Chloride (NaCl) (ACS reagent grade, ≥ 99%) were purchased from Fisher Scientific, Canada.

3.2.2. Methods

3.2.2.1. Preparation of AC

Used water bottles were cut into small pieces of approximately 1 cm x 1 cm dimensions after removing caps and attached labels. They were then soaked in liquid nitrogen, ground, and sieved to obtain flakes of 2-3.35 mm particle size. The ground product was agitated within a KOH solution (1:1 mass ratio of PET: KOH) at room temperature for 1 h in batch sizes of 1.5 g of PET. The water was then boiled off by heating at 80 °C overnight. The KOH coated PET was carbonized under nitrogen flow using a tube furnace (Thermo Scientific Lindberg/Blue M 18.4L B2 Moldatherm Box Furnace) by heating at a rate of 10 ºC/min to a temperature of 600 ºC, 700 ºC and 800 ºC and holding for 1 h and 2 h. Additionally, one sample of sieved PET before KOH impregnation was treated at 600 ºC for 1 h to observe the effects of chemical activation. The samples are designated based on their activation conditions according to the labels in **Table 7**. After carbonization, the samples were washed with 1M Hydrochloric Acid (HCl) for 1 h. The carbon was removed from the HCl solution by centrifugation (Heraeus Megafuge 1.0 Centrifuge) and washed thrice with DI water. The final product was obtained after drying overnight at 80 ºC and grinding using a mortar and pestle.

Table 7: Activation conditions used to produce PET AC.

Sample	Treatment Conditions
Control	Carbonization at 600 ºC for 1 h
AC-600C1h	KOH activation at 600 ºC for 1 h
AC-600C2h	KOH activation at 600 ºC for 2 h
AC-700C1h	KOH activation at 700 ºC for 1 h
AC-700C2h	KOH activation at 700 ºC for 2 h
AC-800C1h	KOH activation at 800 ºC for 1 h
AC-800C2h	KOH activation at 800 ºC for 2 h

3.2.2.2. Surface area analysis and yield of ACs

The surface area of the carbon was characterized by nitrogen adsorption at 77 K using a Micromeritics Gemini VII 2390a. The samples were first degassed at 300 °C for 1 h under vacuum, and then analyzed using relative pressures of $0.005 \leq p/p^o \leq 0.05$. The surface areas were calculated using the BET (Brunauer–Emmett–Teller) method in the specified pressure range. The mass percentage yield for each activated carbon product was calculated using **Equation (7)**, in which m_{PET} is the initial mass of PET carbonized and m_{AC} is the final mass of activated carbon recovered after the acid wash and drying procedure. Duplicate runs of the optimized product were used to estimate the percentage error in the yield values for all samples.

$$\%Yield = 100\, x \frac{m_{AC}}{m_{PET}} \quad \textbf{(7)}$$

3.2.2.3. DLS analysis of ACs

Activated carbon solutions of 0.001 wt.% concentrations in DI water were prepared by sonicating for 20 minutes. The samples were then analyzed using a Malvern Zetasizer Nano-series (Westborough, MA, United States) DLS to measure zeta potential using a folded capillary zeta potential cell (Zetasizer nano series, DTS 1061). Three scans of each sample were collected, and the averages were reported.

3.2.2.4. FTIR analysis and SEM imaging of ACs

FTIR spectra were obtained using a Thermo Scientific Nicolet 6700 equipped with ATR. Data were collected in the range of 650–4000 cm^{-1} in absorbance mode using 16 scans. SEM was conducted using an Oxford Instruments Quanta FEG 250 Environmental SEM (Abingdon, UK) without any sputter coating. The supported energy dispersive X-Ray spectroscopy (EDX) was used to conduct elemental surface analysis and mapping of carbon and oxygen.

3.2.2.5. pH of zero charge

Various solutions were prepared by adjusting 25 mL of 0.1M NaCl in DI water to pH values between 2-12 using HCl and NaOH. Activated carbon (10 mg) was sonicated in 5 mL of their respective solution, then added to the remaining 20mL and placed in a shaker for 24 h at 72 rpm. The pH of the solutions was measured after reaching equilibrium at 24h and plotted against the initial solution pH. The pH of zero charge was determined by plotting this curve against the x = y line and taking the intersection point.

3.2.2.6. UV-vis spectroscopy

UV-Vis spectrophotometry (Cary 300 Bio UV-Visible Spectrophotometer) was used to calculate the concentrations of Methylene Blue (MB), Brilliant Green (BG) and Methyl Orange (MO) dyes. Sample spectra were obtained between 300 - 800 nm, and their absorbance at maximum wavelengths of 664 nm (MB), 624 nm (BG) and 424 nm (MO) were used to calculate concentration. Calibration curves were produced for each dye by preparing a 100 mg/L stock solution and diluting to form a range of concentrations. Absorbances at the corresponding maximum absorbance wavelengths were correlated to the known concentrations to produce a linear calibration equation for all dyes at low concentrations. For MB, an additional calibration curve was produced for concentrations outside the linear region in which a polynomial calibration function was applied. All calibration curves and raw UV-vis data can be found in the Appendix (**Figure 34** - **Figure 37**).

3.2.2.7. Adsorption isotherm study

Methylene blue adsorption tests were carried out in batch sizes of 25 mL using initial concentrations of 100, 150, 200, 250 and 300 mg/L. For each run, 10 mg of AC was sonicated in 5 mL deionized water for 10 min while submerged in cold water for temperature control.

Methylene blue solutions were either adjusted to pH 10 using 0.1 M NaOH, pH 4 using 0.1 M HCl or left at the unadjusted pH of 6. The sonicated AC was added to 20 mL of each methylene blue solution and placed in a shaker for 24 h at 72 rpm. Solutions were then centrifuged, and sequential dilutions (1/10) of the supernatant were used to measure dye concentration via UV-Vis spectroscopy. Similarly, samples of the initial methylene blue solutions were also measured. For each run, the equilibrium adsorption (mg MB/g AC) was determined according to **Equation (8)**, in which C_0 (mg/L), C_e (mg/L), V (L), and m (g) refer to initial dye concentration, equilibrium dye concentration, batch volume, and mass of AC respectively.

$$q_e = \frac{(C_0 - C_e)V}{m} \quad \textbf{(8)}$$

Langmuir, Freundlich and Sips adsorption isotherm models were fitted to the experimental data by non-linear regression using excel's solver function. Parameters were determined based on the minimization of the sum of squared errors (SSE). The Langmuir model was expressed using **Equation (9)**, in which q_{max} is the maximum monolayer adsorption capacity (mg/g) and K_L is the Langmuir constant (L/mg) which represents the affinity of the binding sites. This model assumes a homogenous adsorbent surface and monolayer formation [137].

$$q_e = \frac{q_m K_L C_e}{1 + K_L C_e} \quad \textbf{(9)}$$

The Freundlich model was expressed by **Equation (10)**, in which K_F is the Freundlich constant ($L^{1/n} m g^{1-\frac{1}{n}} g^{-1}$) and n_F indicates the heterogeneity of adsorbate sites [138]. The Freundlich model is often used to describe multilayer adsorption on heterogenous surfaces [86].

$$q_e = K_F C_e^{\frac{1}{n_F}} \quad \textbf{(10)}$$

Lastly, the Sips model, a combination of Langmuir and Freundlich models, is expressed by **Equation (11)**, in which K_s ($L^{\beta} mg^{1-\beta} g^{-1}$), α ($L^{\beta} mg^{-\beta}$) and β are parameters. The model approaches the Langmuir isotherm at high solute concentrations and the Freundlich isotherm at low solute concentrations. Unlike the Langmuir model, it can describe adsorption onto heterogeneous surfaces [138].

$$q_e = \frac{K_s C_e^{\beta}}{1 + \alpha C_e^{\beta}} \quad \textbf{(11)}$$

3.2.2.8. Adsorption kinetics study

Dye Adsorption tests were carried out in batch sizes of 200 mL using activated carbon concentrations of 25, 50 and 75 mg/L. The activated carbon was first sonicated at 1 mg/mL for 10 min while submerged in cold water for temperature control. Next, the sonicated carbon was added to 25 mg/L dye solutions and stirred at 400 rpm for 30 h during which 5 mL samples were collected over time. The samples were centrifuged, and the concentration of the supernatant dye was determined based on UV-Vis spectroscopy. For each run, the adsorption (mg dye/g AC) was determined over time according to **Equation (12)**, in which C_t (mg/L) is the dye concentration at time t (min). Additionally, the percentage recovery of dye was calculated according to **Equation (13)** and plotted over time. For one experiment, a dye mixture containing 8 mg/L MB, and 10 mg/L methyl orange was used as the initial dye solution. Due to negligible peak overlapping, UV-Vis spectrophotometry was used to determine the concentration of each dye in the mixture over time.

$$q_t = \frac{(C_0 - C_t)V}{m} \quad \textbf{(12)}$$

$$\% \text{ Removal} = 100 \times \left(1 - \frac{C_t}{C_0}\right) \quad \textbf{(13)}$$

Pseudo First Order (PFO), Pseudo Second Order (PSO), Weber and Morris (W&M) intraparticle diffusion (IPD), and Elovich kinetic models were fitted to the experimental data using linear regression using Excel's linear least squares best fit lines. Parameters were determined based on the obtained slope and intercept of the linear least squares model. The PFO model is expressed in its linear form by **Equation (14),** in which K_1(g/mg/min) is a parameter describing how fast equilibrium is reached [139], and t (min) is the adsorption time.

$$\ln(q_e - q_t) = \ln(q_e) - K_1(t) \quad \textbf{(14)}$$

The PSO model was expressed in its linear form by **Equation (15)** in which K_2 (g/mg/min) is the parameter similar to K_1 that describes the speed of equilibrium. For a variety of adsorbent/adsorbate systems it was found that at low initial solute concentrations the PSO model is most suitable [139].

$$\frac{t}{q_t} = \frac{1}{K_2 q_e^2} + \frac{t}{q_e} \quad \textbf{(15)}$$

The Weber and Morris Intraparticle diffusion model was expressed by **Equation (16)** which is already in a linear format. The parameter K_{int} (mg/g/min$^{1/2}$) is the intraparticle diffusion rate constant and C (mg/g) is a constant. The intercept C is zero if intraparticle diffusion is the rate limiting step [139]. This model often exhibits separate regions corresponding to an external mass transfer stage followed by intra particle diffusion [94], so the separate parameters K_{ext} and C_{ext} were used to describe the external mass transfer region.

$$q_t = K_{int} t^{\frac{1}{2}} + C_{int} \quad \textbf{(16)}$$

Lastly, the Elovich model is expressed in its linear form by **Equation (17)**, in which a and b are parameters. This version of the model was derived from its original non-linear form

with the assumption of $abt >> 1$. This model assumes that the adsorption energy increases with adsorption time and that the surface of the adsorbent is heterogenous. It is often used to describe the adsorption of gas onto solid but has also been applied to solid-liquid systems more recently [139].

$$q_t = \frac{1}{b}\ln(ab) + \frac{1}{b}\ln(t) \quad \textbf{(17)}$$

3.3. Results and discussion

To alleviate the impact of PET waste buildup and take advantage of the highly carbonaceous aromatic structure of PET, waste bottles were carbonized to form activated carbon (AC). The conversion of waste PET bottles to a high value activated carbon product is schematically illustrated in **Figure 10**. The process involves the carbonization of PET by thermal decomposition combined with the simultaneous activation of the produced char using KOH. The chemical activation developed the required surface area of the char to produce high-capacity adsorbent material. This activation of PET- carbon by KOH can be described by **Equation (18)** [140,141], resulting from many simultaneous and consecutive reactions. Initially, carbon is consumed by water-gas and water-gas shift reactions to produce H_2, CO, and CO_2 gases, with KOH being consumed towards the production of K_2O followed by K_2CO_3. At temperatures exceeding 700 ^oC a significant amount of potassium metal is produced by reducing the mentioned potassium products [44]. Therefore, the activation occurs through the gasification of carbon, the consumption by redox reactions with potassium products, and the intercalation of potassium metal which helps expand the carbon lattice and enhance pore formation [143].

$$6KOH + 2C \rightarrow 2K + 3H_2 + 2K_2CO_3 \quad \textbf{(18)}$$

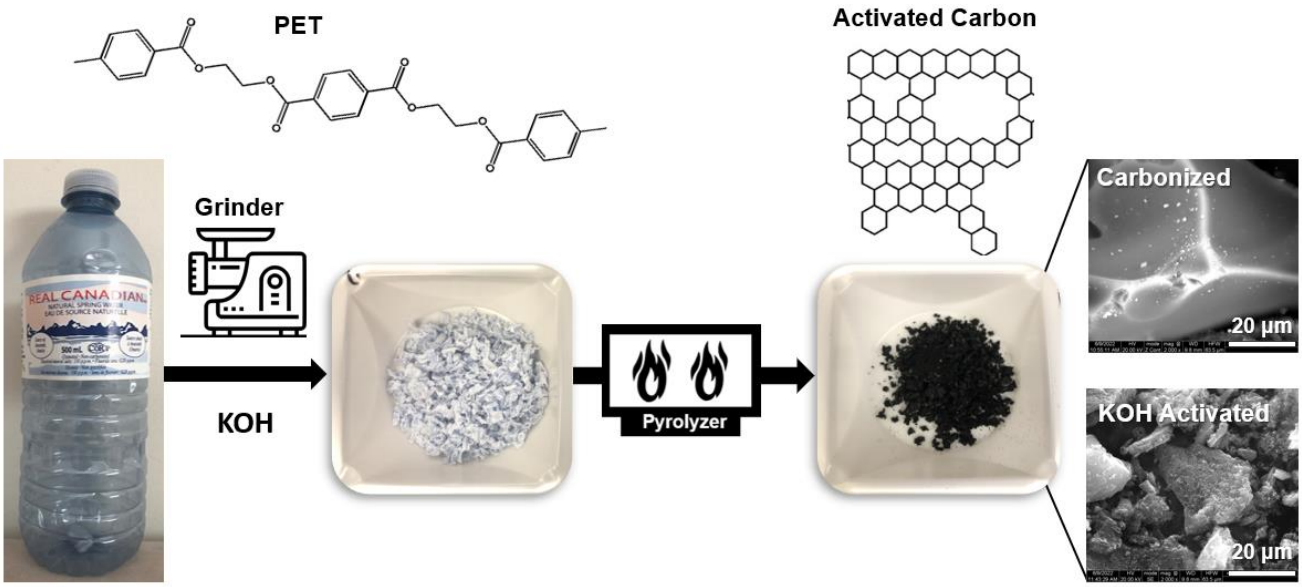

Figure 10: Schematic of activated carbon production from water bottle waste.

In this study, the activation process was carried out at various temperatures and times, as outlined in **Table 7**. Activation performed at 700 ºC and 800 ºC resulted in highly carbonized black char, as shown in **Figure 33** (see Appendix), while activation at 600 ºC resulted in a light grey product. Carbonization at 600 ºC in the absence of KOH resulted in a black char and was used as the control. The yield of all samples and surface properties of the successfully carbonized ACs are presented in **Table 8.**

Table 8: BET surface area, Zeta potential and yield of PET Activated Carbon and carbonized PET.

Sample	Yield (%)	BET Surface Area (m^2/g)*	Zeta Potential (mV)**
Control	17.34 ±1.0	407.50 ±0.87	-34.5 ± 1.6[a]
AC-600C1h	40.0 ± 3.7	-	-
AC-600C2h	39.0 ± 3.7	-	-
AC-700C1h	29.6 ± 2.9	625.63 ± 0.70	-35.3 ± 1.6[a]
AC-700C2h	27.4 ± 2.5	816.48 ± 3.85	-34.1 ± 1.2[a]
AC-800C1h	25.4 ± 2.5	1124.07 ± 1.66	-39.6 ± 0.7[b]

AC-800C2h	21.8 ± 2.1	1214.74 ± 4.90	-39.9 ± 1.8[b]

*BET Surface area uncertainties are model related errors determined by the instrument. **Data = mean ± standard deviation, varying superscript letters within a column indicate statistically different ($P < 0.05$).

3.3.1. BET surface area

The surface area was used as the primary indication of the AC adsorption capability. As seen by the BET surface area data in **Table 8**, there is an increase in surface area as the activation temperature increased from 700 ºC to 800 ºC and time increased from 1 h to 2 h. The produced char from carbonization alone exhibited a substantial surface area of 407 m^2/g (control) but required activation by KOH for further increase. Adibfar et al. [69] also reported a similar surface area of 362 m^2/g for carbonized PET. The extent of activation reaction has substantially increased at 800 ºC where surface areas above 1000 m^2/g were achieved.

The surface areas achieved in this study are comparable to those from literature compiled in **Table 9**. Many of these studies used a higher amount of KOH, with some performing the activation after first carbonizing PET at 600 ºC to achieve surface areas beyond 2000 m^2/g. However, the use of carbonized PET as a precursor to activation is not appealing due to the low yield (17%) observed in this study, which would be further reduced by the subsequent activation. Others have also reported a yield of 17% [116] and 17.1% [144] for the carbonization of PET.

The KOH incorporation methods also cause variations in the achieved surface areas. For example, the higher surface area of 1338 m^2/g achieved by Adibfar et al. [69] using the same amount of KOH may be attributed to the 6 h KOH treatment at an elevated temperature (85-95 ºC) to facilitate its incorporation. In comparison, this study considers the feasibility of the PET conversion process by avoiding long process times, additional energy inputs and unnecessary amounts of the activating agent. For these reasons, activation at 800 ºC for 1 h is suggested. It was concluded that increasing activation time to 2 h is not worth the 100 m^2/g increase in surface

area when considering the effects on the processing time, yield, and ultimately process cost. Overall, the results indicate that high surface areas can be achieved without an excessive amount of KOH, pre-treatment step, or an activation time above 1 h.

Table 9: Comparison of BET surface areas for various ACs produced by KOH activation of PET.

KOH: PET Ratio	Pre-treatment	Activation Conditions	BET Surface Area (m^2/g)	Reference
1:1	-	800 ºC 1 h	1124	This study
2:1	-	700 ºC	1334	[75]
2:1	-	700 ºC	1418	[74]
2:1	-	800 ºC 30 min	1439	[68]
2:1	Carbonize 600 ºC 1 h	850 ºC 1.5 h	2831	[50]
2:1	Carbonize 600 ºC 1 h	800 ºC 1 h	2006	[66]
2:1	-	800 ºC 1 h	844	[99]
1:1	-	800 ºC 1h	817	[70]
1:1	-	850 ºC 2 h	1060	[127]
1:1	-	400 ºC 1 h, 800 ºC 1 h	1338	[69]

3.3.2. AC yield

The mass yield of carbon obtained from PET is an important parameter affecting the cost efficiency of the overall conversion process. Additionally, it has been used as an indication of the degree of activation due to the reduction in yield as pore development progresses [99]. This trend was clearly observed as both activation time and temperature increased (**Table 8**), leading to a decrease in yield from 40.0% (AC-600C1h) to 21.8% (AC-800C2h). Similar yields of 30.07%, 28.45%, and 24.62% were reported at activation temperatures of 700 ºC, 800 ºC and 850 ºC [99], in addition to a higher yield of 31% at a maximum activation temperature of 800 ºC [116].

The decrease in yield upon increasing the temperature from 600 ºC to 700 ºC is mainly due to the increased carbonization of PET. Both the FTIR spectra and colour of the product

(**Figure 33**) indicated that the 600 ºC treatments did not completely carbonize PET leaving behind a higher yield of lower carbon material. At 700 ºC and 800 ºC the decreasing yield correlates with the increased surface area due to activation reactions. Both trends were considered when choosing the most suitable processing conditions of 800 ºC 1 h.

3.3.3. Zeta potential

The zeta potential is used to indicate the surface charge and therefore affinity of the adsorbent towards charged dye molecules. The primary dye of interest in this work is cationic methylene blue, so a negative surface charge would facilitate the attraction of the dye to its surface. The charge on the AC is generated from residual functional groups on the surface, which participate in ion or electron exchange [145]. The control (carbonized PET) likely has residual oxygen groups that cause it to exhibit a negative zeta potential (-34.5 mV) as presented in **Table 8**. This zeta potential ultimately remained the same after activation at 700 ºC but decreased to almost -40 mV after activation at 800 ºC. This can be explained by the surface functional groups imparted onto the AC due to the activating agent. According to **Equation (19)** the KOH activating agent can incorporate oxygen into the carbon structure to form R-O-K groups. Upon washing the AC with aqueous solutions, the incorporated O-K groups can become -OH groups via ion exchange [146].

$$K_2O + R \rightarrow K + R - O - K \xrightarrow{H_2O\ wash} R - OH \quad \textbf{(19)}$$

Surface charges can then be generated by the interaction of the functional groups with the surrounding environment. Typically, acidic and basic sites can be formed on the AC surface based on the following two reactions proposed by Ko et al. [147].

$$R - OH + H^+ \rightarrow R - OH_2^+ \quad \textbf{(20)}$$

$$R - OH \rightarrow R - O^- + H^+ \quad \textbf{(21)}$$

The development of acidic groups, as expressed by **Equation (21)**, contributes to the negative surface charge of the material. This proposed generation of surface charge due to the KOH activation significantly affected the zeta potential of the produced ACs at the higher activation temperature (800 ºC). Still, it did not change upon increasing the activation time. Therefore, the activation at 800 ºC is expected to enhance the affinity toward cationic dyes. The effect of pH on the surface charge and adsorbent/adsorbate charge interactions will be discussed in the adsorption analysis of AC-800C1h.

3.3.4. FTIR analysis

The characteristic IR peak of PET is the carbonyl (C=O) typically seen at ~1730 cm^{-1} [148,149], which provides a good indication of PET conversion based on its disappearance. This peak occurred at around 1718 cm^{-1} in pristine PET and 1685 cm^{-1} in the treated samples. As seen in **Figure 11**, its intensity reduced greatly through carbonization but remained prominent in the samples treated at 600 ºC, indicating incomplete conversion of PET at this temperature. Thus, higher pyrolysis temperatures (700 ºC and 800 ºC) were necessary to cause the significant conversion of PET to carbon. The carbonized PET control exhibits the greatest reduction of all peaks, indicating that the carbonization proceeds more effectively in the absence of the competing KOH activation reactions.

The activated carbons treated at 600 ºC exhibit a new group of peaks at 2963, 2826, 2665 and 2578 cm^{-1}. These peaks indicate a carboxylic acid intermediate, such as benzoic acid, which exhibits an OH stretching vibration from the carboxylic acid group between 2500 and 3300 cm^{-1} [150]. The specific benzoic acid peaks have been reported at 3072, 2839, 2677 and 2561 cm^{-1} [150], which match up very closely with those observed. The presence of this intermediate can explain the lighter colour of samples (**Figure 33** in the Appendix) treated at 600 ºC, since

benzoic acid is a white solid that would not have solubilized during the aqueous washing step. Due to the significant impurity, AC-600C1h and AC-600C2h were excluded from the surface characterization analyses.

For the high conversion activated carbons, the C-H peak at 2960 cm^{-1} [151] can no longer be seen and is replaced by the broad peak around 1550 cm^{-1} attributed to the C=C vibration of aromatic rings [152,153]. It is understood that the unsaturated carbon remaining after devolatilization reactions leads to aromatic crosslinking during polymer decomposition [148]. The other broad peak around 1150 cm^{-1} indicates the bending and stretching of OH groups in C-OH [153,154]. This supports the formation of OH surface groups due to the KOH activator, which contributes to surface charge generation when in solution. Although there are no peaks seen in the typical OH group region (3200-3600cm^{-1}), similar results were reported by Liakos et al. [154], in which the peak around 1150 cm^{-1} was the only indication of C-OH in activated carbons produced from various agricultural sources.

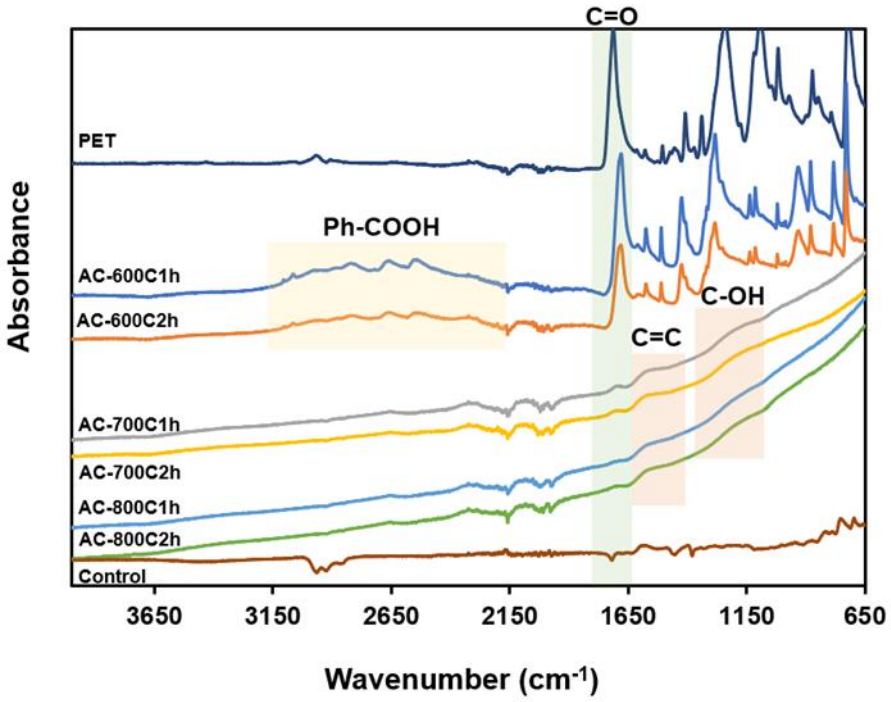

Figure 11: FTIR Spectra of PET Activated carbon, carbonized PET, and untreated PET.

3.3.5. SEM imaging

The EDX elemental mapping of carbon and oxygen onto the AC-700C1h, AC-800C1h and the control are shown in **Figure 12**. The results agree with the FTIR spectra, which exhibit increased carbonization with activation temperature and the highest level of conversion observed in the control samples. This can be seen by the increased density of carbon detected on the surface of AC-800C1h compared to AC-700C1h. As expected, the control, which does not entail KOH activation, exhibited a much higher amount of carbon and lower amount of oxygen than the AC samples due to the high level of carbonization. However, the oxygen content in the AC does not change significantly as activation temperature increases due to the competing effect of oxygen incorporation by the activating agent.

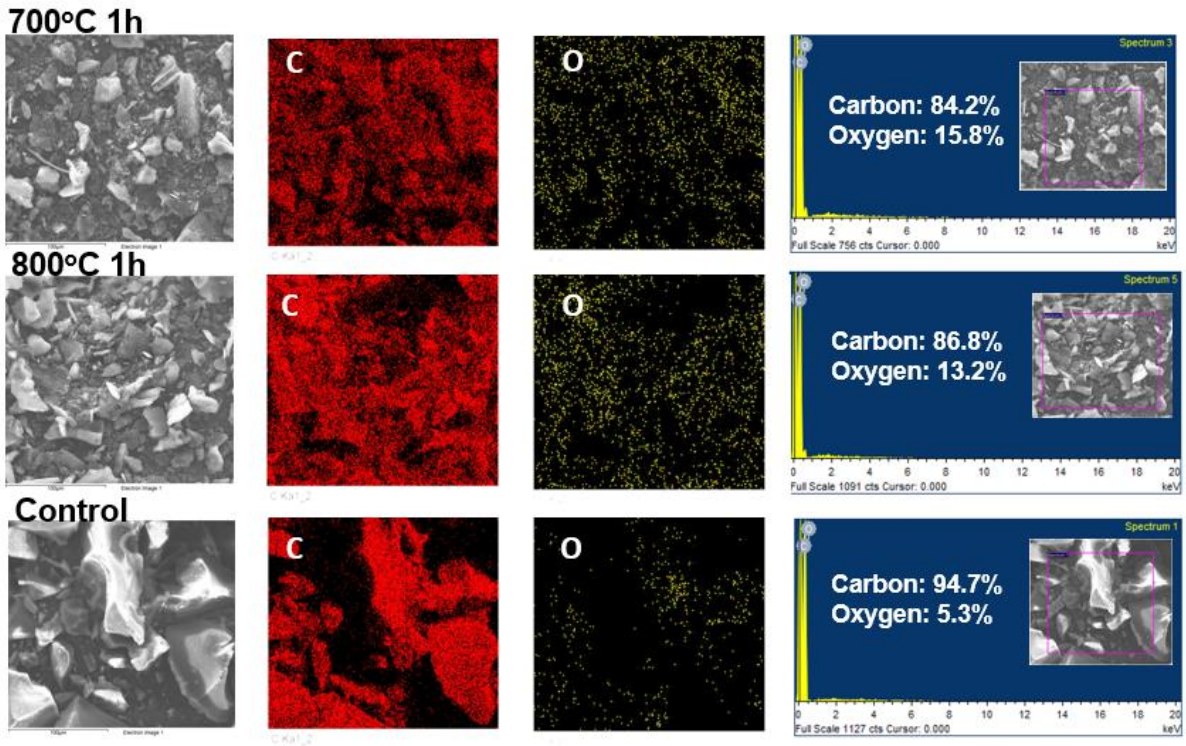

Figure 12: Surface elemental spectra and EDX mapping of carbon and oxygen on PET activated carbons and carbonized PET.

The SEM images of all samples presented in **Figure 13** support the development of a porous structure after activation. Compared to the control, the ACs are highly textured with a distribution of pores that are especially defined in some areas of AC-800C2h (**Figure 13e**). The other ACs exhibit more depth in their structure due to the progressive KOH reactions towards the inside of the carbon [66,99]. It is possible that the highest activation treatment (800 ºC 2h) caused the breakdown of the macropores in some areas, leaving a flatter mesoporous structure. This may explain the relatively lower increase in surface area between AC-800C1h and AC-800C2h (**Table 8**). Others have even reported decreases in surface area of PET activated carbon when increasing activation temperature past 800 ºC [66] and increasing to 2 h activation time at 800 ºC [99] based on similar reasoning.

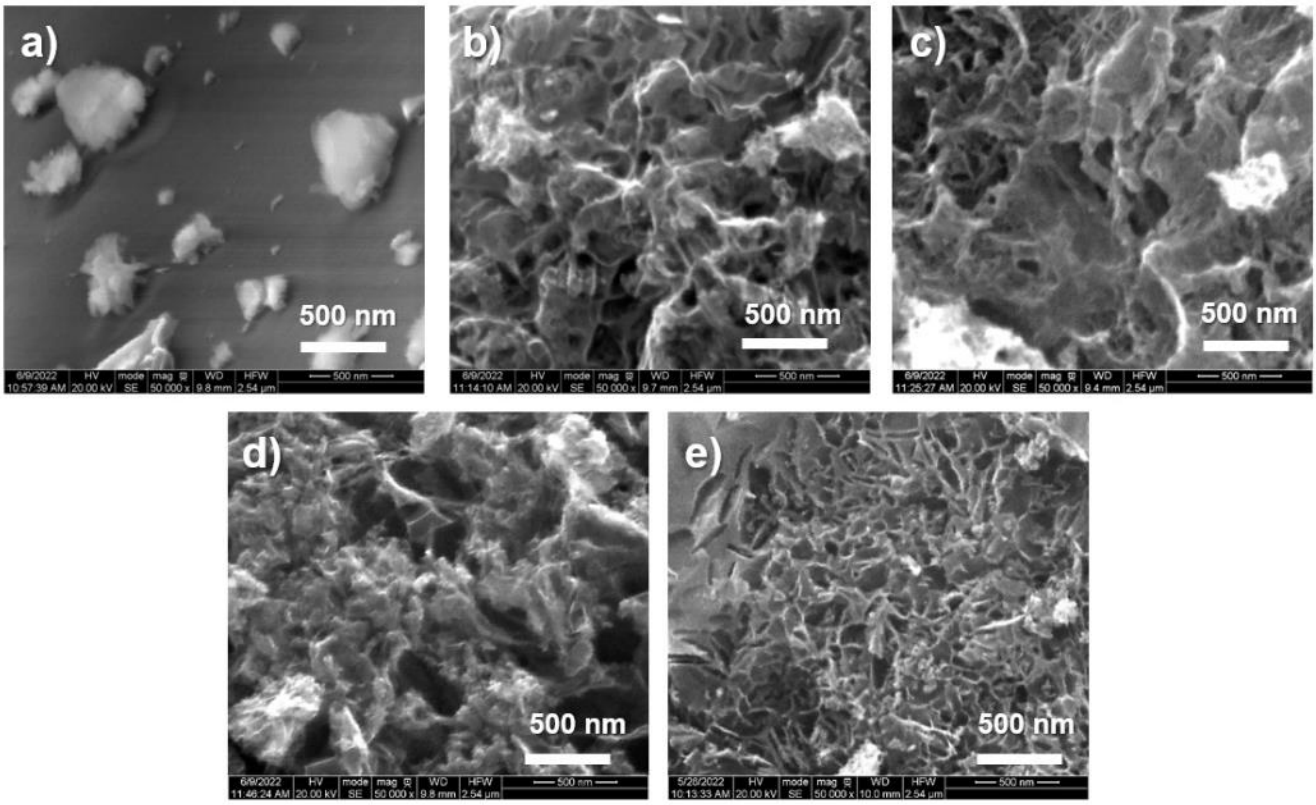

Figure 13: SEM images of a) control; b) AC-700C1h; c) AC-700C2h; d) AC-800C1h; e) AC-800C2h at 50,000X magnification.

3.3.6. pH of zero charge

The ACs exhibited surface charges due to the surface functional groups containing oxygen, as demonstrated by their negative zeta potentials. However, the magnitude is highly dependant on the solution pH surrounding these oxide particles. To understand the effect of pH on the tendency towards a positive or negative surface charge, the pH of Zero charge (pH_{zc}) is often used as an index [155]. This pH value indicates the point above which the surface is negatively charged and below which the surface becomes positively charged. As shown in **Figure 14a**, the pH_{zc} of AC-800C1h was determined to be around 3.7. This confirms that the AC

sustains a negative surface charge for all pH values greater than 3.7, making it an ideal adsorbent for cationic dyes.

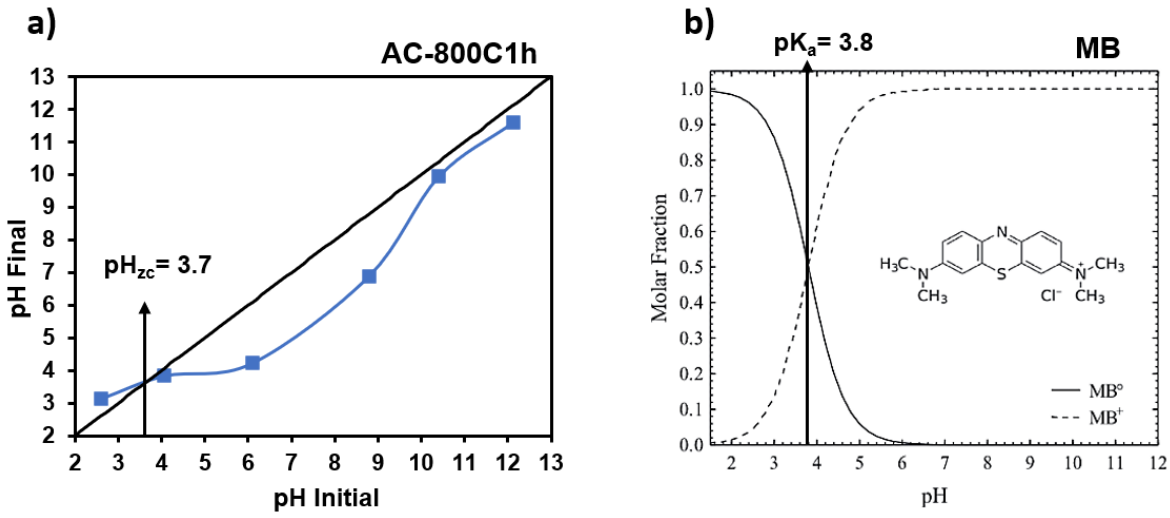

Figure 14: Effect of solution pH on electrostatic charge as indicated by a) pH_{zc} analysis of AC-800C1h; and b) speciation of MB.

Another important consideration is the speciation of the solute dye molecule, which may also change with respect to pH. Methylene blue (MB) can exist with a positive (MB^+) or neutral (MB^o) surface charge according to the speciation diagram (**Figure 14b**) obtained from Salazar-Rabago et al. [156]. According to this diagram, MB exists as both MB^o and MB^+ in equal amounts at the pK_a of 3.8. When pH < pK_a the dye is predominantly in its protonated form, and when pH > Pk_a it is predominantly in its deprotonated form [75]. Therefore, this specific adsorbent/adsorbate system works well because the AC will have an opposite charge to the dye for all pH values in which the dye exhibits a positive charge. Still, the pH will affect this electrostatic attraction due to the changes in surface charge distributions on the dye and the AC.

3.3.7. Methylene blue adsorption isotherm

As shown in **Figure 15a**, the pH affected the adsorption isotherms of MB onto AC-800C1h. At pH 4, the MB is very close to its pK_a where it exists as 50% MB^+ and 50% MB^o. Therefore, around half of the MB molecules possess a neutral charge and do not experience electrostatic attraction to the negatively charged adsorbent. This explains the lower Langmuir monolayer capacity observed at pH 4 (288 mg/g) compared to pH 6 (324 mg/g) and pH 10 (335 mg/g). In addition to the Langmuir model, the Freundlich and Sips isotherm models were applied to the data, with the resulting parameters presented in **Table 10**. The Langmuir adsorption model provided a good fit for pH 4 (R^2= 0.946), pH 6 (R^2= 0.991), and pH 10 (R^2= 0.989) indicating that adsorption follows monolayer formation. However, the Sips model provided a better representation of the isotherm curvature, as illustrated by the pH 4 isotherm in **Figure 15b**. Although a monolayer is formed on the AC, the mechanism does not follow ideal monolayer adsorption likely due to the heterogenous nature of the surface. Therefore, the Sips model provided the best fit for all solution pH values because it approaches Freundlich adsorption at low adsorbate concentrations, which describes the curvature better but approaches Langmuir adsorption at high adsorbate concentrations, which describes the monolayer equilibrium [139].

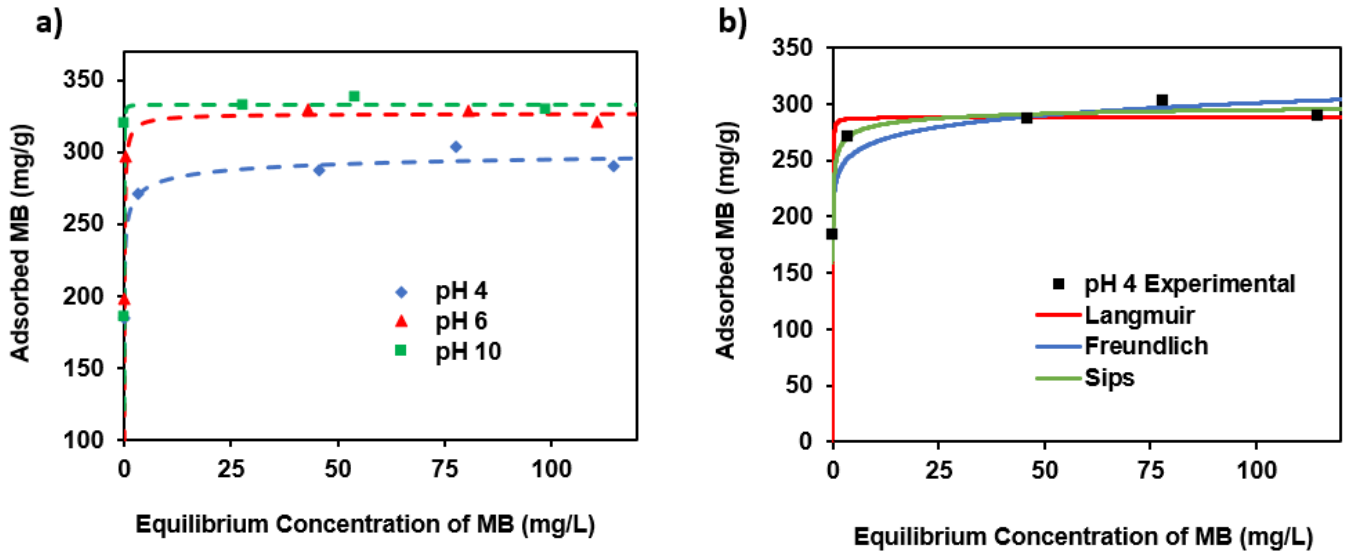

Figure 15: a) Effect of pH on the adsorption isotherm of MB onto AC-800C1h with dotted lines representing Sips model prediction; b) model comparison to adsorption of MB onto AC-800C1h at solution pH 4.

Table 10: Isotherm model parameters describing adsorption of MB onto AC-800C1h at pH 4, pH 6, and pH 10.

Isotherm model	Parameter	pH 4	R^2	pH 6	R^2	pH 10	R^2
Langmuir	q_m	288.22	0.946	324.49	0.991	335.60	0.989
	K_L	63.51		22.43		70.62	
Freundlich	K_F	235.66	0.925	263.39	0.774	281.60	0.623
	n_F	18.79		19.33		22.38	
Sips	K_s	1465.35		4486.84		84339.78	
	α	4.74	0.986	13.72	0.996	253.29	0.998
	β	0.325		0.816		1.323	

Based on the isotherm plots, increasing the pH from 6 to 10 does not significantly affect the monolayer capacity of the material. Presumably, the speciation of MB has the most influence on the adsorption capacity because 100% of the molecules are in their positive form at pH 6 and

above (**Figure 14b**). The speciation of negative and positive charge sites on AC is not as influential because the existence of some positively charged groups does not change the overall negative surface charge on each particle at pH values above 3.7. At pH 6, only negative charges are likely present with increasing charge density at higher pH values. This is expected because the hydroxide ions may cause unreacted surface hydroxyl groups to be converted to acidic groups (**Equation (21)**) to a greater extent as pH increases. It should be noted that the hydroxyl groups are likely to be associated with carboxylic acid groups due to their lower pKa. The increased electrostatic attraction would explain the lower concentration and driving force required to reach the maximum monolayer capacity at pH 10 compared to pH 6. This proposed explanation for the observed changes in adsorption isotherms is illustrated in **Figure 16**.

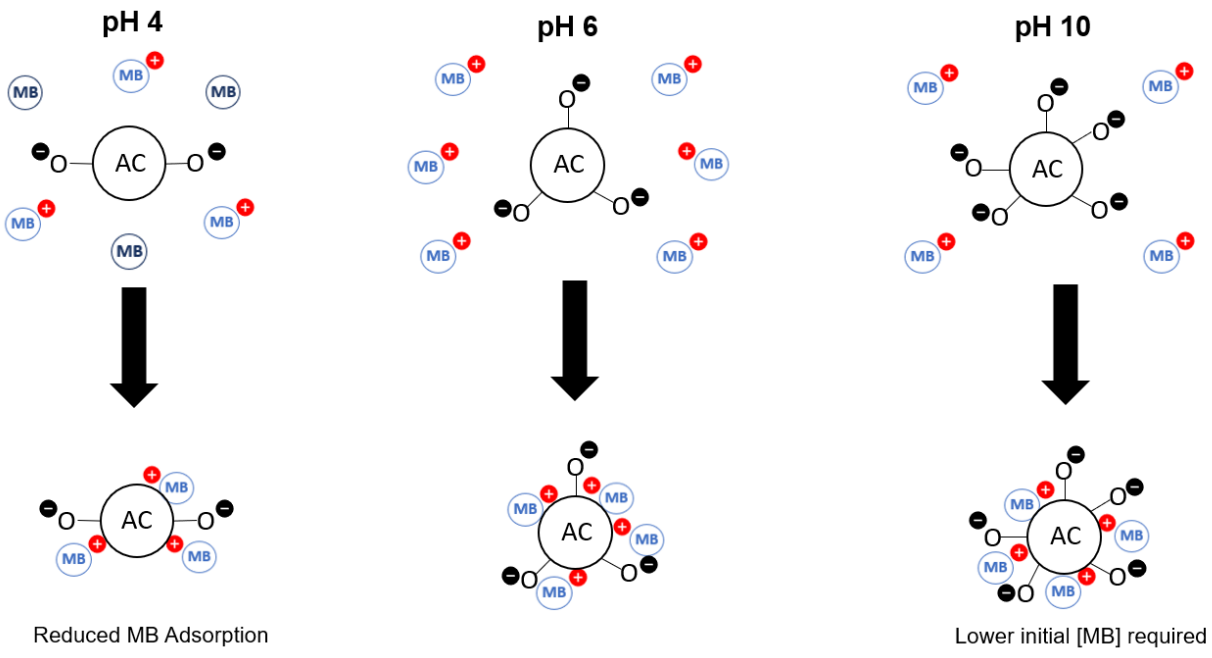

Figure 16: Proposed explanation for pH dependent changes in MB adsorption.

As a result of this analysis, the monolayer capacity at pH 10 (335 mg/g) is taken as the maximum adsorption capacity of the material across all pH values. This value is compared to

ACs produced from other feedstocks in **Table 11**. The high adsorption capacity is attributed to the surface area of the highly activated carbon providing many adsorption sights combined with the charge interaction from functional groups. The effect of functional groups alone was demonstrated in the work of Cheng et al. [157] by the adsorption of charged metal ions onto biochar of low BET surface area. Overall, the AC produced from PET is very competitive with other feedstocks without requiring a separate carbonization pre-treatment like many of the listed products. It should be noted that this adsorption capacity has only reduced by about 47 mg/g at the low (pH = 4), so the adsorbent is expected to perform well across all wastewater pH values. Alternatively, pH adjustment can be used to enhance the charge characteristic of the specific dye in relation to the AC.

Table 11: Comparison of the methylene blue adsorption capacity of AC-800C1h to other ACs.

Feedstock	Pre-treatment	Activating agent	Impregnation Ratio	Activation conditions	Surface Area (m^2/g)	Methylene Blue adsorption (mg/g)	Reference
Commercial Product	-	-	-	-	950-1050	355	[158]
PET	**-**	**KOH**	**1**	**800 °C 1 h**	**1124**	**335**	**This study**
Coconut shell	Carbonization 300 °C	Steam	NA	700 °C	-	278	[159]
Rice husk						454	
Straw						472	
Rattan saw dust	-	KOH	1	700 °C 1 h	-	294	[160]
Peach stone	-	H_3PO_4	0.68	500 °C 2 h	1298	412	[161]
Oil Palm Shell	Carbonization 700 °C	KOH and CO_2	1 (KOH)	850 °C 2 h	596	244	[153]
Tire Char	-	Steam	NA	900 °C	602	227	[162]
S. Vermiculata Leaves	Carbonization 600 °C	$ZnCl_2$	-	650 °C 2 h	-	130	[163]
Rubber seed coat	Carbonization 700 °C	KOH	1	850 °C 2h	1225	227	[164]

3.3.8. Methylene blue adsorption kinetics

The kinetics of the methylene blue (MB) adsorbent was analyzed using a constant MB concentration of 25 mg/L. Based on the results presented in **Figure 17,** the adsorption reached equilibrium after 24 h and achieved 100% dye recovery at an AC loading of 75 mg/L. The lower loading levels (25 mg/L and 50 mg/L) resulted in 40% and 72% dye recovery. In agreement with the maximum monolayer adsorption of 335 mg/g, the equilibrium adsorption of 333 mg/g was observed at the lowest AC concentration of 25 mg/L. This indicates that the AC has reached its maximum adsorption at this AC concentration due to the higher ratio of MB to the adsorbent. It also supports the previous conclusion that the adsorption capacity at pH 6 approaches the same value as pH 10.

The adsorption curves for each AC loading were modelled by four kinetic models and their respective parameters are presented in **Table 12**. The regression was performed using the linearized forms of the model equations and are plotted in **Figure 18**. Evidently, the PFO model did not describe the data well, resulting in large discrepancies between the predicted and experimental equilibrium adsorption (q_e). The PSO model provided the best fit of the linearized data with R^2 values of 0.999 for all three concentrations. However, when observing the modelled adsorption curves compared to experimental data (**Figure 17c**) it was evident that the Elovich model captured the curvature of the two lower AC concentrations more precisely. The PSO model was better suited for the highest concentration AC in which 100% dye recovery was achieved. This model exhibits a steeper rise at the onset of adsorption, which is more applicable to high AC concentrations but provides very accurate equilibrium data (q_e) for all AC concentrations.

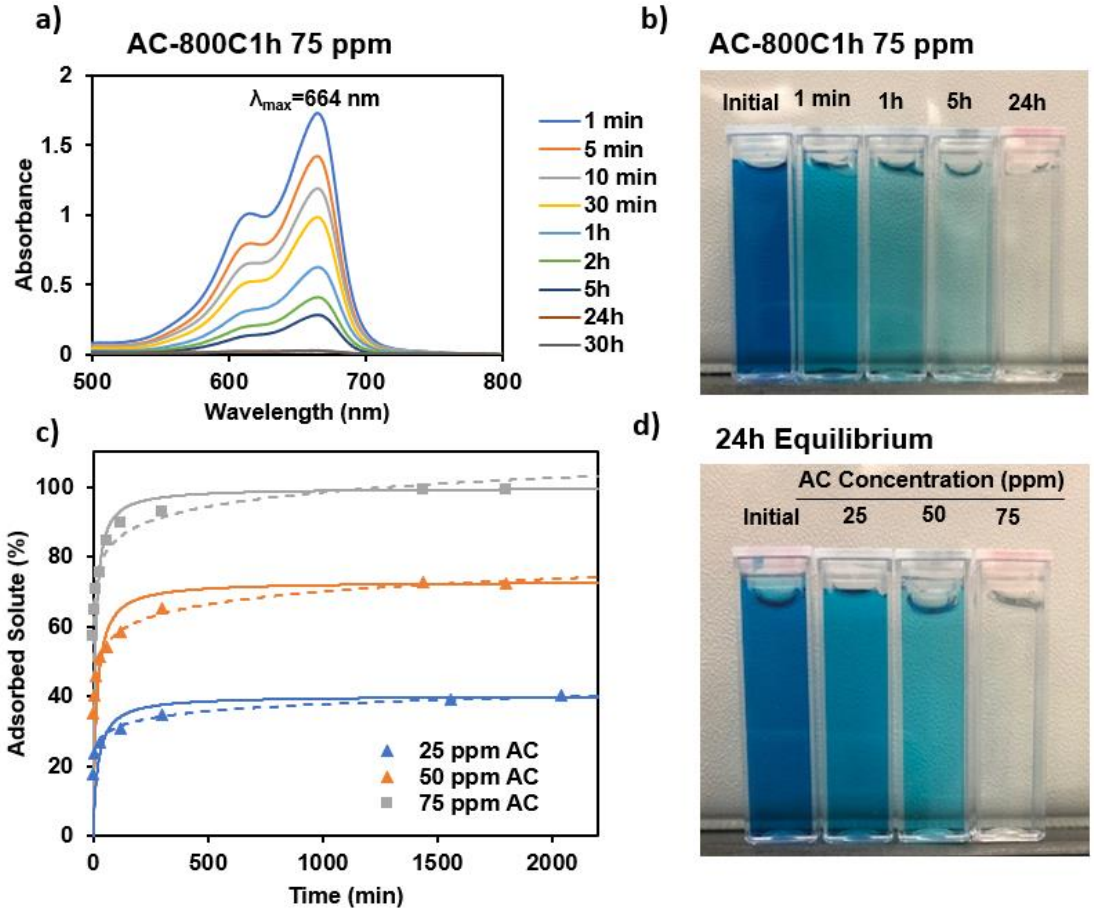

Figure 17: a) UV-vis Spectra of MB over time with 75mg/L AC-800C1h; b) MB solution over time after addition of 75 mg/L AC-800C1h; c) Percentage removal of MB using different AC concentrations over time with dotted lines representing Elovich model predictions and solid lines representing PSO model predictions; f) MB solutions after addition of different AC-800C1h concentrations after 24 h.

Table 12: Kinetic model parameters describing the adsorption of MB (25 mg/L solution) onto AC-800C1h (25 mg/L, 50 mg/L, 75 mg/L) based on regression of linearized data.

Kinetic models		Parameter*	Concentration of AC (mg/L)		
			25	50	75
Experimental		**q_e (mg/g)**	333.81	300.61	275.29
Pseudo First Order		**q_e (mg/g)**	147.14	119.68	81.760
		K_1 (g/mg/min)	0.00406	0.00502	0.00595
		R^2	0.906	0.909	0.826
Pseudo Second Order		**q_e (mg/g)**	334.21	303.31	276.59
		K_2 (g/mg/min)	0.000141	0.000223	0.000425
		h (mg/mg/min)	15.749	20.515	32.513
		R^2	0.999	0.999	0.999
Elovich		**a**	10293.363	12297.441	256671.053
		b	0.0413	0.0455	0.0606
		R^2	0.992	0.993	0.976
Intra-Particle Diffusion	**Stage 1**	**K_{int} (g/g/min)**	40.115	20.348	17.019
		C (mg/g)	105.286	124.004	141.925
		R^2	NA	0.992	0.999
	Stage 2	**K_{int} (g/g/min)**	6.042	5.504	7.132
		C (mg/g)	185.221	179.650	173.591
		R^2	0.991	0.970	0.972
	Stage 3	**K_{int} (g/g/min)**	1.697	1.269	0.844
		C (mg/g)	257.987	249.854	241.547
		R^2	0.998	0.960	0.973

*Correlation of parameters was not investigated and should be considered when applying these models to other data.

The last kinetic intraparticle diffusion model can exhibit three distinct stages: external diffusion, intraparticle diffusion, and slow equilibrium [165]. All three stages were reported in the adsorption of MB via bamboo-activated carbon, which was attributed to the strong electrostatic attraction of the dye to the adsorbent surface followed by the diffusion of dye into adsorbent pores, then the slow diffusion under low solute concentrations in the final stage [166]. As shown in **Figure 18c** these stages were also observed in this study for all AC concentrations.

The initial stage of external diffusion lasted up to 10 min for the two higher AC concentrations and only 5 min for the lowest concentration. The second stage lasted up to 5 h for the two lower AC concentrations and only 2 h for the highest concentration due to the solute being eliminated before the adsorbent reached its capacity. The intraparticle diffusion model fits very well with each stage, but the nonzero intercepts indicate that intraparticle diffusion was not the only rate-limiting step in each stage. This was also the case for bamboo-activated carbon adsorption [166] and may be due to the differences in mass transfer rate throughout adsorption [157]. The decreased mass transfer rate can be seen by the initial adsorption rate constant (h) based on the pseudo second order model (**Equation (22)**) [157]. As listed in **Table 12**, the K_2 values are much smaller than the initial adsorption rate constant which suggests that the adsorption proceeds much faster at the onset and slows over time [157]. Additionally, both rate constants increase with AC concentration due to the increased number of adsorption sites facilitating faster recovery.

$$h = K_2 q_e^2 \quad \textbf{(22)}$$

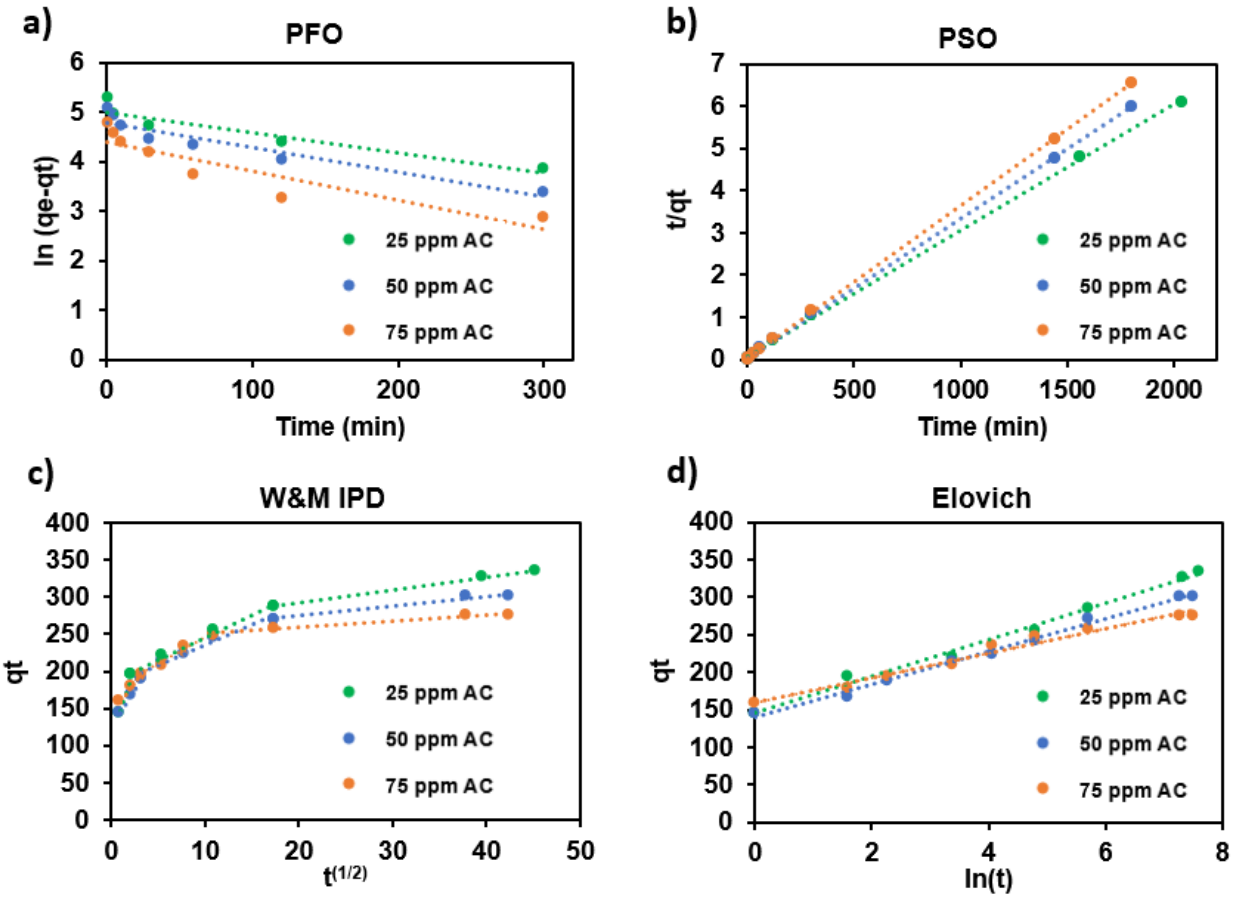

Figure 18: Linear modelling of MB adsorption kinetics onto AC-800C1h at various concentrations using a) PFO; b) PSO; c) M&W Intraparticle diffusion; and d) Elovich models.

3.3.8. Brillian green adsorption

AC-800C1h was also used to treat brilliant green (BG) dye, another commonly used cationic dye for paper printing and textile dying [167]. As shown in **Figure 19a,** the AC did not recover as much BG dye as MB dye at the same concentrations. At a loading of 50 mg/L AC the BG dye was adsorbed at an equilibrium capacity of 194 mg/g, while MB was adsorbed at 300 mg/g. BG followed the same adsorption kinetics as MB, with the kinetic parameters of the PSO and Elovich models listed in **Table 13**.

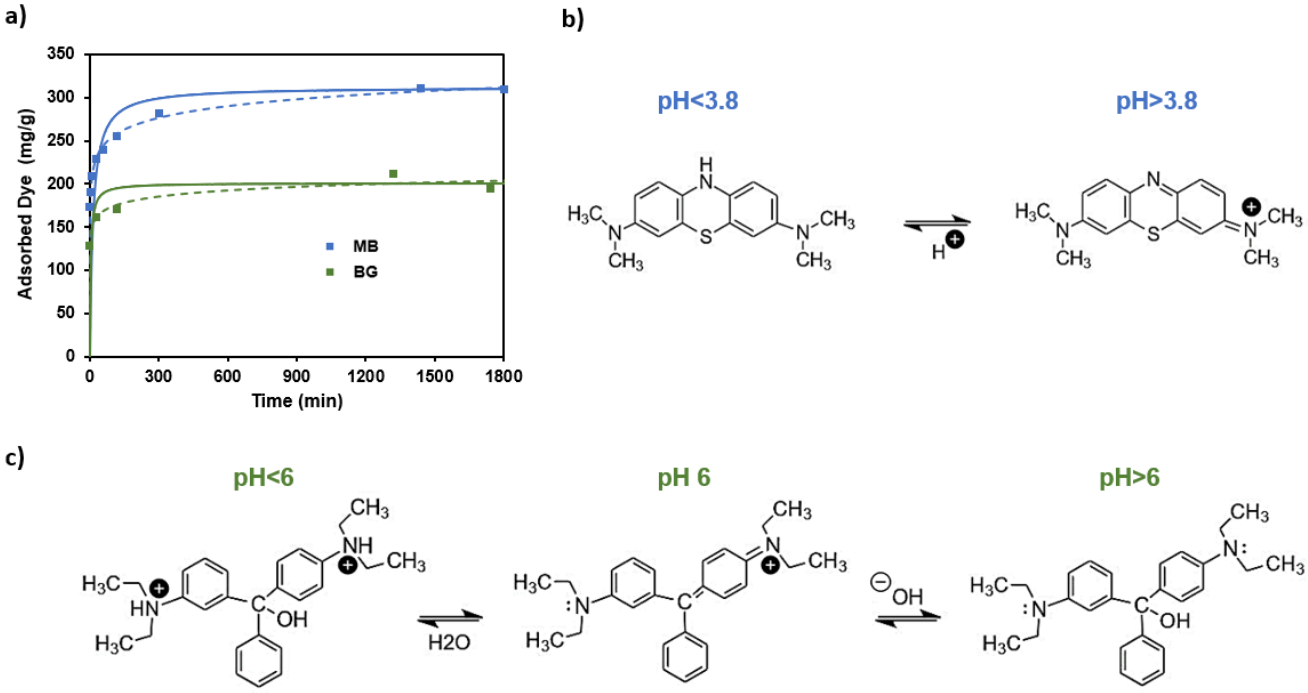

Figure 19: a) Adsorption of MB (25 mg/L pH 6) and BG (25 mg/L pH 7) onto AC-800C1h (50 mg/L) with solid lines representing PSO model prediction and dotted lines representing Elovich model prediction; b) Speciation of Methylene blue; and c) Brilliant green dye with respect to pH.

The differences in adsorption capability for the two dyes result from the difference in charge. As illustrated in **Figure 19c,** BG does not retain a positive charge for as wide a range as methylene blue (**Figure 19b**). The resonance diagram, which was adapted from Rao et al. [168] , indicates that the neutral resonance structure of BG becomes stable at pH values above 6. At the unadjusted adsorption pH of 7, the neutral form of BG is present because at this point a portion of the molecules have undergone reaction with OH^-. The analysis by Rao et al. [168] indicated that the mono-cationic form of BG is still present at the investigated pH values of 7 and 8, and in the opposite direction it does not entirely disappear until below pH 2. For the case of MB, the conversion to the cationic species occurs rapidly above pH 3.8, such that all species exist in this

form at the adsorption pH of 6. Therefore, the adsorption process facilitated by electrostatic attraction to the negatively charged carbon is more robust in the case of MB, leading to a 50% increase in dye recovery compared to BG at their natural pH values. Adjustment of the solution pH below 6 would help enhance the affinity of BG towards the activated carbon.

3.3.9. Methyl orange adsorption

To predict the performance of the AC within a mixture of textile wastewater containing both cationic and anionic dyes, adsorption tests were carried out on a mixture of Methyl Orange (MO) (10 mg/L) and MB (8 mg/L). MO was used as a representative anionic dye which is also applied in the textile, paper, food and cosmetic industries [169]. The UV-vis spectra and solution images of the mixture over time (**Figure 20**) indicate the strong selectivity of the AC towards the cationic MB dye. At an AC concentration of 50 mg/L 96% of the MB was adsorbed while only 31% of the MO was adsorbed after 22 h leaving behind a yellow-coloured solution from the initial green mixture. It should be noted that the AC still adsorbed a significant portion of the methyl orange despite the opposite charge, indicating that the adsorption process takes place through mechanisms other than electrostatic attraction.

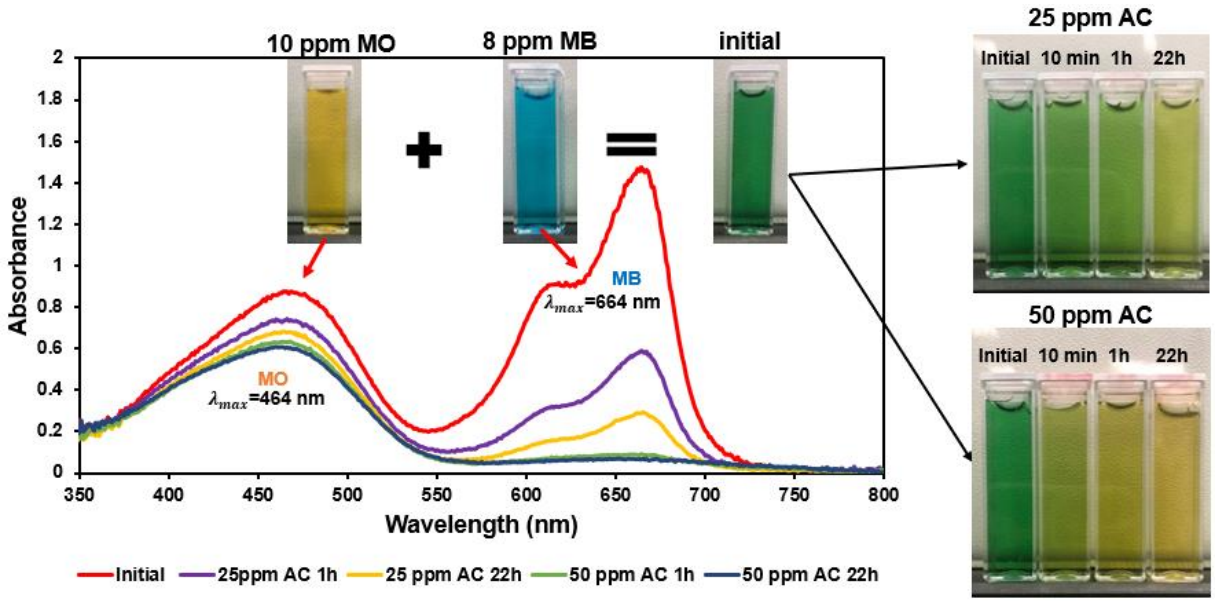

Figure 20: UV-vis spectra of a mixed dye solution (10 mg/L MO, 8 mg/L MB) over time after treatment with 25mg/L and 50mg/L AC-800C1h and corresponding solution images.

The kinetics of the dye mixture adsorption was also analyzed using the PSO and Elovich models, as shown in **Figure 21**. The kinetics of both MB and MO adsorption within the mixture are better described by the Elovich model except at the higher AC concentration, in which the MB adsorption follows the PSO kinetics more closely. This same observation was made in the previous MB study in which the PSO model was more accurate in describing the adsorption at the highest AC concentration, which reached equilibrium faster. Additionally, the PSO model was able to provide very accurate estimations of the equilibrium solute adsorption, as listed in **Table 13**. The overall recovery of dye from the mixture was 47.7% (25 mg/L AC) and 59.3% (50 mg/L AC), which is very good considering one of the dyes carries an opposite charge to the adsorbent. The MO adsorption accounted for 26.1% (25 mg/L AC) and 29.3% (50 mg/L AC) of the total dye recovery despite the greater amount present initially due to it having a much lower affinity toward the adsorbent. The results indicate that the AC favours the adsorption of cationic dyes as expected but can still recover a significant portion of oppositely charged dye.

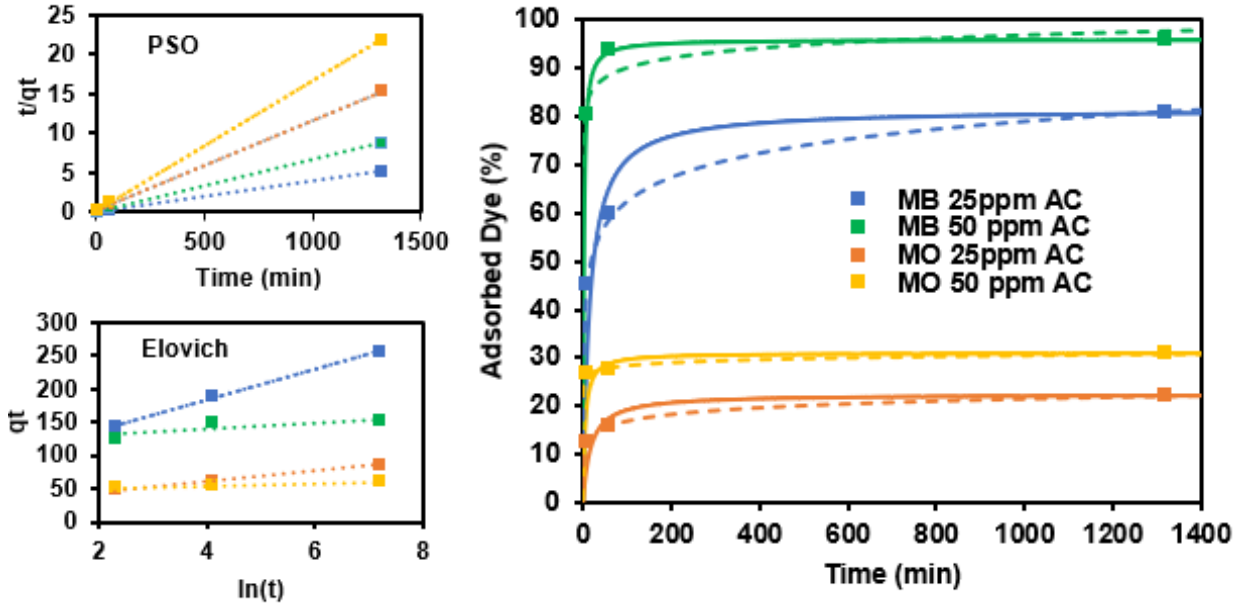

Figure 21: Linearized PSO and Elovich modelling of MB and MO adsorption onto AC-800C1h (25 mg/L and 50 mg/L) from a mixed dye solution and corresponding predictions of percentage removal over time. Solid lines represent PSO model predictions, dotted lines represent Elovich model predictions.

Table 13: Kinetic model parameters describing the adsorption of A) MB and MO dye within a mixture; and B) BG dye onto AC-800C1h based on regression of linearized data.

Kinetic models	Parameter*	A) Mixed Dye Solution				B) BG Solution
		MB (8 mg/L)		MO (10 mg/L)		(25 mg/L)
		AC Concentration (mg/L)				
		25	50	25	50	50
Experimental	**q_e (mg/g)**	243.28	144.56	86.73	60.47	194.74
Pseudo Second Order	**q_e (mg/g)**	247.83	145.88	87.81	60.67	201.05
	K_2 (g/mg/min)	0.000274	0.00407	0.000677	0.00359	0.00139
	R^2	0.999	0.999	0.999	0.999	0.997
Elovich	**a**	1296.153	9.48029×10^{11}	386.032	8.688×10^{11}	263.768×10^{4}
	b	0.0457	0.224	0.128	0.567	0.0982
	R^2	0.997	0.721	0.997	0.969	0.944

*Correlation of parameters was not investigated and should be considered when applying these models to other data.

3.4. Conclusions

Due to the significant need to reduce the growing amount of plastic water bottle waste entering landfills, the conversion of PET waste to activated carbon was optimized and validated for the treatment of dye-contaminated wastewater. The activation conditions required to produce an effective adsorbent of charged dye molecules was determined to be 800 ºC for 1 h based on conversion to carbon, surface area, surface charge, and yield. The resulting product with a yield of 25% exhibited a high surface area (1124 m^2/g) and negative zeta potential (-40 mV) leading to outstanding cationic dye recovery. Through the study of methylene blue dye adsorption (q_m = 335 mg/g) and subsequent comparison to cationic brilliant green and anionic methyl orange, the adsorption behaviour was found to be dependent on the type and speciation of the dye across various pH values. Despite this dependence on the dye chemistry, the adsorbent retains its affinity towards cationic dyes in a wide range of pH values, as indicated by its pH_{zc} of 3.7. Therefore, it has the potential to effectively recover a variety of cationic dyes using pH adjustments to enhance the charge characteristic of the dye. The high surface area of the product also enables it to adsorb a considerable amount of anionic dye, providing sufficient recoveries in dye mixtures. Overall, the charge characteristic and high surface area of the activated carbon produced from PET results in superior potential as an adsorbent of waste dyes from the textile industry. The product should be further investigated for applications in other similar industries requiring negatively charged adsorbents and can potentially become more economically appealing through improvements in process yield.

Chapter 4: Utilization of epoxy thermoset waste to produce activated carbon for the remediation of nano-plastic contaminated wastewater[3]

4.1. Introduction

Plastics continue to be produced and discarded at alarming rates, leading to a build-up of post-consumer waste. Over time, this waste not only persists in the environment but disintegrates into tiny particles called microplastics (MPs) and nano-plastic (NPs), which are highly mobile and have the potential to threaten the health of marine life [4]. These particles are also infiltrating freshwater and land environments due to human activities which introduce plastic debris into wastewater effluents. For example, laundering of synthetic clothing and common products such as exfoliants and toothpaste cause significant release of MPs into water systems. NPs can then be generated from further breakdown of MPs or directly release from exfoliating hygiene products, abrasive cleaning supplies and plastic powders for example [4].

The proposed size ranges for MPs and NPs are 1-1000 μm and 1-1000 nm, respectively [4,170]. While MPs can be treated relatively easily in wastewater treatment plants (WWTP), NPs are more likely to escape during filtration and settling operations, leading to surface water pollution [89]. As a result, WWTP effluents are a major source of plastic particles that end up in freshwater systems [171], eventually impacting drinking water sources as well [172]. Therefore, MPs and NPs pose a human health risk which is expected to be more severe in the case of NPs due to their smaller size [4]. NPs are capable of penetrating cell membranes and accumulating in any organism, which has been shown to cause a variety of health complications in marine

[3] A version of this chapter is published: Blanchard, R., Mekonnen, T., Separation and Purification Technology Volume 326, December 2023, 124755.

animals such as breaching of the blood-brain barrier in Japanese rice fish [173], and physiological and metabolic shifts in crucian carp [174].

The treatment of MP and NP-contaminated waters is primarily accomplished through conventional wastewater treatment plants (WWTPs) that utilize preliminary, primary, and secondary stages. In some cases, subsequent advanced treatments, such as ultrafiltration, reverse osmosis, or chemical disinfection, may be necessary [175]. For MPs, advanced treatments are necessary to achieve over 97% recovery [176]; However, the release of wastewater after the second stage allows MPs to persist in treated effluents[175]. Although some advanced treatments (ultrafiltration, ultracentrifugation) for NPs have shown efficiency rates of up to 99% based on a laboratory study [89], the feasibility and cost of implementing these techniques on a large scale must be considered. The use of advanced filtration, for example, requires high pressures, slow flow rates, and membrane regeneration [175].

Several methods have been investigated for the treatment of NPs and MPs that require modifications to typical WWTPs [177–179]. Of these technologies, activated carbon (AC) is particularly well-suited for NP recovery, due to its small-sized pores and ease of implementation. Consequently, AC and similar carbon adsorbents have been studied for the recovery of MPs within filters [93], as well as in continuous column studies [90–92]. However, when it comes to NPs, only a few studies have explored the use of carbon-based adsorbents, such as the batch adsorption charged poly(styrene) (PS) NPs using biochar [94,95] and granular activated carbon [96]. Additionally, NP studies are limited to commercially available PS, as it is difficult to detect and obtain NP debris for testing [180]. Therefore, there is a need to investigate the adsorption of other common plastics which do not carry a surface charge.

Consequently, this study has investigated the use of activated carbon for treatment of NP contaminated water by adsorption. A key aspect of this investigation involved the use of a cured epoxy waste feedstock to produce the AC product. The choice to produce AC from waste thermoset plastic is important to the study due to the environmental impacts of traditional AC production from fossil-based products and lack of investigation into thermoset plastic waste as a feedstock. While many common plastics have been explored in the literature because of their high carbon content and abundance [23,26,57,181,182], these technologies are often limited to thermoplastics, which can be recycled via thermomechanical processes. This study, therefore, seeks to investigate the utilization of cured epoxy waste, which is a very commonly used thermoset plastic containing cross-linked structures that cannot be conventionally recycled.

Epoxy is widely used in the matrix of composites, adhesives, coatings, and in electronic materials due to its excellent mechanical properties combined with thermal, chemical and electrical resistance [183]. However, most chemical recycling methods utilized to recover value from end-of-life epoxy waste lead to degraded material with significantly reduced value [184]. An alternative method for valorizing non-recyclable plastic waste is by pyrolysis to produce useful products such as fuels and oils [185], and when applied to epoxy resin can produce liquid products such as phenols and brominated organics along with gaseous CO_2, CH_4 and H_2 [186]. On the other hand, an AC product has potential to provide greater value due to its excellent surface properties and can not be obtained from pyrolysis alone, which yields non-porous solid residue [186]. Therefore, the activation of epoxy waste into a high surface area AC was investigated to upcycle this waste to a high valued product. This may also be achieved by activation of the spent chars derived from pyrolysis [187] [188]. However, this work proposes a direct method for producing AC from epoxy waste due to the increasing feedstock of

decommissioned epoxy waste requiring a disposal pathway. This buildup is especially influenced by the growing demand for clean energy and the application of epoxy thermosets in large scale wind turbines [189].

Existing research on the production of activated carbon (AC) from epoxy-based feedstock, has focused on the activation of the epoxy resin component from waste circuit boards using various activating agents [82,190–192]. In general, activation by chemical agents is advantageous compared to physical activation methods using steam or CO_2 due to lower processing temperatures, shorter processing times, higher carbon yields, and more developed surface areas [39]. Among the activating agents used, chemicals such as NaOH and KOH help to improve the product composition and promote new pore formation [193]. Specifically, potassium hydroxide (KOH) is known to be the most effective, producing high surface areas of up to 3000 m^2/g [44,194]. With respect to epoxy, there is a need to investigate and optimize the activation by KOH because, to the best of the authors' knowledge, there is no study investigating the production of AC from cured epoxy. While one study employed KOH as an activator for epoxy resin [82], it was also limited to one activation condition and used a costly two-stage carbonization/ activation process.

Therefore, a chemical activation process using KOH was investigated for the conversion of cured epoxy to AC. Additionally, other potassium containing activating agents were compared to KOH due to the known role of potassium (K) metal in the development of AC surface area and for the prospect of finding less harmful (toxic, corrosive) alternatives to KOH. At high temperature, potassium metal is produced during the activation process and intercalates into the carbon network to further facilitate pore formation [41]. Therefore, two other less toxic potassium compounds including potassium carbonate (K_2CO_3) and potassium Acetate (KOAc)

were compared to the KOH activating agent. Activation by K_2CO_3 has produced high surface areas above 1800 m^2/g in bamboo [195] and lignin feedstocks [196], which was superior to the performance of KOH reported in the latter study. KOAc is an ideal substitute because of its very low hazard rating [41], and has been reported as an effective activating agent in the synthesis of porous carbon from resol [197].

Overall, this study aims to explore the production of activated carbon (AC) from waste epoxy thermosets through a one-stage heating process, and to evaluate the AC product's ability to adsorb NPs in contaminated water. It therefore addresses the current research gaps associated with 1) the chemical activation of epoxy plastic [82,190–192] which have not focused on cured epoxy thermosets and 2) the adsorption of NPs onto carbon material which is limited to the investigation of charged PS particles [94–96]. The optimization of activation conditions was carried out by first comparing the performance of various potassium containing activating agents, then examining the impact of activation temperature and impregnation ratio of the superior activating agent. The AC product was then evaluated for its potential to adsorb polyethylene terephthalate (PET) NPs, which are among the most widely used thermoplastics in textiles, packaging, and containment [198]. As such, the study addresses two key ecological challenges simultaneously: the upcycling of epoxy thermosets into high surface area activated carbon and its utilization for the treatment of NP contaminated wastewater.

4.2. Materials and methods

4.2.1. Materials

Epoxy thermoset was produced using diglycidyl ether of bisphenol A (Araldite 506) and poly(propylene glycol) bis (2-aminopropyl ether) curing agent obtained from Sigma-Aldrich (Oakville, ON, Canada). Potassium hydroxide (KOH) (ACS reagent grade, ≥97%), hydrochloric

acid (HCl) (ACS reagent grade, 37%), trifluoroacetic acid (TFA) (≥99%), and potassium acetate (KOAc) crystals were all purchased from Sigma-Aldrich (Oakville, ON, Canada). Potassium carbonate (K_2CO_3) anhydrous was purchased from VWR Life Science, (Mississauga, ON, Canada). Used water bottles (Real Canadian Brand) were collected as the source of poly(ethylene terephthalate) (PET).

4.2.2. Methods

4.2.2.1. Preparation of AC

Epoxy resin was produced by mixing Araldite 506 with the curing agent poly(propylene glycol) bis (2-aminopropyl ether) in a mass ratio of 10:3. The mixture was homogenized at 7000 rpm for 2 min then cast onto silicone sheets. The resin was cured overnight at 60 ºC then post cured at 120 ºC for 2h. The cured resin was grinded (IKA MF 10 basic) to <1 mm particle size, then agitated within an aqueous solution containing a chemical activating agent at a predetermined impregnation ratio (mass of activating agent: epoxy) at room temperature for 1 h. The water was then boiled off by heating at 80 °C overnight followed by further heating at 110 ºC until completely dry. The activator coated epoxy was carbonized under nitrogen flow using a tube furnace (Thermo Scientific Lindberg/Blue M 18.4L B2 Moldatherm Box Furnace) by heating at 10 ºC/min to the final activation temperature and holding for 2h. After carbonization, the samples were washed with 1M HCl under agitation (400 rpm on a magnetic stir plate) for 1h at room temperature. The carbon was separated from the HCl solution by centrifugation (3500 rpm, 5 min) (Heraeus Megafuge 1.0 Centrifuge) and washed three times with deionized (DI) water. The final product was obtained after drying at 80 ºC overnight and grinding using a mortar and pestle.

An activator study was first conducted using KOH, K_2CO_3, and KOAc activating agents. For this study the samples were treated at an activation temperature of 800 ºC and an

impregnation ratio of 1:1. After choosing the best activator, the activation conditions were investigated using high and low levels of the activation temperature (600 ºC and 800 ºC) and the impregnation ratio (1:1 and 2:1). The samples were designated according to the format AC-**X**C-**YZ,** in which X refers to the activation temperature in Celsius, Y refers to the impregnation ratio, and Z refers to the activating agent as shown in **Table 18** (in the Appendix). An additional sample designated as 'control' was produced by heat treatment at 600 ºC in the absence of an activating agent.

4.2.2.2. Preparation of PET NPs

PET nanoparticles were synthesized based on a trifluoroacetic acid (TFA) precipitation method adapted from Rodriguez-Hernandez et. al. (2019) [199]. PET plastic waste was cut up and grinded (IKA MF 10 basic) to <1 mm particle size, then 50 mg of the powder was dissolved in 10 mL of a 90% (v/v) TFA solution in DI water. The solution was then added dropwise (~0.01 mL/drop) into 80 mL of DI water while agitating vigorously at 550 rpm. The precipitated PET was separated from the TFA solution by centrifugation then washed twice with DI water. It was then diluted with more DI water to an approximate concentration of 400 mg/L and sonicated for 20 min. The sonicated dispersion was further diluted to produce stock dispersions of 100 mg/L, 200 mg/L, and 350 mg/L concentrations.

4.2.2.3. Surface area analysis and yield of AC

The specific surface area of the AC was characterized by nitrogen adsorption at 77 K using a micromeritics ASAP 2020 Plus. The samples were first degassed at 300 ºC for 3 h under vacuum then analyzed based on five adsorptions data points in the relative pressure range of $0.005 \leq P/P^o \leq 0.05$. The surface areas were calculated by the equipment software using the BET (Brunauer–Emmett–Teller) method. The mass percentage yield for each activated carbon product

was calculated using **Equation (23),** in which m_E is the initial mass of cured epoxy , m_{AC} is the final mass of activated carbon recovered after the acid wash and drying procedure. For the control sample the value refers to the yield of char obtained after carbonization. Triplicate runs of the optimized product were used to estimate the percentage error in the yield for all AC samples, and the same was done for the control sample.

$$\%Yield = 100\ x \frac{m_{AC}}{m_E} \quad \textbf{(23)}$$

4.2.2.4. Spectroscopy analysis of AC

Fourier transform infrared spectroscopy (FTIR) analysis was conducted using KBr pellets. The KBr pellets were prepared by mixing 1 mg of AC sample with 200 mg of dried KBr powder and pressed with a pellet mold at 13,000 psi for 1.5 min. The pellets were then analyzed using a Thermo Scientific Nicolet 6700 with a pure KBr pellet as the background. An ATR component was attached for the measurement of pristine epoxy directly in grinded form by ATR FTIR using air as the background. Additionally, ATR FTIR was conducted for analysis of an AC sample before and after adsorption of NP, and for grinded PET such that the adsorption of PET NPs onto AC could be confirmed. Spectra were collected in the absorbance mode using 16 scans and an automatic baseline correction was applied to all spectra before plotting. For X-ray Photoelectric spectroscopy (XPS) analysis, AC samples were dried (48 h at 80 ºC) and the XPS spectra were collected using a ThermoVG ESCALAB 250 X-ray photoelectron spectrometer. The CasaXPS software was used to estimate the overall surface compositions of C, N and O based on the survey spectra, and to produce the deconvoluted peaks associated with the carbon spectra.

4.2.2.5. DLS analysis and SEM imaging

AC samples were prepared by sonicating mixtures of 1 mg/mL AC in DI water for 20 min. The samples were then analyzed using a Malvern Zetasizer Nano-series (Westborough, MA, United States) DLS to measure zeta potential using a folded capillary zeta potential cell (Zetasizer nano series, DTS 1061). Three scans of each sample were collected, and the averages were reported with standard deviation. SEM was conducted on AC samples using an Oxford Instruments Quanta FEG 250 Environmental SEM (Abingdon, UK) without any sputter coating. The supported energy dispersive X-Ray spectroscopy (EDX) was used to conduct elemental surface analysis and mapping of carbon and oxygen on the surface of one AC sample before and after adsorption of NPs to validate the presence of adsorbed PET NPs.

4.2.2.6. Characterization of PET NPs

DLS analysis of the NP dispersion was conducted by sonicating 20 mL of a 200 mg/L stock dispersion of NP for 10 min. For SEM analysis, the NP dispersion was prepared by sonicating 20 mL of a 200 mg/L stock dispersion for 10 min. One drop of the dispersion was then placed on a glass slide and the water was dabbed off using a paper towel. The glass slide was placed on top of a metal stub covered by carbon tape and was then imaged using an Oxford Instruments Quanta FEG 250 Environmental SEM (Abingdon, UK) without any sputter coating. Similarly, the NP dispersion was prepared for transmission electron microscopy (TEM) analysis by the same sonication procedure. One drop of the dispersion was placed on a 300 mesh carbon grid and dried under vacuum for an hour. Images were then taken using a Zeiss Libra 200MC TEM.

4.2.2.7. UV-vis spectroscopy

UV-Vis spectroscopy (Cary 300 Bio UV-Visible Spectrophotometer) was used to calculate the concentrations of NP dispersions. Sample spectra were obtained between 300 - 800

nm, and the absorbance at 400 nm was used to calculate NP concentration based on a fitted calibration equation (R^2=0.999). The calibration curve was produced by preparing a 400 mg/L stock solution of NPs and diluting to form a range of concentrations. The UV-vis spectra were collected for all samples after sonicating for 10 min, and the absorbances values at 400 nm were correlated to the known concentrations. For each sample, two spectra were collected by rotating the cuvette due to the main source of error being the noise affecting the low signal spectra. The average of the two runs were used to calculate concentrations and standard deviations, which were propagated to determine the error in adsorption and percentage recovery. The calibration curve and all raw UV-vis data can be found in the Appendix (**Figure 38**).

4.2.2.8. NP adsorption kinetics

An adsorption test was carried out in a batch size of 200 mL using an initial NP concentration of 250 mg/L. The NP dispersion was first sonicated for 10 min, then the exact initial concentration was measured by UV-vis spectroscopy. Next, the AC (100 mg) was added to the NP dispersion and the mixture was stirred at 400 rpm for 29 h during which 5 mL samples were collected over time. The samples were passed through a syringe equipped with a 20-micron filter to separate the AC, and the NP concentration in the filtrate was measured by UV-Vis spectroscopy. The adsorption (mg NP/g AC) was determined over time according to **Equation (24)** in which C_0 (mg/L) is the initial NP concentration, C_t (mg/L) is the NP concentration at time t (min), m (g) is the mass of AC used, and V (L) is the batch volume. Additionally, the NP percentage recovery was calculated according to **Equation (25)** and plotted over time.

$$q_t = \frac{(C_0 - C_t)V}{m} \quad \textbf{(24)}$$

$$\%\ Recovery = 100\ x\left(1 - \frac{C_t}{C_0}\right) \quad \textbf{(25)}$$

Pseudo First Order (PFO), Pseudo Second Order (PSO), Weber and Morris (W&M) intraparticle diffusion (IPD), and Elovich kinetic models (**Equations (14) - (17)**) were fitted to the data using linear regression. The resulting kinetic parameters were also obtained by non-linear regression for confirmation.

4.2.2.9. NP adsorption isotherm

Adsorption tests were carried out in batch sizes of 20 mL using initial NP concentrations of 100 mg/L, 200 mg/L and 350 mg/L. For each run, the NP dispersion was sonicated for 10 min, then the exact initial concentration was measured by UV-vis spectroscopy. Next, AC (2.5 mg, 5 mg, 10 mg, 15 mg, and 25 mg) was added to the dispersion and the mixture was stirred at 400 rpm for 20 h. After treatment, the mixture was passed through a 20-micron filter by vacuum filtration to separate the AC, and the NP concentration in the filtrate was measured by UV-Vis spectroscopy. For each run the adsorption (mg NP/g AC) and NP percentage recovery were determined according to **Equation (26)** and **Equation (27)** in which C_e (mg/L) is the equilibrium NP concentration.

$$q_e = \frac{(C_e - C_t)V}{m} \quad \textbf{(26)}$$

$$\%\ Recovery = 100\ x\left(1 - \frac{C_e}{C_0}\right) \quad \textbf{(27)}$$

The Brunauer-Emmett-Teller (BET) adsorption isotherm model was then fitted to the experimental data by non-linear regression. This model developed by Brunauer et. al. (1938) [200] is a very widely known physical adsorption isotherm that can describe various phenomenon such as monolayer and multilayer filling. Due to its capabilities, it is well known for its application in surface area calculations of various materials. It was originally developed to describe adsorption of gases, but it has been adapted for application in liquid phase systems

[201]. This version of the isotherm model (**Equation (28)**) is defined by the adsorption equilibrium parameter for the first layer K_{BET1} (L/mg), the adsorption equilibrium parameter for upper layers K_{BET2} (L/mg), and the BET monolayer adsorption capacity q_{mBET} (mg/g) [87].

$$q_e = q_{mBET} \frac{K_{BET1} C_e}{(1 - K_{BET2} C_e)(1 - K_{BET2} C_e + K_{BET2} C_e)} \quad \textbf{(28)}$$

The Aranovich model (**Equation (29)**) developed by Aranovich (1992) [202] was also applied to the adsorption isotherm data. The Aranovich model is another physical adsorption isotherm known to describe multilayer adsorption and is intended to model adsorption over broader adsorbate concentrations. It contains three parameters which are the Aranovich constant C_A (mg/L), the adsorbate monolayer saturation concentration C_{sA} (mg/L), and the Aranovich monolayer adsorption capacity q_{mA} (mg/g) [87].

$$q_e = \frac{q_{mA} C_A \left(\frac{C_e}{C_A}\right)}{\left(1 - \left(\frac{C_e}{C_A}\right)\right)^{0.5} \left(1 + C_A \left(\frac{C_e}{C_A}\right)\right)} \quad \textbf{(29)}$$

Additionally, the equilibrium data was modelled by the AD-Langmuir isotherm model developed by Aranovich and Donohue (1995) [203]. This model, intended for multilayer adsorption of gas molecules, uses two additional parameters to extend the Langmuir monolayer isotherm for the modelling of multilayer filling [204]. In this work it was adapted to describe liquid phase adsorption by expressing the isotherm equation in terms of concentration rather than pressure. The resulting version of the AD-Langmuir model is described by **Equation (30)** based on the AD model parameters including the adsorbate saturation concentration C_{sAD} (mg/L) and the AD exponent n, in addition to the Langmuir model parameters including the Langmuir constant K_L (L/mg) and the Langmuir monolayer adsorption capacity q_{mL} (mg/g).

$$q_e = \frac{\frac{q_{mL} K_L C_e}{1 + K_L C_e}}{\left(1 - \frac{C_e}{C_{sAD}}\right)^{n_{AD}}} \quad \textbf{(30)}$$

Lastly, the Frenkel-Halsey-Hill (FHH) model for multilayer adsorption was used to describe the equilibrium data. This model is also intended to describe adsorption of gas molecules but was adapted to describe liquid phase adsorption. The resulting version of the FHH model (**Equation (31)**) is defined by the constant K_{FHH} (mg/g), index n_{FHH}, and the adsorbate saturation concentration C_{sFHH} (mg/L) [203].

$$q_e = \frac{K_{FHH}}{\left(\ln\left(\frac{C_{sFHH}}{C_e}\right)\right)^{n_{FHH}}} \quad \textbf{(31)}$$

4.3. Results and discussion

4.3.1. Activation by K compounds

In the first study on epoxy activation, the effectiveness of potassium hydroxide (KOH), potassium carbonate (K_2CO_3), and potassium acetate (KOAc) activating agents was compared. One of the main performance indicators used to assess the ACs is the BET surface area because of its known correlation with the amount of material which can be adsorbed [205]. All activating agents caused a significant increase in BET surface area, from 52 m^2/g in the carbonized epoxy (control) to above 1000 m^2/g (**Figure 22a**). The sample AC-800C-1K_2CO_3 exhibited the highest surface area (1844 m^2/g) due to the thermal stability of K_2CO_3, which enabled direct activation solely at high temperature. On the other hand, KOH first decomposes into K_2O and K_2CO_3 (**Equations (32)-(33)**), which then participate in activation reactions above 700 °C (**Equations (34)-(35)**) [196]. While some activation occurs through the release of H_2O and CO_2 at low temperature [43], the decomposition products of KOH react directly with carbon at high

temperature (**Figure 23a**). In a study of AC production from lignin, the superior surface area produced using K_2CO_3 (1803 m^2/g) compared to KOH (1562 m^2/g) was also attributed to K_2CO_3 being the effective activating agent at high temperature [196].

$$2KOH \rightarrow K_2O + H_2O \quad \textbf{(32)}$$

$$K_2O + CO_2 \rightarrow K_2CO_3 \quad \textbf{(33)}$$

$$K_2CO_3 + 2C \rightarrow 2K + 3CO \quad (> 700^oC) \quad \textbf{(34)}$$

$$K_2O + C \rightarrow 2K + CO \quad (> 700^oC) \quad \textbf{(35)}$$

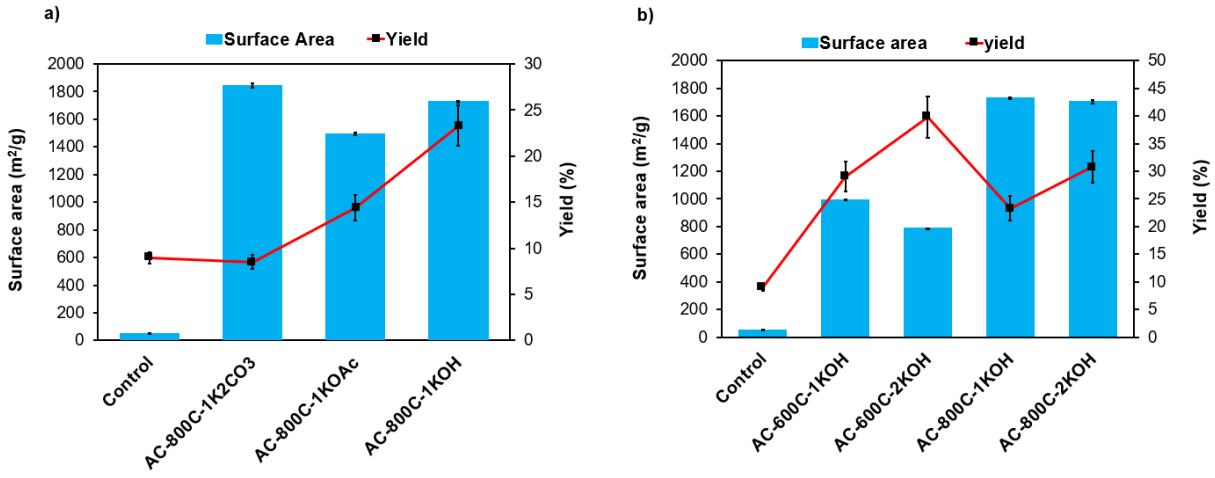

Figure 22: a) Comparison of BET surface area and yield of ACs produced using different K-containing activating agents, and b) using KOH under various activation conditions. See the Appendix (**Table 19**, **Table 20**) for tabulated values.

Similarly, the surface area of AC-800C-1KOAc (1495 m^2/g) was less than that of AC-800C-1 K_2CO_3 due to KOAc first decomposing into K_2CO_3 (**Equation (36)**) at around 303 °C before activation [197]. Still, KOAc was able to achieve a high surface area and could potentially provide value in some applications as a less corrosive alternative to KOH. It was also reported to produce a high surface area (1201 m^2/g) in the activation of resol (3:1 impregnation ratio) at 800 °C [197].

$$CH_3COOK \rightarrow CO_2 + K_2CO_3 \quad (303^oC) \qquad \textbf{(36)}$$

During the thermal decomposition of bisphenol A diglycidyl ether (DGEBA) epoxy, there is a significant release of bisphenol A (BPA), among other volatile molecules, as illustrated in **Figure 23b** [206]. Typically, the bonds between epoxy monomer units are weaker than those within them, leading to the predominant release of BPA molecules at temperatures below 600 °C [207]. The introduction of KOH may suppress the release of fragmented decomposition products, such as BPA, through the formation of more stable compounds. This results in the observed reduction in epoxy volatilization. A similar effect on yield was observed during the activation of PE with KOH, in which the yield increased with elevated activation conditions [47]. The study also reported an opposite trend in yield in the absence of KOH, indicating that the effect was a result of the interaction with KOH.

a)

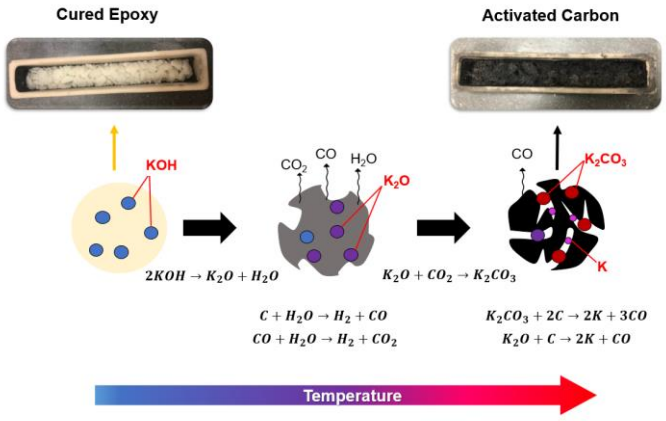

b)

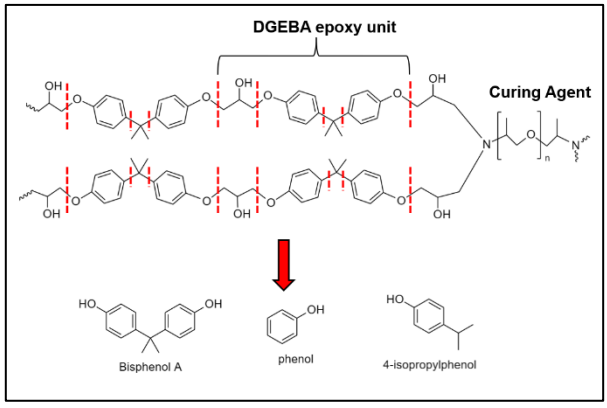

Figure 23: a) Schematic of the KOH activation of epoxy (low temperature activation reactions referenced from [44] and high temperature activation reactions referenced from [43]), and b) Illustration of a main epoxy thermal degradation pathway [207].

The use of KOAc as an activating agent also resulted in an improved yield (14.4%), although not to the same extent as the more reactive KOH activator. Both activating agents still produced a higher yield compared to K_2CO_3, which is a much less reactive and more thermally stable. For comparison, K_2CO_3 melts at 891 ºC and decomposes above 1200 ºC while KOH melts at 380 ºC and decomposes at 769 ºC [208]. Although these transition temperatures are reduced after impregnation onto AC [208], K_2CO_3 still does not interact with AC until very high temperature is achieved. This means that carbon consumption by activation occurs after complete carbonization, resulting in a lower yield (8.55%) than that of the control. Therefore, KOH is the superior activating agent when considering yield and was further investigated in the following section. Tabulated yield and surface area data for the activator study can be found in the Appendices (**Table 19**).

Although it is known that KOH is an effective activating agent for producing high surface areas in activated carbon, its effect on yield is not often reported. This is a very important consideration because not only does increased yield improve the economic feasibility of the process, but it also corresponds with the suppression of gaseous emissions. Therefore, there is an environmental benefit of using KOH despite the hazards associated with its use (toxic, corrosive). More work is required to fully understand the mechanism of yield increase and potentially investigate less harmful alternatives to KOH which show similar effect on activated carbon yield.

4.3.2. Activation by KOH

The main observation of the KOH activation study is that temperature has a significant impact on the BET surface area, with values increasing from below 1000 m^2/g at 600 ºC to above 1700 m^2/g at 800 ºC (**Figure 22b**). This can be attributed to the effectiveness of the high-temperature activation reactions (**Equations (34)-(35)**), which cause extensive pore development. Furthermore, at temperatures above 700 ºC, the formation of potassium metal further facilitates pore development by intercalating into the carbon network and causing expansion (**Figure 2a**) [43]. Still, there was significant activation occurring at 600 ºC as evident by the increases in surface area from 52 m^2/g in the control to 788 m^2/g and 996m^2/g. At this temperature the porosity is developed through physical activation by H_2O and CO_2 rather than by redox reactions of the potassium compounds [43]. Therefore, the dehydration of KOH (**Equation (32)**) and the subsequent water-gas reaction (**Equation (37)**) and water-gas shift reaction (**Equation (38)**) occurring below 700 ºC [44] contribute greatly to pore development despite the superior activation at 800 ºC.

$$C + H_2O \rightarrow H_2 + CO \quad \textbf{(37)}$$

$$CO + H_2O \rightarrow H_2 + CO_2 \quad \textbf{(38)}$$

A comparison of the maximum surface area sample (AC-800C-1KOH) with other ACs produced by KOH activation of plastic feedstocks is presented in **Table 14**. The surface areas were contextualized by comparison to the typical surface areas of commercial products (500-1500 m^2/g). Evidently, the ACs obtained from epoxy and other plastic feedstocks meet or exceed that of commercial ACs, so the epoxy AC is expected to possess a comparable capacity to these commercial products. The key distinction which incentivizes the epoxy AC and was the

motivation for this activation study, is the environmental impact of utilizing a non-recyclable waste plastic feedstock.

Table 14: Comparison of BET surface areas achieved through KOH activation of various plastic feedstocks.

Feedstock	Pre-treatment	KOH impregnation ratio	Activation conditions	BET Surface Area (m^2/g)	Reference
Cured Epoxy	-	1	800 °C 2 h	1728	This study
Commercial products	-	-	-	500-1500	[38]
Epoxy Resin	Carbonization	3	800 °C 1 h	2572	[82]
PET	-	1	800 °C 2 h	1215	[57]
PVC	Oxidation	3	800 °C 2 h	2507	[49]
PE	Sulfonation	3	900 °C	1803	[47]
PS foam	Carbonization	4	800 °C 1 h	2712	[52]
Tires	-	4	800 °C	411	[209]

When comparing the BET surface areas of ACs obtained from cured epoxy to other plastic precursors (**Table 14**), it was observed that most plastic feedstocks necessitate pre-treatment to achieve higher surface areas than observed in this study. However, epoxy activation proved to be an effective one-step process, as it does not require oxidation due to the composition of epoxy, and the KOH treatment during carbonization helps restore the carbon yield. While a previous study on epoxy resin activation reported a higher surface area of 2572 m^2/g [82], they utilized a two-step process that incurs higher costs in terms of processing time and low yield of the carbonization step. In contrast, the simultaneous carbonization and activation process used in this study improved the yield while still achieving a maximum surface area of 1728 m^2/g.

Increasing the KOH impregnation ratio was observed to decrease the BET surface area (**Figure 22b**), which can be explained by the inverse relationship between yield and pore development [41]. This relationship between yield and surface area has been observed in the KOH activation of PE as well, where yield increased as surface area decreased with respect to temperature [47].The decrease in surface area with respect to KOH impregnation ratio was much more pronounced at the lower activation temperature (600 ^{o}C) because the associated suppression of gaseous carbonization products may have hindered the physical activation which dominates at lower temperatures (**Figure 23a**). At the higher activation temperature (800 °C), the resulting decrease in surface area was not as significant (~23 m^2/g), so the effect of KOH on yield is more consequential to the high temperature conversion process.

The positive impact of KOH on the yield was further demonstrated by the increase associated with the impregnation ratio (**Figure 22b**). On the other hand, decreasing yield was observed with respect to activation temperature due to the increased effect of pore-forming reactions [41]. As activation at 800 °C is necessary to develop surface areas above 1700 m^2/g, an impregnation ratio of 2:1 should be used to mitigate the loss in yield. Consequently, the product AC-800C-2KOH was deemed optimal based on both surface area and yield. For a tabulated account of yield and surface area data for the KOH activation study, please refer to **Table 20** in the Appendices. Future work is required to further optimize the conversion process by investigation of a wider range of activation conditions. For example, it would be worthwhile to investigate further increases in the yield of activated carbon to ensure that the conversion process is economically feasible.

4.3.3. FTIR analysis

The degradation of epoxy resin was confirmed by the conversion of characteristic epoxy peaks into a broad AC spectrum (**Figure 24**). The pristine epoxy featured distinct DGEBA peaks, such as the oxirane group C-O-C (823 cm^{-1}), oxirane group C-O stretching (936 cm^{-1}), aromatic ring C=C stretching (1600 cm-1), ether C-O-C stretching (1040 cm-1), and C-H stretching (2870-2960 cm^{-1}) [43]. In the control sample, the visible peaks at 2870-2960 cm^{-1} indicated the presence of aliphatic C-H after carbonization. These peaks almost fully disappeared in the ACs treated by KOH due to their conversion to more stable aromatic bonds, which is known to occur during thermal decomposition at high temperature [210]. This evidence suggests that interactions with KOH facilitated the formation of an aromatic structure during decomposition.

The ACs exhibited peaks at 1700 cm^{-1}, 1600 cm^{-1}, and 1420 cm^{-1}, along with a broad peak centered at 1090 cm^{-1}. These peaks were attributed to COOH [47,82], C=C (1600 cm^{-1} and 1420 cm^{-1}) [186,211], and the general C-O bond group [211]. The broad C-O peak suggests the presence of oxygen from various functional groups. In aromatic carbon materials, the C-O peak at 1090 cm^{-1} may indicate the presence of hydroxyl (1000-1220 cm^{-1}), carboxylic acid (1120-1200 cm^{-1}), or lactone (1160-1370 cm^{-1}) groups [212]. However, the presence of COOH and OH can be confirmed based on the carboxyl peak at 1700 cm^{-1} and the broad hydroxyl peak at 3400 cm^{-1} [213,214].

The incorporation of oxygen in the form of OH is known to be affected by KOH activation according to **Equation (39)**, which may also extend to the formation of COOH based on the increased carboxylic peak in the ACs compared to the control. However, the surface functional groups are not entirely due to KOH activation, as indicated by the presence of hydroxyl groups in the control sample. In the pyrolysis of epoxy resin from waste circuit boards,

the pyrolysis char was also found to be rich in functional groups such as OH and C=O in addition to C=C bonds from benzene ring backbones [186]. Overall, the FTIR results indicated the presence of oxygen containing functional groups in the control and KOH activated ACs in addition to the aromatic structure of the ACs. Although COOH and OH bonds were confirmed, the presence of other oxygen containing functionalities were unclear due to overlapping peak locations. Therefore, the surface structure is further analyzed by XPS in the subsequent section to identify all surface bond types and their trends with respect to activation conditions.

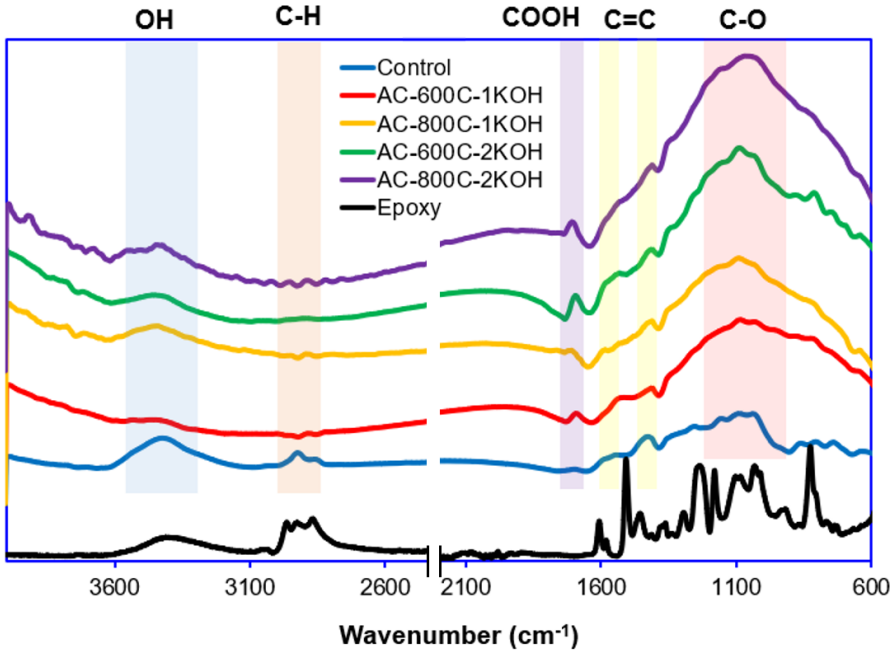

Figure 24: FTIR spectra of ACs produced by KOH activation of cured epoxy at various conditions.

4.3.4. XPS analysis

XPS analysis was carried out to investigate the presence of oxygen-containing bonds on the surface of the ACs, which can affect their polarity as an adsorbent material. The deconvoluted carbon spectra (**Figure 25a**) revealed four peaks at binding energies of 284.6-284.9 eV, 285.8-286.0 eV, 288.6-288.9 eV, and 290.4-291.9 eV. These peaks were assigned based

on the relative peak locations reported for commercial ACs as C-C/C-H, C-O (hydroxyl or ether), C=O, and O-C=O (carboxyl or ester), respectively [215]. The C-C peak was specifically identified as predominantly C=C in this study based on its alignment with the aromatic carbon bond typically located at 284.5 eV [212].

The contribution of each carbon bond type to the overall carbon peak was quantified and is presented in **Figure 25b**. Based on the 9% decrease in C=C/C-H proportion in AC-600C-1KOH compared to the control, there is indication that KOH may facilitate the development of surface functional groups on the AC. According to **Equation (39)**, KOH can react with carbon to form C-O-K groups, which later transform into OH groups after the washing step [145]. This effect of KOH was also observed during the activation of PET, where the oxygen content increased from 18.99% to 34.33% by increasing the KOH impregnation ratio from 1 to 3 [76]. The surface atomic compositions of the synthesized epoxy ACs were also estimated (**Figure 26b**) based on the XPS survey spectra (**Figure 26a**), indicating increased oxygen content in the activated samples (13.3-19.1%) compared to the control (10.6%).

$$K_2O + R \rightarrow K + R - O - K \xrightarrow{H_2O\ wash} R - OH \quad \textbf{(39)}$$

a)

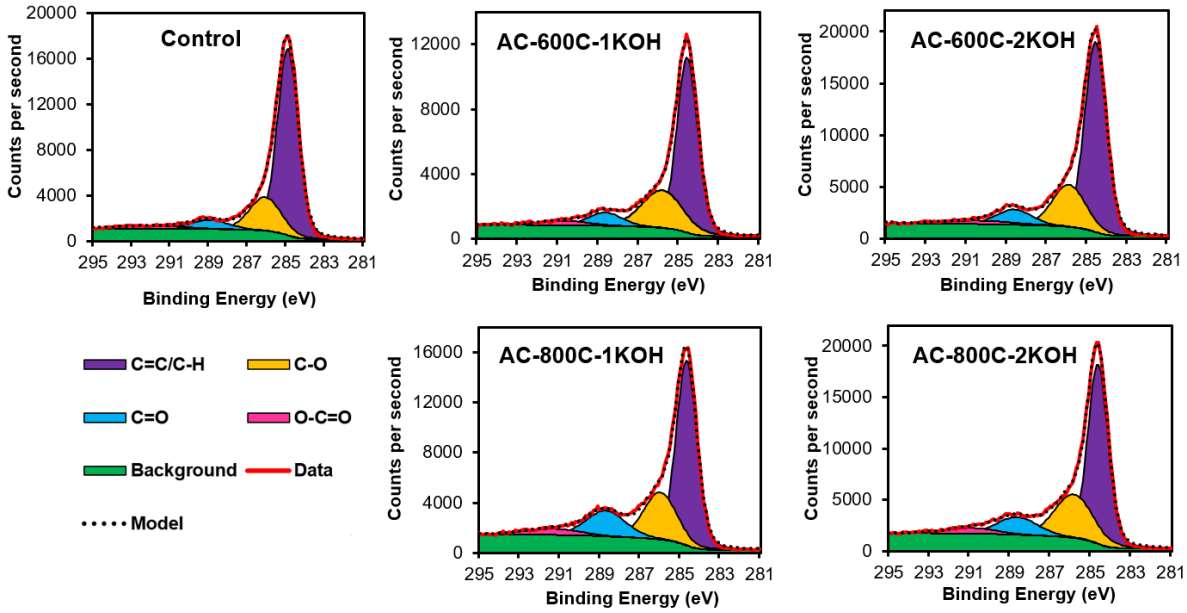

b)

Sample	Surface carbon bond Composition (%)			
	C=C/C-H	C-O	C=O	O-C=O
Control	71.35	19.42	6.07	3.16
AC-600C-1KOH	62.32	26.55	7.63	3.5
AC-600C-2KOH	65.27	22.2	8.56	3.97
AC-800C-1KOH	57.48	22.77	14.9	4.85
AC-800C-2KOH	57.75	26.44	11.44	4.36

Figure 25: a) Deconvoluted XPS carbon spectra of ACs produced by KOH activation of cured epoxy at various conditions and b) the corresponding estimates of carbon bond composition.

The changes in surface functional groups through activation were also observed based on the composition of carbon bond types (**Figure 25b**). Although C-O bonds represent the majority of oxygen bonds, there were also increases in other bond types as a result of KOH activation. The higher O-C=O composition supports the indication from FTIR that carboxyl groups may also be imparted by KOH. The composition of O-C=O is small in all samples, but it is much

more apparent in the ACs activated at the higher temperature of 800 ºC (**Figure 25a**). In terms of the activation conditions, the proportion of oxygen containing functionalities increased at a higher activation temperature (800 ºC) while the KOH impregnation ratio did not have a significant effect. Therefore, the selection of AC-800C-2KOH as the optimal sample was further supported by the increase in oxygen containing functional groups achieved through activation at 800 °C.

a)

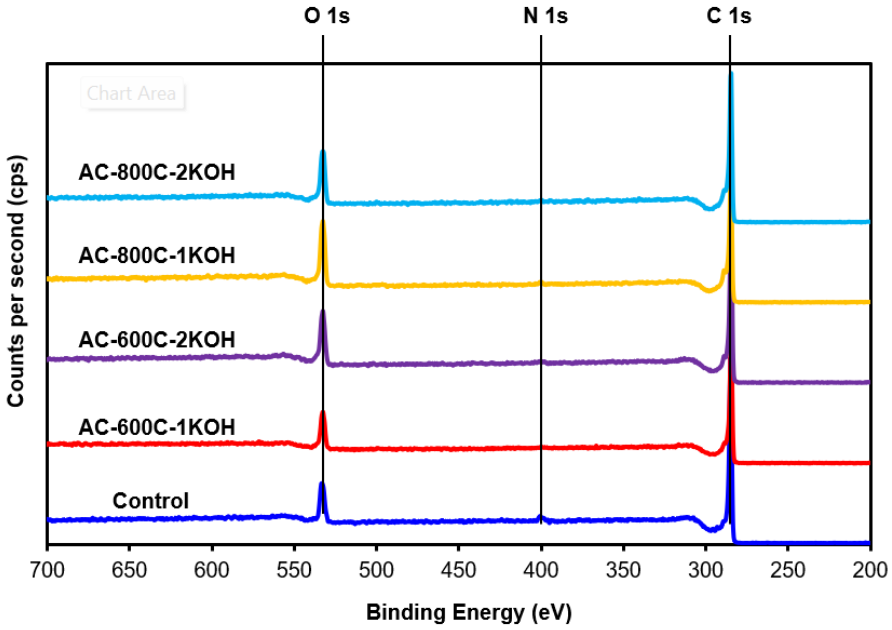

b)

Sample	Surface atomic composition (%)		
	Oxygen	Carbon	Nitrogen
Control	10.61	87.62	1.76
AC-600C-1KOH	13.3	86.7	-
AC-600C-2KOH	15.5	84.5	-
AC-800C-1KOH	19.13	80.17	0.7
AC-800C-2KOH	15.24	84.76	-

Figure 26: a) XPS survey spectra of Acs produced by KOH activation of cured epoxy at various conditions and b) the corresponding atomic composition estimates.

The increased oxygen content in the ACs will likely enhance the affinity of the carbon towards organic solutes due to the imparted surface polarity [145]. Additionally, the negative

surface charges of all ACs (< -30 mV) determined by zeta potential measurements (**Figure 27a**), suggest the presence of acidic OH and COOH surface groups. The zeta potential of the ACs is fully analyzed in the following section.

4.3.5. Zeta potential

The zeta potential of the ACs (**Figure 27a**) was measured to further investigate the surface chemistry based on electrostatic charge. The KOH activation was expected to influence the surface charge through the introduction of oxygen groups. Because this charge characteristic is affected by pH, it is often expressed in terms of surface acidity or basicity, quantified by the point of zero charges (PZC). The PZC refers to the pH above which the surface charge is positive and below which the surface charge is negative [216]. The high proportion of acidic surface groups causes a PZC below 7, while predominantly basic surface groups increase the PZC above 7 [217]. Therefore, in a system at neutral pH an acidic AC surface would correlate with a negative net charge, while a basic surface would result in a positive net charge.

The acidic nature of AC is imparted by functional groups such as carboxylic acids and phenol groups due to the deprotonation of the hydroxyl group [217,218] (**Figure 27b**). The negative charge is then generated on the deprotonated oxygen as expressed in **Equations (40)-(41)**[147]. Therefore, the negative zeta potential exhibited by the control (-45 mV) indicates the acidic hydroxyl groups, which comprise the majority of the oxygen bond types (C-O). However, it is likely that the carboxyl groups contribute more to the negative charge (**Equation (40)**) due to their lower pKa. Although the oxygen groups increased with KOH activation based on XPS, the zeta potential did not change significantly after activation at 600 ºC and even became less negative after activation at 800 ºC. This is due to the increasing content of basic functionalities along with the acidic hydroxyl-containing groups.

$$R - COOH \rightarrow R - COO^- + H^+ \quad \textbf{(40)}$$

$$R - OH \rightarrow R - O^- + H^+ \quad \textbf{(41)}$$

One of the features causing surface basicity in carbon is functional groups, such as N-containing groups, ketones, and pyrones [218]. Therefore, the increase in the more basic C=O groups indicated by XPS is likely limiting the development of a negative charge. It has been suggested that the basicity of carbonyl-containing groups like pyrones is significant when existing across a double ring [219] as shown in **Figure 27b**. The occurrence of such groups in the ACs is a possibility, given the variety of surface oxygen bonds observed. Another cause of surface basicity is delocalized pi electrons of the aromatic structure, which can attract positive hydrogen ions to the surface (**Figure 27b**) [218]. This phenomenon is a major contributor to the basic nature of ACs due to the high proportion of aromatic carbon compared to other functional groups [217]. Therefore, the trend towards less negative zeta potentials with elevated activation conditions may result from a combination of aromatization and increases in basic groups like pyrones.

Overall, the negative zeta potentials exhibited by all samples confirm the presence of acidic functional groups such as COOH and OH. Additionally, the trend in zeta potential indicates the presence of basic groups in addition to acidic groups. Therefore, the FTIR, XPS and zeta potential results all indicate the abundance of various types of oxygen-containing groups, which may improve the interaction of the AC with solute molecules. However, further studies are required to confirm the effect of oxygen content at various levels on NP adsorption.

a)

Sample	Zeta potential (mV)
Control	-44.93 ±0.90
AC-600C-1KOH	-46.73 ±1.60
AC-600C-2KOH	-46.17 ±2.02
AC-800C-1KOH	-40.30 ±0.98
AC-800C-2KOH	-33.77 ±0.32

b)

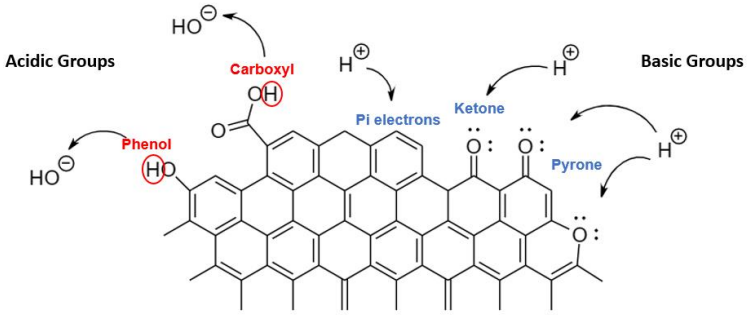

Figure 27: a) Comparison of ACs produced by KOH activation at various conditions, and b) illustration of the acidic and basic groups expected on the AC surface [219].

4.3.6. SEM imaging

The SEM images of the epoxy ACs (**Figure 28**) confirmed their highly porous structure compared to the carbonized epoxy control, which exhibited a completely smooth surface due to the absence of activation by KOH. Furthermore, the ACs activated at 800°C exhibit smaller particle and pore sizes, consistent with the increase in BET surface area with increasing activation temperature (**Figure 22b**). The SEM images also confirmed the general magnitude of pore sizes which dictates the size of molecules that can be adsorbed. At higher magnification, the optimal sample AC-800C-2KOH shows the presence of micron sized pores (**Figure 28f**), which can effectively accommodate the targeted nano-sized plastic particles. Overall, the BET surface areas confirmed that the ACs have a high capacity for adsorption while the SEM images confirmed that the NPs are of an appropriate size to be adsorbed in the AC porous structure.

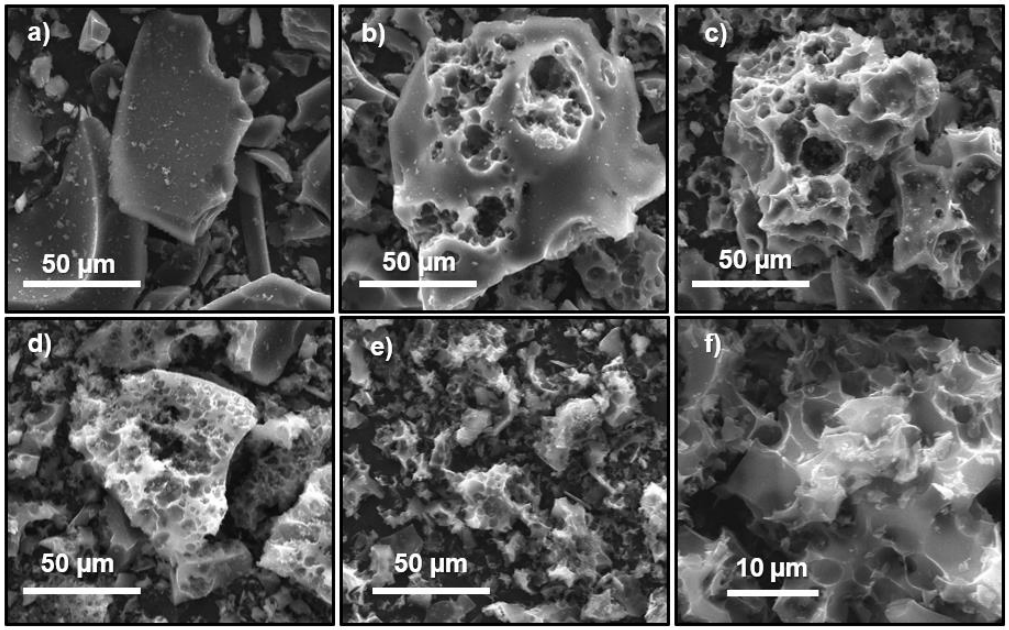

Figure 28: SEM images of a) Control, b) AC-600C-1KOH, c) AC-600C-2KOH, d) AC-800C-1KOH, e) AC-800C-2KOH, and f) AC-800C-2KOH (high magnification).

4.3.7. Characterization of NPs

The size distribution of the PET NPs was analyzed using DLS, and it was found that all particles had sizes below 350 nm, with an average size of 148 nm (**Figure 29a and c**). SEM imaging confirmed that the particles were uniformly distributed and were consistent with the DLS data (**Figure 29b**) while TEM imaging revealed that the particles had an irregular shape (**Figure 29d**). The zeta potential of the NP dispersion was measured to be -0.074 mV (**Figure 29c**), indicating a neutral surface charge. Thus, electrostatic interactions are not expected to be the primary mechanism for adsorption of the NPs by the AC or other particles.

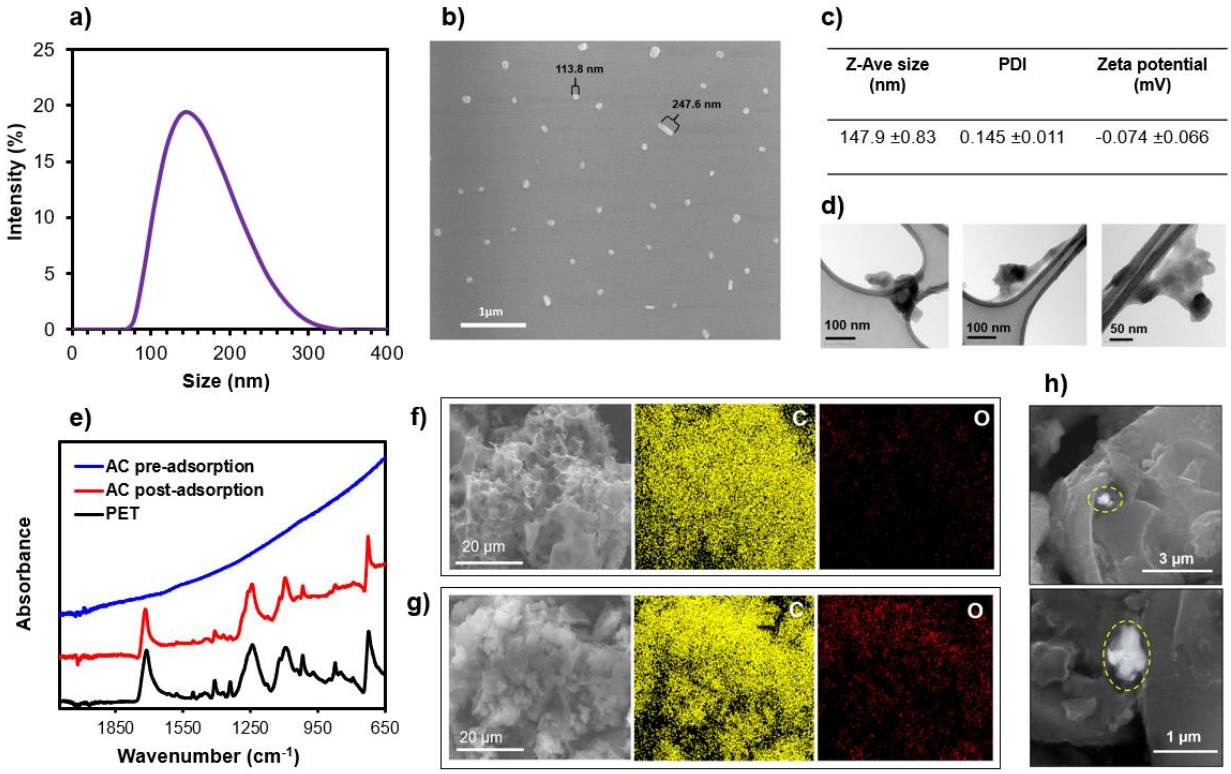

Figure 29: a) DLS particle size distribution of PET NPs, b) SEM images of PET NPs, c) Average particle size and zeta potential of PET NPs, d) TEM images of PET NPs, e) ATR-FTIR of AC-800C-2KOH before and after adsorption of PET NPs (1.6:1 mass ratio of NP:AC) and corresponding EDX elemental mapping f) before and g) after adsorption, and h) SEM images of PET NPs lodged in the crevices of AC-800C-2KOH after adsorption of NP (NP:AC ratio of 0.16).

4.3.8. NP adsorption confirmation

Confirmation of NP adsorption onto the surface of AC-800C-2KOH was achieved through analysis of the AC after treatment with an NP dispersion (NP:AC mass ratio of 1.6). The appearance of PET peaks in the FTIR spectrum (**Figure 29e**) provided evidence of the PET NPs on the surface of the AC. Furthermore, EDX elemental mapping of the same sample before

(**Figure 29f**) and after (**Figure 29g**) adsorption indicated an increased density of oxygen and carbon due to the adsorption of PET particles. The NPs formed layers on the surface of the AC, which reduced the visibility of underlying pores. After the adsorption of a more dilute NP dispersion (NP:AC ratio of 0.16), SEM imaging showed clusters of NPs located within the pores and crevices of AC-800C-2KOH (**Figure 29h**), highlighting the importance of the surface features in the adsorption process. The effect of surface area on adsorption was observed by the drastic increase in adsorption when comparing treatment using AC-800C-2KOH to the low surface area control sample (**Figure 31d**).

4.3.9. NP adsorption kinetics

To determine the equilibrium time for NP adsorption onto AC-800C-2KOH, the adsorption process was monitored over time. As illustrated in **Figure 30a**, the adsorption reached equilibrium after 19 hours of agitation, so 20h was used as the treatment time in subsequent studies. Adsorption kinetics were then analyzed by fitting the data to several models, as shown in **Figure 30b**. The pseudo second order (PSO) model proved to be the most accurate with an R^2 value of 0.999, closely predicting the experimental data (**Figure 30a**). Based on the PSO model, the initial adsorption rate constant (h) was calculated according to **Equation (42)** [220]. As shown in **Table 15**, the initial adsorption rate (h = 5.22) is larger than the average adsorption rate constant (K_2 = 3.21 x10^{-5}), indicating that the adsorption rate is much faster at the start of the process and decreases over time [220]. All the kinetic parameters for the fitted models are presented in **Table 15** with comparison to the values obtained by non-linear regression.

$$h = K_2^2 q_e^2 \quad \textbf{(42)}$$

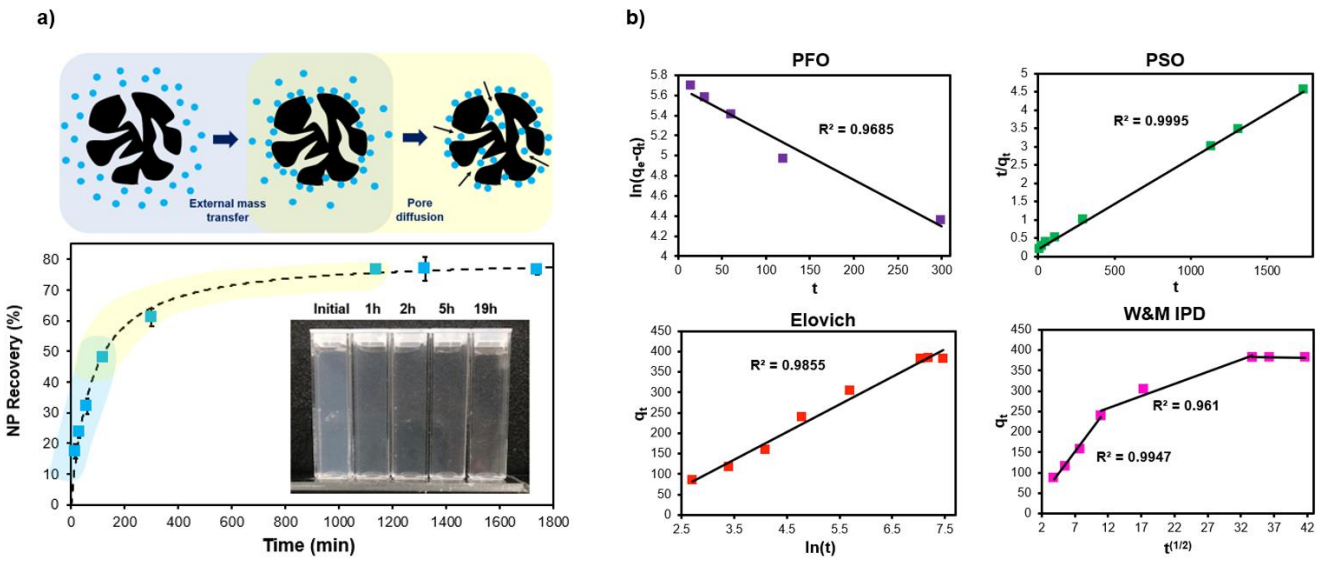

Figure 30: a) Recovery of NP (250 mg/L) by AC-800C-2KOH (500 mg/L) over time compared to PSO model prediction and b) linearized kinetic modelling of the data.

The Weber & Morris Intraparticle Diffusion (W&M IPD) model was used to gain insight into the adsorption process, as shown in **Figure 30b**. The appearance of three separate regions was observed and based on the analysis of other NP adsorption studies [94,96], these stages were attributed to external mass transfer, intraparticle diffusion, and equilibrium phases. Similar to adsorption reported by granular activated carbon (GAC), the rate constant for intraparticle diffusion (K_{int}) was much smaller than that of external mass transfer (K_{ext}), indicating that external mass transfer occurs much more quickly [96]. This makes sense because the tortuosity of the diffusion is affected by porosity [221], which is high in the AC. As a result, the external mass transfer phase was concluded after 2 h, while the intraparticle diffusion extended until around 19 h. Additionally, the zero intercept of the IPD model indicates that intraparticle diffusion is the rate limiting step of the adsorption process [222].

Table 15: Kinetic model parameters describing the adsorption of NP onto AC-800C-2KOH based on linear and non-linear regression.

Model		Parameter*	Value	
			Linear	**Non-linear**
Pseudo First Order		q_e (mg/g)	360.930	366.55
		K_1 (1/min)	0.00675	0.00954
		R^2	0.968	0.951
Pseudo Second Order		q_e (mg/g)	403.32	402.21
		K_2 (g/mg/min)	3.21 $x10^{-5}$	3.09 $x10^{-5}$
		h (g/mg/min)	5.22	4.99
		R^2	0.999	0.991
Elovich		a	15.288	15.288
		b	0.0148	0.0148
		R^2	0.985	0.985
Weber & Morris Intraparticle diffusion	External mass transfer	K_{int} (mg/g/min$^{(1/2)}$)	21.52	21.52
		C_{int} (mg/g)	-0.10	0.00
		R^2	0.995	0.995
	Intraparticle diffusion	K_{int} (mg/g/min$^{(1/2)}$)	5.98	5.98
		C_{int} (mg/g)	185.40	185.40
		R^2	0.961	0.961

*Correlation of parameters was not investigated and should be considered when applying these models to other data.

4.3.10. NP adsorption isotherm

The results of the NP adsorption experiments (**Figure 31a**) show that the adsorption increases with increasing NP concentration, which acts as the driving force for mass transfer. The observed decrease in adsorption (mg NP/g AC) with increasing AC concentration has previously been attributed to the reduction in exposed surface area due to aggregation at high carbon

loadings [223]. Another factor that can explain this trend is the reduction in concentration driving force as adsorption progresses with the addition of more AC. Furthermore, the percentage recovery of NPs (**Figure 31b**) is shown to increase with AC concentration as expected, while the trend with respect to NP concentration is not as clear. This is because percentage recovery is a measure of adsorption relative to the initial NP concentration, so this trend is dependant on the underlying adsorption isotherm describing the relationship between NP concentration and adsorption. Although the isotherm plot reports the equilibrium NP concentration, it is correlated with the initial NP concentration such that the effect of solely increasing initial concentration can be understood from the plot. Therefore, the equilibrium isotherm curve was plotted in order to better understand the nature of adsorption.

The equilibrium data from all runs was used to produce the isotherm plot (**Figure 31c**). At lower equilibrium concentrations the adsorption follows a convex shaped isotherm curve indicative of monolayer filling, while at higher equilibrium concentration the adsorption follows a convex shaped isotherm curve indicative of multilayer filling. Therefore, the BET, Aranovich, FHH, and AD-Langmuir multilayer adsorption models were used to describe the data, resulting in predictions of $R^2 > 0.95$. The AD-Langmuir model provided the best prediction of the data with $R^2 = 0.963$ and an estimated monolayer adsorption capacity of 325 mg/g, as shown in **Table 16**. The FHH model also described the data with the same R^2 value, but the AD-Langmuir model was favoured due to the more fitting curvature at equilibrium concentrations approaching zero (**Figure 31c**). This may indicate that the initial adsorption of NPs resembles that of the Langmuir isotherm model, in which each adsorption site is held by one adsorbate molecule [224]. Therefore, interaction of NPs with AC is likely greater than between NPs such that monolayer filling predominantly occurs prior to the formation of layers.

Table 16: Isotherm model parameters describing the adsorption of NP onto AC-800C-2KOH based on non-linear regression.

Model	Parameter	Value
BET	K_{BET1} (L/mg)	0.0369
	K_{BET2} (L/mg)	0.0450
	q_{mBET} (mg/g)	532.24
	R^2	0.957
Aranovich	C_A (mg/L)	3.418
	C_{sA} (mg/L)	182.42
	Q_{mA} (mg/g)	870.58
	R^2	0.954
FHH	K_{FHH} (mg/g)	1264.34
	C_{sFHH} (mg/L)	357.29
	n_{FHH}	1.52
	R^2	0.963
AD-Langmuir	K_L (L/mg)	0.0967
	q_{mL} (mg/g)	325.03
	C_{sAD} (mg/L)	1952.89
	n_{AD}	20.54
	R^2	0.963

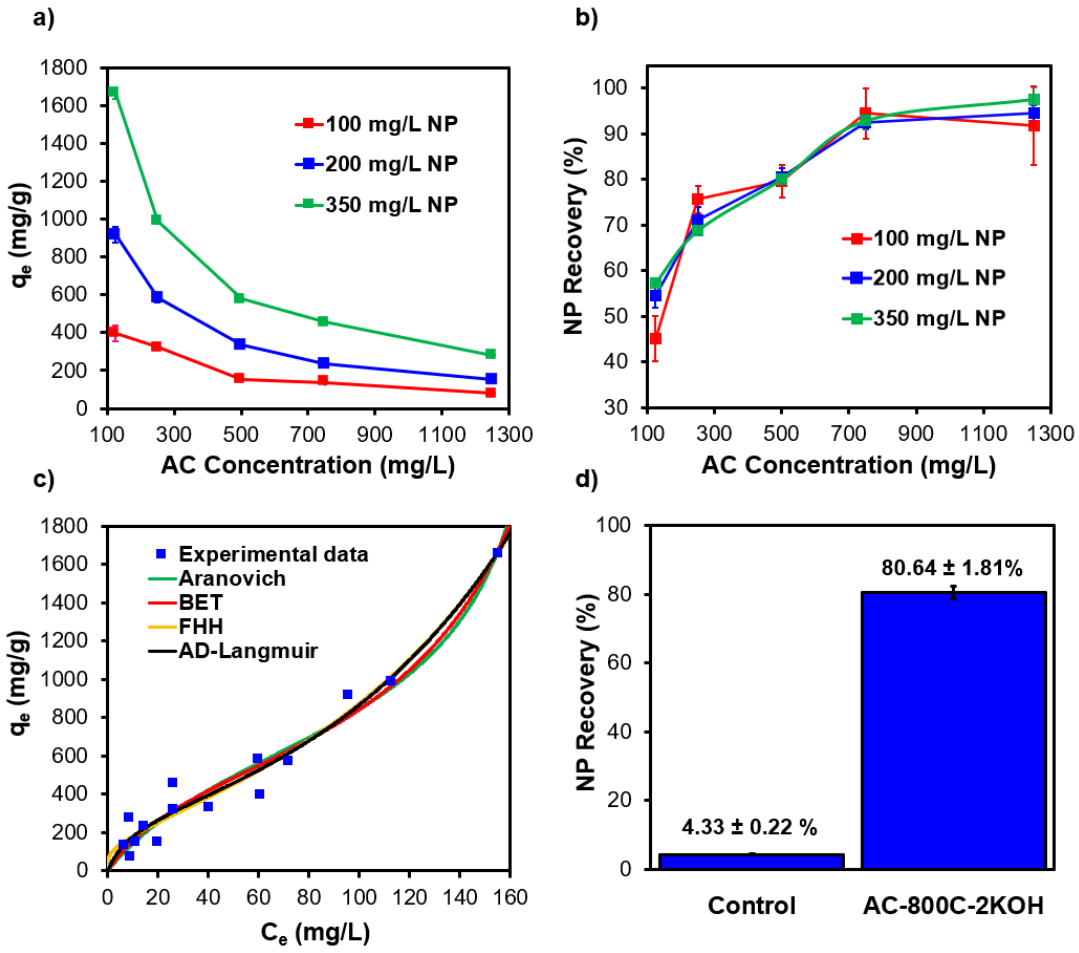

Figure 31: Analysis of NP adsorption onto AC-800C-2KOH as shown by (a) adsorption (mg/g) at various concentrations, (b) NP recovery at various concentrations, (c) the corresponding adsorption isotherm with model predictions, (d) comparison of NP recovery (200 mg/L dispersion) by AC-800C-2KOH (500 mg/L) and the control (500 mg/L carbonized epoxy).

To explain the NP percentage recovery trends, the effects of both AC and NP concentration on adsorption were illustrated in relation to the isotherm curve (**Figure 32**). As shown, increases in both NP and AC concentrations lead to a greater total mass of adsorbed NPs (**Figure 32b and c**); However, the recovery is dependent on the adsorbed NPs relative to the initial amount. Therefore, under a constant initial NP concentration the recovery increased with respect to AC concentration (**Figure 32b**). On the other hand, as the initial NP concentration

increases the resulting change in recovery is dependent on the proportionality between adsorption and NP concentration, which varies due to the changing curvature of the isotherm plot (**Figure 32a**). Furthermore, an increasing NP concentration may cause the adsorption to progress into different adsorption regions (**Figure 32b**) leading to unpredictable trends in recovery. Still, it can be noted that there is not much change in percentage recoveries for all NP concentrations (**Figure 31b**) because the observed isotherm plot (**Figure 31c**) does not present extreme curvature. Therefore, it can be concluded that the effect of NP concentration is minimal and high AC levels are required to achieve high recoveries regardless of the initial NP concentration. For the NP concentrations tested, an AC level of 750 mg/L was required to achieved recoveries above 90%, but further increases began to level off significantly beyond this point.

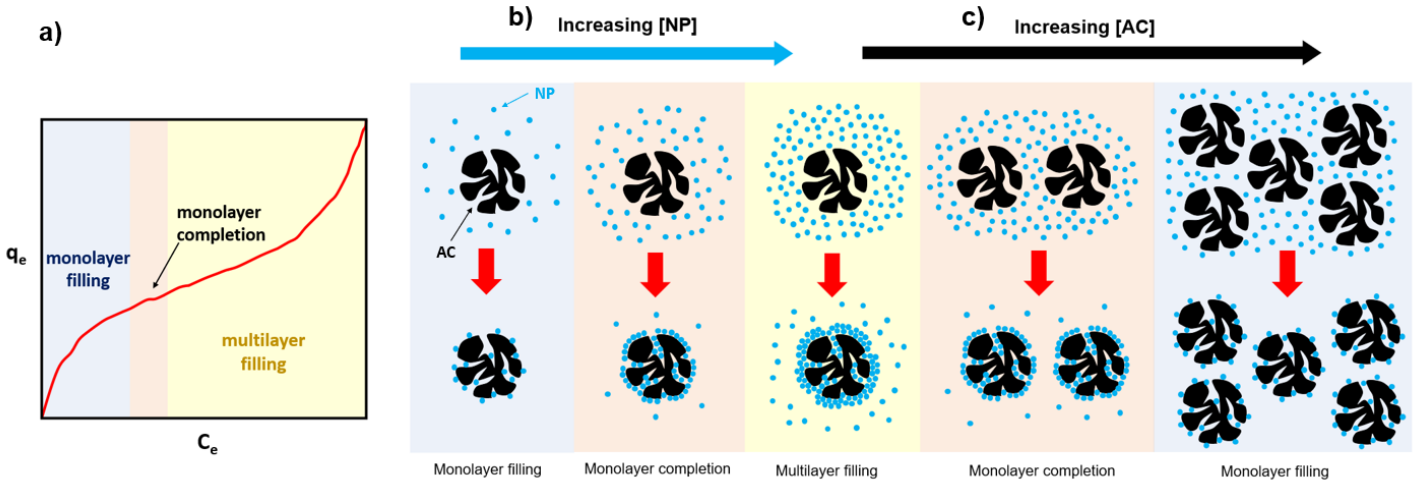

Figure 32: a) Multilayer isotherm model labeled with filling stages and corresponding illustrations of NP adsorption onto AC under b) varying initial NP concentration and c) varying AC concentration.

The main observation from the adsorption isotherm analysis is that the adsorption of NPs onto AC-800C-2KOH follows multilayer physical adsorption, which was best described by the AD-Langmuir model. In contrast, previous research examining NP adsorption has used charged

PS [94–96], and have shown that electrostatic charges can impact the adsorption process. All studies found that the Langmuir adsorption model best described their data, which is consistent with the chemical adsorption of charged NP molecules and inhibited formation of successive layers. In the case of PET NPs, the zeta potential was determined to be approximately zero, allowing the particles to form multiple layers mainly through physical adsorption. Still, it is expected that monolayer filling occurs prior to NP layering since the charge difference with respect to the AC is larger than that of another NP. Additionally, the many oxygen functionalities on the AC likely aided the physical adsorption process.

The trends in NP recovery (**Figure 31b**) indicate that it may not be worthwhile to increase the AC concentration beyond 750 mg/L. Most notably, at the lowest NP concentration tested (100 mg/L) the recovery at 750 mg/L AC (94%) was not significantly changed when the AC concentration was increased to 1150 mg/L AC. This performance was compared with previous studies examining polystyrene (PS) NP recovery, as shown in **Table 17**. Comparatively, AC-800C-2KOH was able to treat a much greater NP concentration with a generally low AC loading. For example, a significantly greater amount of commercial GAC (5 g/L) was used to treat a more diluted NP dispersion (40 mg/L), achieving only 26% recovery [96]. Evidently AC-800C-2KOH shows a much greater adsorption capacity than commercial AC, which can be attributed to the higher surface area of AC-800C-2KOH (1705 m^2/g) compared to the GAC (1150 m^2/g) which can accommodate more NPs. Despite the increased capacity, the achieved percentage NP recovery does not exceed those reported in previous NP studies (**Table 17**) due to the limited driving force for adsorption. Because the observed adsorption is a physical process it is facilitated mainly by Van der Waals forces which are relatively weak bonds.

Table 17: Comparison of NP recovery and adsorbent dose to other NP/carbon systems.

NP type	Solute concentration (mg/L)	Adsorbent type	Adsorbent concentration (g/L)	NP recovery	Reference
PET	100	Epoxy AC	0.75	94%	This study
PS	10	Bagasse Biochar	0.3	99%	[94]
PS	5	Commercial GAC	5	98%	[96]
	40			26%	

Overall, the adsorption analysis was used to identify the multilayer adsorption of NPs onto the epoxy AC and the high capacity of the product (q_m = 325 mg/g). There was also indication of high efficiency in NP recovery (>90%) within the tested NP concentrations. Due to the method of NP detection by UV-Vis the study was limited to a minimum NP concentration of 100 mg/L, under which the signal was too low for accurate analysis. Therefore, future work is required to confirm the adsorption efficiency of NPs onto AC at the even lower concentrations. Additionally, the results indicated that percentage recoveries begin to level off significantly beyond AC loadings of 750 mg/L making it difficult to approach 100% NP recovery. It is suspected that increased attraction between AC and NP is required to achieve higher recovery as a result of the weak physical bonds dictating the adsorption process. Improvements to the interaction between AC and NP should be investigated by modification of the AC structure in order to achieve higher NP recovery without significant increase in AC loading.

4.4. Conclusions

This study investigated the production of activated carbon (AC) from cured epoxy waste via controlled pyrolysis and activation, with a focus on utilizing the generated AC for NP adsorption from contaminated wastewater. It was found that KOH was an appealing activating agent due to its ability to increase the low char yield of epoxy (8.98%) to an observed maximum

of 39.8%. Although the maximum BET surface area was achieved by K_2CO_3 (1843 m^2/g), its decreased reactivity at low temperatures resulted in the lowest yield product (8.53%). Therefore, KOH activation was preliminarily optimized to produce an AC product of high surface area (1705 m^2/g), yield (31%) and significant oxygen content based on activation conditions of 800 ^oC and a 2:1 KOH impregnation ratio. The epoxy AC demonstrated adsorption of synthesized PET NPs (<350 nm) through multilayer physical adsorption with an estimated monolayer capacity of 325 mg/g based on the AD-Langmuir model (R^2 = 0.963). At low NP concentration (100 mg/L), the product achieved 94% NP recovery, indicating an improved capacity compared to that of commercial AC. In general, AC loadings of only 750 mg/L resulted in NP recoveries > 90%, but there was difficulty in achieving full recovery. It is recommended for future research to explore milder activating agents, refine the activation process, and enhance NP adsorption efficiency through AC modification. Despite these limitations, the epoxy AC has shown potential to significantly reduce NP contamination in water by a simple batch agitation technique. Not only is this product effective and easier to implement in WWTPs compared to the alternative advanced treatment techniques, but the use of cured epoxy waste would simultaneously help divert this non-recyclable waste stream from the inevitable accumulation in landfills.

Chapter 5: Concluding remarks

Plastic waste recycling is necessary to ensure the sustainability of the mass-produced and petroleum-based products being used daily. However, it is not an issue that can be easily solved, as recycling implementation faces many challenges which have limited recycling rates across the globe. As waste continues to grow it is of high interest to find sustainable methods of disposal and divert these plastics from the buildup in landfill sites. To address the concerns surrounding the current overflow of plastic waste in the environment, this thesis explored the validity of a specific disposal pathway involving the carbonization of plastics to produce activated carbon (AC) for wastewater treatment applications. Two distinct polymer types were converted to AC through chemical activation and applied as adsorbents for two prevalent wastewater pollutants. The conclusions from these studies are summarized below:

PET bottle waste to AC for treatment of dye contaminated wastewater: KOH chemical activation was used to convert PET bottle waste into AC. It was found that increased activation temperature and time enhanced the surface area development, but the inverse relationship of carbon yield led to an optimal product at a lower activation time of 1 h. The higher activation temperature of 800 ºC was also found to increase the negative surface charge, which was ideal for interaction with cationic dye molecules. The product exhibiting a surface area of 1214 m^2/g and zeta potential of -40 mV was found to adsorb cationic methylene blue (MB) dye through monolayer adsorption with a maximum capacity of 335 mg/g, aligning with commercial products. The adsorption was enhanced at higher pH values and the selectivity of the AC for cationic dyes was confirmed through the increased recovery of MB dye within a mixture containing anionic methyl orange dye. Lastly, the effects of cationic dye charge characteristics were observed by the

reduced adsorption capacity of brilliant green dye resulting from the lower proportion of positively charged molecules at the test pH. Overall, this work showcased the substantial capacity of PET AC for adsorption of cationic dyes and the expected impacts of AC surface composition, dye type, and their relation to solution pH.

1) **Epoxy thermoset plastic to AC for treatment of nano-plastic contaminated wastewater:** Chemical activation by various potassium-based activators was used to convert cured epoxy plastic to AC. It was found that KOH was the best activator due to its ability to substantially improve yield, resulting in an optimal product at a higher impregnation ratio (2:1) to conserve yield and a high activation temperature (800 ^{o}C) to produce a large surface area. The resulting product exhibiting a surface area of 1705 m^2/g and yield of 31% was found to adsorb neutral PET nano-plastics (NPs) through multilayer physical adsorption with an estimated monolayer capacity of 325 mg/g. This adsorption capability is very impressive compared to existing studies limited to adsorption of charged PS NPs; However, the NP recovery at representatively low NP concentrations did not exceed 94% due to the relatively weak polar interactions dictating the adsorption process. The neutrality of the NP surface limited electrostatic interaction with the AC; However, the resulting lack of inter-particle repulsion enables the NP particles to form multiple adsorption layers. Overall, this work showcased the potential of epoxy AC in adsorbing PET NPs, and provided valuable insight into both the chemical activation of thermoset waste and the adsorption mechanism of neutral NPs onto AC.

In conclusion, there is a lot of potential for plastics as feedstocks to AC as they produce high surface area material with surface features that can facilitate adsorption through both electrostatic

interaction with charged molecules and polar interaction with neutral particles. This work exhibited the success in the conversion of both thermoplastic and thermoset material into AC and demonstrated the general adsorption behaviors that may be expected when treating textile dyes and nano-plastics in water. The applications of plastic derived AC may also extend beyond wastewater treatment applications, but these areas should be individually investigated due to the unique features of each absorbent/ adsorbate system.

In terms of next steps, it is recommended that the feasibility of AC production from real waste plastic streams is fully analyzed for this conversion pathway to be realized. Although this method can produce a high value product from low quality and non-recyclable plastic waste, it must still overcome the issues of waste sorting due to the different degradation pathways for each plastic type. Additionally, the production cost and life cycle of the product must be analyzed to justify its implementation. One key aspect of this is the disposal of the AC post adsorption and the potential removal or decomposition of the adsorbed dye/ NP for reuse of the adsorbent. Lastly, the intended adsorption applications should be further validated through testing of real wastewater samples, which contain a variety of components and may exhibit lower NP concentrations than could be accurately tested in this work. Still, plastic wastes should not be overlooked as a precursor to AC products, as this usage could divert a significant portion of plastic waste from being landfilled while providing a sustainable alternative feedstock for valuable wastewater pollutant adsorbents.

References

[1] J. Choi, I. Yang, S.-S. Kim, S.Y. Cho, S. Lee, Upcycling Plastic Waste into High Value-Added Carbonaceous Materials, Macromol Rapid Commun 43 (2022) 2100467. https://doi.org/https://doi.org/10.1002/marc.202100467.

[2] S. Chen, Z. Liu, S. Jiang, H. Hou, Carbonization: A feasible route for reutilization of plastic wastes, Science of The Total Environment 710 (2020) 136250. https://doi.org/https://doi.org/10.1016/j.scitotenv.2019.136250.

[3] D.K.A. Barnes, F. Galgani, R.C. Thompson, M. Barlaz, Accumulation and Fragmentation of Plastic Debris in Global Environments, Philosophical Transactions: Biological Sciences 364 (2009) 1985–1998. http://www.jstor.org/stable/40485977.

[4] K. Boyle, B. Örmeci, Microplastics and Nanoplastics in the Freshwater and Terrestrial Environment: A Review, Water (Basel) 12 (2020). https://doi.org/10.3390/w12092633.

[5] M. Cole, P. Lindeque, C. Halsband, T.S. Galloway, Microplastics as contaminants in the marine environment: a review, Mar Pollut Bull 62 (2011) 2588–2597.

[6] S.D. Anuar Sharuddin, F. Abnisa, W.M.A. Wan Daud, M.K. Aroua, A review on pyrolysis of plastic wastes, Energy Convers Manag 115 (2016) 308–326. https://doi.org/https://doi.org/10.1016/j.enconman.2016.02.037.

[7] A. Dorigato, Recycling of polymer blends, Advanced Industrial and Engineering Polymer Research 4 (2021) 53–69. https://doi.org/https://doi.org/10.1016/j.aiepr.2021.02.005.

[8] K. Ragaert, L. Delva, K. Van Geem, Mechanical and chemical recycling of solid plastic waste, Waste Management 69 (2017) 24–58. https://doi.org/https://doi.org/10.1016/j.wasman.2017.07.044.

[9] J.-P. Lange, Managing Plastic Waste─Sorting, Recycling, Disposal, and Product Redesign, ACS Sustain Chem Eng 9 (2021) 15722–15738. https://doi.org/10.1021/acssuschemeng.1c05013.

[10] S.H. Gebre, M.G. Sendeku, M. Bahri, Recent Trends in the Pyrolysis of Non-Degradable Waste Plastics, ChemistryOpen 10 (2021) 1202+. https://link-gale-com.proxy.lib.uwaterloo.ca/apps/doc/A688145542/AONE?u=uniwater&sid=bookmark-AONE&xid=8659723c.

[11] Y. Wang, B.P. Chang, A. Veksha, A. Kashcheev, A. ling Y. Tok, V. Lipik, R. Yoshiie, Y. Ueki, I. Naruse, G. Lisak, Processing plastic waste via pyrolysis-thermolysis into hydrogen and solid carbon additive to ethylene-vinyl acetate foam for cushioning applications, J Hazard Mater 464 (2024) 132996. https://doi.org/https://doi.org/10.1016/j.jhazmat.2023.132996.

[12] S. Kumar, A.K. Panda, R.K. Singh, A review on tertiary recycling of high-density polyethylene to fuel, Resour Conserv Recycl 55 (2011) 893–910.

[13] T. Ueno, E. Nakashima, K. Takeda, Quantitative analysis of random scission and chain-end scission in the thermal degradation of polyethylene, Polym Degrad Stab 95 (2010) 1862–1869.

[14] G. Elordi, M. Olazar, G. Lopez, M. Artetxe, J. Bilbao, Product yields and compositions in the continuous pyrolysis of high-density polyethylene in a conical spouted bed reactor, Ind Eng Chem Res 50 (2011) 6650–6659.

[15] P. Das, P. Tiwari, The effect of slow pyrolysis on the conversion of packaging waste plastics (PE and PP) into fuel, Waste Management 79 (2018) 615–624. https://doi.org/https://doi.org/10.1016/j.wasman.2018.08.021.

[16] T.M. Kruse, O.S. Woo, H.-W. Wong, S.S. Khan, L.J. Broadbelt, Mechanistic modeling of polymer degradation: a comprehensive study of polystyrene, Macromolecules 35 (2002) 7830–7844.

[17] J. Zhou, Y. Qiao, W. Wang, E. Leng, J. Huang, Y. Yu, M. Xu, Formation of styrene monomer, dimer and trimer in the primary volatiles produced from polystyrene pyrolysis in a wire-mesh reactor, Fuel 182 (2016) 333–339.

[18] J.A. Onwudili, N. Insura, P.T. Williams, Composition of products from the pyrolysis of polyethylene and polystyrene in a closed batch reactor: Effects of temperature and residence time, J Anal Appl Pyrolysis 86 (2009) 293–303. https://doi.org/https://doi.org/10.1016/j.jaap.2009.07.008.

[19] Y. Luo, X. Lin, E. Lichtfouse, H. Jiang, C. Wang, Conversion of waste plastics into value-added carbon materials, Environ Chem Lett 21 (2023) 3127–3158. https://doi.org/10.1007/s10311-023-01638-7.

[20] S. Ren, X. Xu, K. Hu, W. Tian, X. Duan, J. Yi, S. Wang, Structure-oriented conversions of plastics to carbon nanomaterials, Carbon Research 1 (2022) 15. https://doi.org/10.1007/s44246-022-00016-2.

[21] J. Gong, X. Chen, T. Tang, Recent progress in controlled carbonization of (waste) polymers, Prog Polym Sci 94 (2019) 1–32. https://doi.org/https://doi.org/10.1016/j.progpolymsci.2019.04.001.

[22] L. Dai, O. Karakas, Y. Cheng, K. Cobb, P. Chen, R. Ruan, A review on carbon materials production from plastic wastes, Chemical Engineering Journal 453 (2023) 139725. https://doi.org/https://doi.org/10.1016/j.cej.2022.139725.

[23] D. Choi, D. Jang, H.-I. Joh, E. Reichmanis, S. Lee, High Performance Graphitic Carbon from Waste Polyethylene: Thermal Oxidation as a Stabilization Pathway Revisited, Chemistry of Materials 29 (2017) 9518–9527. https://doi.org/10.1021/acs.chemmater.7b03737.

[24] J.M. Younker, T. Saito, M.A. Hunt, A.K. Naskar, A. Beste, Pyrolysis Pathways of Sulfonated Polyethylene, an Alternative Carbon Fiber Precursor, J Am Chem Soc 135 (2013) 6130–6141. https://doi.org/10.1021/ja3121845.

[25] D. Hines, A. Bagreev, T.J. Bandosz, Surface Properties of Porous Carbon Obtained from Polystyrene Sulfonic Acid-Based Organic Salts, Langmuir 20 (2004) 3388–3397. https://doi.org/10.1021/la0360613.

[26] C. Zou, D. Wu, M. Li, Q. Zeng, F. Xu, Z. Huang, R. Fu, Template-free fabrication of hierarchical porous carbon by constructing carbonyl crosslinking bridges between polystyrene chains, Journal of Materials Chemistry - J MATER CHEM 20 (2010). https://doi.org/10.1039/b917960g.

[27] W.M. Qiao, S.H. Yoon, I. Mochida, J.H. Yang, Waste polyvinylchloride derived pitch as a precursor to develop carbon fibers and activated carbon fibers, Waste Management 27 (2007) 1884–1890. https://doi.org/https://doi.org/10.1016/j.wasman.2006.10.002.

[28] B.E. Barton, J. Patton, E. Hukkanen, M. Behr, J.-C. Lin, S. Beyer, Y. Zhang, L. Brehm, B. Haskins, B. Bell, B. Gerhart, A. Leugers, M. Bernius, The chemical transformation of hydrocarbons to carbon using SO3 sources, Carbon N Y 94 (2015) 465–471. https://doi.org/https://doi.org/10.1016/j.carbon.2015.07.029.

[29] A.R. Postema, H. De Groot, A.J. Pennings, Amorphous carbon fibres from linear low density polyethylene, J Mater Sci 25 (1990) 4216–4222. https://doi.org/10.1007/BF00581075.

[30] P.J. Kim, H.D. Fontecha, K. Kim, V.G. Pol, Toward High-Performance Lithium–Sulfur Batteries: Upcycling of LDPE Plastic into Sulfonated Carbon Scaffold via Microwave-Promoted Sulfonation, ACS Appl Mater Interfaces 10 (2018) 14827–14834. https://doi.org/10.1021/acsami.8b03959.

[31] C. Li, H. Zhu, N. V Salim, B.L. Fox, N. Hameed, Preparation of microporous carbon materials via in-depth sulfonation and stabilization of polyethylene, Polym Degrad Stab 134 (2016) 272–283. https://doi.org/https://doi.org/10.1016/j.polymdegradstab.2016.10.019.

[32] S. Villagómez-Salas, P. Manikandan, S.F. Acuña Guzmán, V.G. Pol, Amorphous Carbon Chips Li-Ion Battery Anodes Produced through Polyethylene Waste Upcycling, ACS Omega 3 (2018) 17520–17527. https://doi.org/10.1021/acsomega.8b02290.

[33] X. Yang, C. Li, G. Zhang, C. Yang, Polystyrene-derived carbon with hierarchical macro–meso–microporous structure for high-rate lithium-ion batteries application, J Mater Sci 50 (2015) 6649–6655. https://doi.org/10.1007/s10853-015-9214-7.

[34] W.M. Qiao, Y. Song, S.-H. Yoon, Y. Korai, I. Mochida, S. Yoshiga, H. Fukuda, A. Yamazaki, Carbonization of waste PVC to develop porous carbon material without further activation, Waste Management 26 (2006) 592–598. https://doi.org/https://doi.org/10.1016/j.wasman.2005.06.010.

[35] T. Saito, Magnetic properties of carbon materials prepared from polyvinyl chloride, J Appl Phys 105 (2009) 013902. https://doi.org/10.1063/1.3054176.

[36] Y. Bai, Z. Wang, C. Wu, R. Xu, F. Wu, Y. Liu, H. Li, Y. Li, J. Lu, K. Amine, Hard Carbon Originated from Polyvinyl Chloride Nanofibers As High-Performance Anode Material for Na-Ion Battery, ACS Appl Mater Interfaces 7 (2015) 5598–5604. https://doi.org/10.1021/acsami.5b00861.

[37] R. Bhattacharya, A review on production and application of activated carbon from discarded plastics in the context of 'waste treats waste,' J Environ Manage 325 (2023) 116613. https://doi.org/https://doi.org/10.1016/j.jenvman.2022.116613.

[38] A. Sharma, J. Jindal, A. Mittal, K. Kumari, S. Maken, N. Kumar, Carbon materials as CO2 adsorbents: a review, Environ Chem Lett 19 (2021) 875–910. https://doi.org/10.1007/s10311-020-01153-z.

[39] Y. Gao, Q. Yue, B. Gao, A. Li, Insight into activated carbon from different kinds of chemical activating agents: A review, Science of The Total Environment 746 (2020) 141094. https://doi.org/https://doi.org/10.1016/j.scitotenv.2020.141094.

[40] Z. Heidarinejad, M.H. Dehghani, M. Heidari, G. Javedan, I. Ali, M. Sillanpää, Methods for preparation and activation of activated carbon: a review, Environ Chem Lett 18 (2020) 393–415. https://doi.org/10.1007/s10311-019-00955-0.

[41] T.S. Hui, M.A.A. Zaini, Potassium hydroxide activation of activated carbon: A commentary, Carbon Letters (2015). https://doi.org/10.5714/CL.2015.16.4.275.

[42] R. Blanchard, T.H. Mekonnen, Utilization of epoxy thermoset waste to produce activated carbon for the remediation of nano-plastic contaminated wastewater, Sep Purif Technol 326 (2023) 124755. https://doi.org/https://doi.org/10.1016/j.seppur.2023.124755.

[43] F. Hussin, M.K. Aroua, M.A. Kassim, U.F. Md. Ali, Transforming Plastic Waste into Porous Carbon for Capturing Carbon Dioxide: A Review, Energies (Basel) 14 (2021). https://doi.org/10.3390/en14248421.

[44] T. Otowa, R. Tanibata, M. Itoh, Production and adsorption characteristics of MAXSORB: High-surface-area active carbon, Gas Separation and Purification (1993). https://doi.org/10.1016/0950-4214(93)80024-Q.

[45] A. Spence, Activated carbon breakthrough offers solution to global plastic crisis, The Lead (2019). https://theleadsouthaustralia.com.au/industries/technology/activated-carbon-breakthrough-offers-solution-to-global-plastic-crisis/ (accessed December 12, 2023).

[46] A. Milbrandt, K. Coney, A. Badgett, G.T. Beckham, Quantification and evaluation of plastic waste in the United States, Resour Conserv Recycl 183 (2022) 106363. https://doi.org/https://doi.org/10.1016/j.resconrec.2022.106363.

[47] I. Yang, J.H. Mok, M. Jung, J. Yoo, M.-S. Kim, D. Choi, J.C. Jung, Polyethylene-Derived Activated Carbon Materials for Commercially Available Supercapacitor in an Organic

Electrolyte System, Macromol Rapid Commun 43 (2022) 2200006. https://doi.org/https://doi.org/10.1002/marc.202200006.

[48] W.M. Qiao, S.H. Yoon, Y. Korai, I. Mochida, S. Inoue, T. Sakurai, T. Shimohara, Preparation of activated carbon fibers from polyvinyl chloride, Carbon N Y 42 (2004) 1327–1331. https://doi.org/https://doi.org/10.1016/j.carbon.2004.01.035.

[49] X. Liu, F. Yang, M. Li, S. Wang, C. Sun, From polyvinyl chloride waste to activated carbons: the role of occurring additives on porosity development and gas adsorption properties, Science of The Total Environment 833 (2022) 154894. https://doi.org/https://doi.org/10.1016/j.scitotenv.2022.154894.

[50] F. Lian, C. Chang, Y. Du, L. Zhu, B. Xing, C. Liu, Adsorptive removal of hydrophobic organic compounds by carbonaceous adsorbents: A comparative study of waste-polymer-based, coal-based activated carbon, and carbon nanotubes, J Environ Sci (China) (2012). https://doi.org/10.1016/S1001-0742(11)60984-4.

[51] L. Gonsalvesh, S.P. Marinov, G. Gryglewicz, R.Carleer, J.Yperman, Preparation, characterization and application of polystyrene based activated carbons for Ni(II) removal from aqueous solution, Fuel Processing Technology 149 (2016) 75–85. https://doi.org/https://doi.org/10.1016/j.fuproc.2016.03.024.

[52] F.G.F. de Paula, M.C.M. de Castro, P.F.R. Ortega, C. Blanco, R.L. Lavall, R. Santamaría, High value activated carbons from waste polystyrene foams, Microporous and Mesoporous Materials 267 (2018) 181–184. https://doi.org/10.1016/j.micromeso.2018.03.027.

[53] N. Deka, J. Barman, S. Kasthuri, V. Nutalapati, G.K. Dutta, Transforming waste polystyrene foam into N-doped porous carbon for capacitive energy storage and deionization applications, Appl Surf Sci 511 (2020) 145576. https://doi.org/https://doi.org/10.1016/j.apsusc.2020.145576.

[54] G. Gatti, M. Errahali, L. Tei, E. Mangano, S. Brandani, M. Cossi, L. Marchese, A Porous Carbon with Excellent Gas Storage Properties from Waste Polystyrene, Nanomaterials 9 (2019) 726. https://doi.org/10.3390/nano9050726.

[55] Z. Li, R. Wang, J. Ye, F. Liu, Z. Sha, Preparation of activated carbon from polycarbonate by chemical activation, CHISA 2006 - 17th International Congress of Chemical and Process Engineering (2006).

[56] Z. Li, K. Wang, J. Song, Q. Xu, N. Kobayashi, Preparation of activated carbons from polycarbonate with chemical activation using response surface methodology, J Mater Cycles Waste Manag 16 (2014) 359–366. https://doi.org/10.1007/s10163-013-0196-8.

[57] R. Blanchard, T.H. Mekonnen, Synchronous pyrolysis and activation of poly (ethylene terephthalate) for the generation of activated carbon for dye contaminated wastewater treatment, J Environ Chem Eng 10 (2022) 108810. https://doi.org/https://doi.org/10.1016/j.jece.2022.108810.

[58] L. Wei, N. Yan, Q. Chen, Converting Poly(ethylene terephthalate) Waste into Carbon Microspheres in a Supercritical CO2 System, Environ Sci Technol 45 (2011) 534–539. https://doi.org/10.1021/es102431e.

[59] J.B. Parra, C.O. Ania, A. Arenillas, F. Rubiera, J.J. Pis, High value carbon materials from PET recycling, Appl Surf Sci 238 (2004) 304–308. https://doi.org/https://doi.org/10.1016/j.apsusc.2004.05.229.

[60] J.B. Parra, C.O. Ania, A. Arenillas, F. Rubiera, J.M. Palacios, J.J. Pis, Textural development and hydrogen adsorption of carbon materials from PET waste, J Alloys Compd 379 (2004) 280–289. https://doi.org/https://doi.org/10.1016/j.jallcom.2004.02.044.

[61] A. Esfandiari, T. Kaghazchi, M. Soleimani, Preparation and evaluation of activated carbons obtained by physical activation of polyethyleneterephthalate (PET) wastes, J Taiwan Inst Chem Eng 43 (2012) 631–637. https://doi.org/https://doi.org/10.1016/j.jtice.2012.02.002.

[62] W. Bratek, A. Świątkowski, M. Pakuła, S. Biniak, M. Bystrzejewski, R. Szmigielski, Characteristics of activated carbon prepared from waste PET by carbon dioxide activation, J Anal Appl Pyrolysis 100 (2013) 192–198. https://doi.org/https://doi.org/10.1016/j.jaap.2012.12.021.

[63] R. Mendoza-Carrasco, E.M. Cuerda-Correa, M.F. Alexandre-Franco, C. Fernández-González, V. Gómez-Serrano, Preparation of high-quality activated carbon from polyethyleneterephthalate (PET) bottle waste. Its use in the removal of pollutants in aqueous solution, J Environ Manage (2016). https://doi.org/10.1016/j.jenvman.2016.06.070.

[64] K. László, A. Bóta, L.G. Nagy, Comparative adsorption study on carbons from polymer precursors, Carbon N Y (2000). https://doi.org/10.1016/S0008-6223(00)00038-5.

[65] E. Lorenc-Grabowska, M.A. Diez, G. Gryglewicz, Influence of pore size distribution on the adsorption of phenol on PET-based activated carbons, J Colloid Interface Sci 469 (2016) 205–212. https://doi.org/https://doi.org/10.1016/j.jcis.2016.02.007.

[66] X. Yuan, J.G. Lee, H. Yun, S. Deng, Y.J. Kim, J.E. Lee, S.K. Kwak, K.B. Lee, Solving two environmental issues simultaneously: Waste polyethylene terephthalate plastic bottle-derived microporous carbons for capturing CO2, Chemical Engineering Journal (2020). https://doi.org/10.1016/j.cej.2020.125350.

[67] C.S. de Castro, L.N. Viau, J.T. Andrade, T.A.P. Mendonça, M. Gonçalves, Mesoporous activated carbon from polyethyleneterephthalate (PET) waste: pollutant adsorption in aqueous solution, New Journal of Chemistry 42 (2018) 14612–14619. https://doi.org/10.1039/C8NJ02715C.

[68] I.P. da Paixão Cansado, C.R. Belo, P.A. Mira Mourão, Pesticides abatement using activated carbon produced from a mixture of synthetic polymers by chemical activation

with KOH and K2CO3, Environ Nanotechnol Monit Manag (2019). https://doi.org/10.1016/j.enmm.2019.100261.

[69] M. Adibfar, T. Kaghazchi, N. Asasian, M. Soleimani, Conversion of Poly(Ethylene Terephthalate) Waste into Activated Carbon: Chemical Activation and Characterization, Chem Eng Technol (2014). https://doi.org/10.1002/ceat.201200719.

[70] Ç. Sarıcı-Özdemir, Y. Önal, Synthesis of new activated carbons produced from polymer waste, Fullerenes Nanotubes and Carbon Nanostructures (2018). https://doi.org/10.1080/1536383X.2018.1447930.

[71] S. Ayyalusamy, S. Mishra, V. Suryanarayanan, Promising post-consumer PET-derived activated carbon electrode material for non-enzymatic electrochemical determination of carbofuran hydrolysate, Sci Rep 8 (2018) 13151. https://doi.org/10.1038/s41598-018-31627-8.

[72] X. Yuan, M.-K. Cho, J.G. Lee, S.W. Choi, K.B. Lee, Upcycling of waste polyethylene terephthalate plastic bottles into porous carbon for CF4 adsorption, Environmental Pollution 265 (2020) 114868. https://doi.org/https://doi.org/10.1016/j.envpol.2020.114868.

[73] B. Kaur, J. Singh, R.K. Gupta, H. Bhunia, Porous carbons derived from polyethylene terephthalate (PET) waste for CO2 capture studies, J Environ Manage 242 (2019) 68–80. https://doi.org/https://doi.org/10.1016/j.jenvman.2019.04.077.

[74] I.P.P. Cansado, P.A.M. Mourão, A.I. Falcão, M.M.L.R. Carrott, P.J.M. Carrott, The influence of the activated carbon post-treatment on the phenolic compounds removal, Fuel Processing Technology (2012). https://doi.org/10.1016/j.fuproc.2011.10.015.

[75] I.P.P. Cansado, C. Galacho, Á.S. Nunes, M.L.R. Carrott, P.J.M. Carrott, Adsorption properties of activated carbons prepared from recycled pet in the removal of organic pollutants from aqueous solutions, Adsorption Science and Technology (2010). https://doi.org/10.1260/0263-6174.28.8-9.807.

[76] B. Kaur, J. Singh, R.K. Gupta, H. Bhunia, Porous carbons derived from polyethylene terephthalate (PET) waste for CO2 capture studies, J Environ Manage 242 (2019) 68–80. https://doi.org/10.1016/J.JENVMAN.2019.04.077.

[77] X. Dong, J. Wang, M. Yan, B. Ren, J. Miao, L. Zhang, Z. Liu, Y. Xu, Hierarchically Fe-doped porous carbon derived from phenolic resin for high performance supercapacitor, Ceram Int 47 (2021) 5998–6009. https://doi.org/https://doi.org/10.1016/j.ceramint.2020.10.175.

[78] X. Xiang, E. Liu, H. Xie, Y. Tian, Y. Wu, Z. Wu, Y. Zhu, Highly stable performance of supercapacitors using microporous carbon derived from phenol–melamine–formaldehyde resin, Journal of Solid State Electrochemistry 16 (2012) 2661–2666. https://doi.org/10.1007/s10008-012-1692-9.

[79] Z. Zheng, Q. Gao, Hierarchical porous carbons prepared by an easy one-step carbonization and activation of phenol–formaldehyde resins with high performance for supercapacitors, J Power Sources 196 (2011) 1615–1619. https://doi.org/https://doi.org/10.1016/j.jpowsour.2010.09.010.

[80] H. Teng, S.-C. Wang, Influence of Oxidation on the Preparation of Porous Carbons from Phenol−Formaldehyde Resins with KOH Activation, Ind Eng Chem Res 39 (2000) 673–678. https://doi.org/10.1021/ie990473i.

[81] Y. Kan, Q. Yue, B. Gao, Q. Li, Preparation of epoxy resin-based activated carbons from waste printed circuit boards by steam activation, Mater Lett 159 (2015) 443–446. https://doi.org/https://doi.org/10.1016/j.matlet.2015.07.053.

[82] Y. Kan, Q. Yue, B. Gao, Q. Li, Comparison of activated carbons from epoxy resin of waste printed circuit boards with KOH activation by conventional and microwave heating methods, J Taiwan Inst Chem Eng 68 (2016) 440–445. https://doi.org/https://doi.org/10.1016/j.jtice.2016.08.047.

[83] C. Zhao, S. Chen, N. Sun, W. Jiang, W. Cai, C. Zhao, Bisphenol A Epoxy Resin-Derived Activated Carbon with High Performance for Supercapacitors, The Journal of Physical Chemistry C 127 (2023) 18821–18831. https://doi.org/10.1021/acs.jpcc.3c03756.

[84] M.A. Tadda, A. Ahsan, A. Shitu, M. Elsergany, A. Thirugnanasambantham, B. Jose, M. Razzaque, N. Norsyahariati, A review on activated carbon: process, application and prospects, 2 (2016) 7–13.

[85] X. Wang, H. Cheng, G. Ye, J. Fan, F. Yao, Y. Wang, Y. Jiao, W. Zhu, H. Huang, D. Ye, Key factors and primary modification methods of activated carbon and their application in adsorption of carbon-based gases: A review, Chemosphere 287 (2022) 131995. https://doi.org/https://doi.org/10.1016/j.chemosphere.2021.131995.

[86] S. Husien, R.M. El-taweel, A.I. Salim, I.S. Fahim, L.A. Said, A.G. Radwan, Review of activated carbon adsorbent material for textile dyes removal: Preparation, and modelling, Current Research in Green and Sustainable Chemistry 5 (2022) 100325. https://doi.org/https://doi.org/10.1016/j.crgsc.2022.100325.

[87] J. Wang, X. Guo, Adsorption isotherm models: Classification, physical meaning, application and solving method, Chemosphere (2020). https://doi.org/10.1016/j.chemosphere.2020.127279.

[88] Y. Kuang, X. Zhang, S. Zhou, Adsorption of methylene blue in water onto activated carbon by surfactant modification, Water (Switzerland) 12 (2020) 1–19. https://doi.org/10.3390/w12020587.

[89] A. Murray, B. Örmeci, Removal Effectiveness of Nanoplastics (<400 nm) with Separation Processes Used for Water and Wastewater Treatment, Water (Basel) 12 (2020). https://doi.org/10.3390/w12030635.

[90] V. Siipola, S. Pflugmacher, H. Romar, L. Wendling, P. Koukkari, Low-Cost Biochar Adsorbents for Water Purification Including Microplastics Removal, Applied Sciences 10 (2020). https://doi.org/10.3390/app10030788.

[91] M. Tong, L. He, H. Rong, M. Li, H. Kim, Transport behaviors of plastic particles in saturated quartz sand without and with biochar/Fe3O4-biochar amendment, Water Res 169 (2020) 115284. https://doi.org/https://doi.org/10.1016/j.watres.2019.115284.

[92] Z. Wang, M. Sedighi, A. Lea-Langton, Filtration of microplastic spheres by biochar: removal efficiency and immobilisation mechanisms, Water Res 184 (2020) 116165. https://doi.org/https://doi.org/10.1016/j.watres.2020.116165.

[93] Z. Wang, T. Lin, W. Chen, Occurrence and removal of microplastics in an advanced drinking water treatment plant (ADWTP), Science of The Total Environment 700 (2020) 134520. https://doi.org/https://doi.org/10.1016/j.scitotenv.2019.134520.

[94] Z.A. Ganie, N. Khandelwal, E. Tiwari, N. Singh, G.K. Darbha, Biochar-facilitated remediation of nanoplastic contaminated water: Effect of pyrolysis temperature induced surface modifications, J Hazard Mater 417 (2021) 126096. https://doi.org/https://doi.org/10.1016/j.jhazmat.2021.126096.

[95] A.S.I. Abdoul Magid, Md.S. Islam, Y. Chen, L. Weng, J. Li, J. Ma, Y. Li, Enhanced adsorption of polystyrene nanoplastics (PSNPs) onto oxidized corncob biochar with high pyrolysis temperature, Science of The Total Environment 784 (2021) 147115. https://doi.org/https://doi.org/10.1016/j.scitotenv.2021.147115.

[96] L. Ramirez Arenas, S. Ramseier Gentile, S. Zimmermann, S. Stoll, Nanoplastics adsorption and removal efficiency by granular activated carbon used in drinking water treatment process, Science of The Total Environment 791 (2021) 148175. https://doi.org/https://doi.org/10.1016/j.scitotenv.2021.148175.

[97] F. Welle, Twenty years of PET bottle to bottle recycling - An overview, Resour Conserv Recycl (2011). https://doi.org/10.1016/j.resconrec.2011.04.009.

[98] J.B. Parra, C.O. Ania, A. Arenillas, F. Rubiera, J.M. Palacios, J.J. Pis, Carbonaceous materials from recycled Pet, in: Boletin de La Sociedad Espanola de Ceramica y Vidrio, 2004. https://doi.org/10.3989/cyv.2004.v43.i2.1043.

[99] R. Mendoza-Carrasco, E.M. Cuerda-Correa, M.F. Alexandre-Franco, C. Fernández-González, V. Gómez-Serrano, Preparation of high-quality activated carbon from polyethyleneterephthalate (PET) bottle waste. Its use in the removal of pollutants in aqueous solution, J Environ Manage 181 (2016) 522–535. https://doi.org/10.1016/J.JENVMAN.2016.06.070.

[100] B. Geyer, G. Lorenz, A. Kandelbauer, Recycling of poly(ethylene terephthalate) – A review focusing on chemical methods, Express Polym Lett (2016). https://doi.org/10.3144/expresspolymlett.2016.53.

[101] US EPA, Plastics: Material-Specific Data, United States Environmental Protection Agency (2018).

[102] B. Saha, A.K. Ghoshal, Thermal degradation kinetics of poly(ethylene terephthalate) from waste soft drinks bottles, Chemical Engineering Journal (2005). https://doi.org/10.1016/j.cej.2005.04.018.

[103] S. Sharifian, N. Asasian-Kolur, Polyethylene terephthalate (PET) waste to carbon materials: Theory, methods and applications, J Anal Appl Pyrolysis (2022). https://doi.org/10.1016/j.jaap.2022.105496.

[104] Y. Xue, P. Johnston, X. Bai, Effect of catalyst contact mode and gas atmosphere during catalytic pyrolysis of waste plastics, Energy Convers Manag (2017). https://doi.org/10.1016/j.enconman.2017.03.071.

[105] R. Sadeghbeigi, FCC Feed Characterization, in: Fluid Catalytic Cracking Handbook, 2012. https://doi.org/10.1016/b978-0-12-386965-4.00003-3.

[106] M.S. Reza, C.S. Yun, S. Afroze, N. Radenahmad, M.S.A. Bakar, R. Saidur, J. Taweekun, A.K. Azad, Preparation of activated carbon from biomass and its' applications in water and gas purification, a review, Arab J Basic Appl Sci 27 (2020) 208–238. https://doi.org/10.1080/25765299.2020.1766799.

[107] M.K.B. Gratuito, T. Panyathanmaporn, R.-A. Chumnanklang, N. Sirinuntawittaya, A. Dutta, Production of activated carbon from coconut shell: Optimization using response surface methodology, Bioresour Technol 99 (2008) 4887–4895. https://doi.org/https://doi.org/10.1016/j.biortech.2007.09.042.

[108] C. Seto, B.P. Chang, C. Tzoganakis, T.H. Mekonnen, Lignin derived nano-biocarbon and its deposition on polyurethane foam for wastewater dye adsorption, Int J Biol Macromol (2021). https://doi.org/10.1016/j.ijbiomac.2021.06.185.

[109] Suhas, P.J.M. Carrott, M.M.L. Ribeiro Carrott, Lignin – from natural adsorbent to activated carbon: A review, Bioresour Technol 98 (2007) 2301–2312. https://doi.org/https://doi.org/10.1016/j.biortech.2006.08.008.

[110] W.E. Rashwan, B.S. Girgis, Adsorption capacities of activated carbons derived from rice straw and water hyacinth in the removal of organic pollutants from water, Adsorption Science and Technology (2004). https://doi.org/10.1260/0263617041503471.

[111] A. Esfandiari, T. Kaghazchi, M. Soleimani, Preparation and evaluation of activated carbons obtained by physical activation of polyethyleneterephthalate (PET) wastes, J Taiwan Inst Chem Eng (2012). https://doi.org/10.1016/j.jtice.2012.02.002.

[112] Yuliusman, Nasruddin, A. Sanal, A. Bernama, F. Haris, I.T. Ramadhan, Preparation of activated carbon from waste plastics polyethylene terephthalate as adsorbent in natural gas storage, IOP Conf Ser Mater Sci Eng 176 (2017) 012055. https://doi.org/10.1088/1757-899X/176/1/012055.

[113] C. Akmil-Başar, Y. Önal, T. Kiliçer, D. Eren, Adsorptions of high concentration malachite green by two activated carbons having different porous structures, J Hazard Mater (2005). https://doi.org/10.1016/j.jhazmat.2005.06.025.

[114] I.P.P. Cansado, M.M.L.R. Carrott, P.J.M. Carrott, P.A.M. Mourão, Textural development of activated carbon prepared from recycled PET with different chemical activation agents, in: Materials Science Forum, 2008. https://doi.org/10.4028/www.scientific.net/msf.587-588.753.

[115] S. Ayyalusamy, S. Mishra, Optimization of preparation conditions for activated carbons from polyethylene terephthalate using response surface methodology, Brazilian Journal of Chemical Engineering (2018). https://doi.org/10.1590/0104-6632.20180353s20160724.

[116] M. Adibfar, T. Kaghazchi, N. Asasian, M. Soleimani, Conversion of Poly(Ethylene Terephthalate) Waste into Activated Carbon: Chemical Activation and Characterization, Chem Eng Technol 37 (2014) 979–986. https://doi.org/10.1002/ceat.201200719.

[117] R.P.K. Dasanayaka, APPLICATIONS OF ACTIVATED CARBON IN WASTE WATER TREATMENT AS A LOW COST MEDIA, International Journal of Engineering Applied Sciences and Technology (2021). https://doi.org/10.33564/ijeast.2021.v05i11.001.

[118] A. Ullah, The influence of interfacial tension on rejection and permeation of the oil droplets through a slit pore membrane, Sep Purif Technol 266 (2021) 118581. https://doi.org/https://doi.org/10.1016/j.seppur.2021.118581.

[119] A. Ullah, J. Ahmad, H. Khan, S.W. Khan, F. Zamani, S.W. Hasan, V.M. Starov, J.W. Chew, Membrane oscillation and slot (pore) blocking in oil–water separation, Chemical Engineering Research and Design 142 (2019) 111–120. https://doi.org/https://doi.org/10.1016/j.cherd.2018.12.007.

[120] I.D. Charry Prada, R. Rivera-Tinoco, C. Bouallou, Biogas industry: Novel acid gas removal technology using a superacid solvent. Process design, unit specification and feasibility study compared with other existing technologies, Chemical Engineering Research and Design 154 (2020) 212–231. https://doi.org/https://doi.org/10.1016/j.cherd.2019.12.007.

[121] A. Ullah, K. Shahzada, S.W. Khan, V. Starov, Purification of produced water using oscillatory membrane filtration, Desalination 491 (2020) 114428. https://doi.org/https://doi.org/10.1016/j.desal.2020.114428.

[122] P.A. Sosa-Fernandez, J.W. Post, M.S. Ramdlan, F.A.M. Leermakers, H. Bruning, H.H.M. Rijnaarts, Improving the performance of polymer-flooding produced water electrodialysis through the application of pulsed electric field, Desalination 484 (2020) 114424. https://doi.org/https://doi.org/10.1016/j.desal.2020.114424.

[123] S. Cheng, S. Zhao, B. Xing, Y. Liu, C. Zhang, H. Xia, Preparation of magnetic adsorbent-photocatalyst composites for dye removal by synergistic effect of adsorption and

photocatalysis, J Clean Prod 348 (2022) 131301. https://doi.org/https://doi.org/10.1016/j.jclepro.2022.131301.

[124] S. Cheng, S. Zhao, H. Guo, B. Xing, Y. Liu, C. Zhang, M. Ma, High-efficiency removal of lead/cadmium from wastewater by MgO modified biochar derived from crofton weed, Bioresour Technol 343 (2022) 126081. https://doi.org/https://doi.org/10.1016/j.biortech.2021.126081.

[125] A. Arenillas, F. Rubiera, J.B. Parra, C.O. Ania, J.J. Pis, Surface modification of low cost carbons for their application in the environmental protection, in: Appl Surf Sci, 2005. https://doi.org/10.1016/j.apsusc.2005.02.076.

[126] B. Kaur, R.K. Gupta, H. Bhunia, Chemically activated nanoporous carbon adsorbents from waste plastic for CO2 capture: Breakthrough adsorption study, Microporous and Mesoporous Materials (2019). https://doi.org/10.1016/j.micromeso.2019.03.025.

[127] V. Gómez-Serrano, M. Adame-Pereira, M. Alexandre-Franco, C. Fernández-González, Adsorption of bisphenol A by activated carbon developed from PET waste by KOH activation, Environmental Science and Pollution Research (2021). https://doi.org/10.1007/s11356-020-08428-6.

[128] Y. El Maguana, N. Elhadiri, M. Benchanaa, R. Chikri, Activated Carbon for Dyes Removal: Modeling and Understanding the Adsorption Process, J Chem (2020). https://doi.org/10.1155/2020/2096834.

[129] P.K. Navin, S. Kumar, M. Mathur, Textile wastewater treatment: A critical review, in: International Journal of Engineering Research & Technology (IJERT), 2018.

[130] P. Kalivel, Treatment of Textile Dyeing Waste Water Using TiO 2 /Zn Electrode by Spray Pyrolysis in Electrocoagulation Process , in: Dyes and Pigments - Novel Applications and Waste Treatment, 2021. https://doi.org/10.5772/intechopen.95325.

[131] P. Kalivel, Treatment of Textile Dyeing Waste Water Using TiO 2 /Zn Electrode by Spray Pyrolysis in Electrocoagulation Process , in: Dyes and Pigments - Novel Applications and Waste Treatment, 2021. https://doi.org/10.5772/intechopen.95325.

[132] W.A. Khanday, F. Marrakchi, M. Asif, B.H. Hameed, Mesoporous zeolite–activated carbon composite from oil palm ash as an effective adsorbent for methylene blue, J Taiwan Inst Chem Eng 70 (2017) 32–41. https://doi.org/https://doi.org/10.1016/j.jtice.2016.10.029.

[133] F. Marrakchi, M.J. Ahmed, W.A. Khanday, M. Asif, B.H. Hameed, Mesoporous-activated carbon prepared from chitosan flakes via single-step sodium hydroxide activation for the adsorption of methylene blue, Int J Biol Macromol 98 (2017) 233–239. https://doi.org/https://doi.org/10.1016/j.ijbiomac.2017.01.119.

[134] Md.A. Islam, M.J. Ahmed, W.A. Khanday, M. Asif, B.H. Hameed, Mesoporous activated carbon prepared from NaOH activation of rattan (Lacosperma secundiflorum) hydrochar

for methylene blue removal, Ecotoxicol Environ Saf 138 (2017) 279–285. https://doi.org/https://doi.org/10.1016/j.ecoenv.2017.01.010.

[135] Md.A. Islam, S. Sabar, A. Benhouria, W.A. Khanday, M. Asif, B.H. Hameed, Nanoporous activated carbon prepared from karanj (Pongamia pinnata) fruit hulls for methylene blue adsorption, J Taiwan Inst Chem Eng 74 (2017) 96–104. https://doi.org/https://doi.org/10.1016/j.jtice.2017.01.016.

[136] F. Marrakchi, W.A. Khanday, M. Asif, B.H. Hameed, Cross-linked chitosan/sepiolite composite for the adsorption of methylene blue and reactive orange 16, Int J Biol Macromol 93 (2016) 1231–1239. https://doi.org/https://doi.org/10.1016/j.ijbiomac.2016.09.069.

[137] W.A. Khanday, M. Asif, B.H. Hameed, Cross-linked beads of activated oil palm ash zeolite/chitosan composite as a bio-adsorbent for the removal of methylene blue and acid blue 29 dyes, Int J Biol Macromol 95 (2017) 895–902. https://doi.org/https://doi.org/10.1016/j.ijbiomac.2016.10.075.

[138] S. Tripathi, N. Arora, P. Gupta, P.A. Pruthi, K.M. Poluri, V. Pruthi, Microalgae, in: Advanced Biofuels, 2019. https://doi.org/10.1016/b978-0-08-102791-2.00004-0.

[139] N. Ayawei, A.N. Ebelegi, D. Wankasi, Modelling and Interpretation of Adsorption Isotherms, J Chem (2017). https://doi.org/10.1155/2017/3039817.

[140] J. Wang, X. Guo, Adsorption kinetic models: Physical meanings, applications, and solving methods, J Hazard Mater (2020). https://doi.org/10.1016/j.jhazmat.2020.122156.

[141] A. Linares-Solano, M.A. Lillo-Ródenas, J.P. Marco-Lozar, M. Kunowsky, A.J. Romero-Anaya, NaOH and KOH for preparing activated carbons used in energy and environmental applications, International Journal of Energy, Environment and Economics (2012).

[142] M.A. Lillo-Ródenas, J. Juan-Juan, D. Cazorla-Amorós, A. Linares-Solano, About reactions occurring during chemical activation with hydroxides, in: Carbon N Y, 2004. https://doi.org/10.1016/j.carbon.2004.01.008.

[143] J. Wang, S. Kaskel, KOH activation of carbon-based materials for energy storage, J Mater Chem (2012). https://doi.org/10.1039/c2jm34066f.

[144] V. Gómez-Serrano, M. Adame-Pereira, M. Alexandre-Franco, C. Fernández-González, Adsorption of bisphenol A by activated carbon developed from PET waste by KOH activation, (n.d.). https://doi.org/10.1007/s11356-020-08428-6/Published.

[145] V.L. Snoeyink, W.J. Weber, The Surface Chemistry of Active Carbon; A Discussion of Structure and Surface Functional Groups, Environ Sci Technol (1967). https://doi.org/10.1021/es60003a003.

[146] B. Viswanathan, P. Neel, T. Varadarajan, Methods of activation and specific applications of carbon materials, … for Catalysis Research, Indian Institute of … (2009).

[147] D.C.K. Ko, D.H.K. Tsang, J.F. Porter, G. McKay, Applications of multipore model for the mechanism identification during the adsorption of dye on activated carbon and bagasse pith, Langmuir (2003). https://doi.org/10.1021/la020654g.

[148] J.W.F. Chia, O. Sawai, T. Nunoura, Reaction pathway of poly(ethylene) terephthalate carbonization: Decomposition behavior based on carbonized product, Waste Management (2020). https://doi.org/10.1016/j.wasman.2020.04.035.

[149] A.P. Dos Santos Pereira, M.H.P. Da Silva, É.P. Lima, A. Dos Santos Paula, F.J. Tommasini, Processing and characterization of PET composites reinforced with geopolymer concrete waste, in: Materials Research, 2017. https://doi.org/10.1590/1980-5373-MR-2017-0734.

[150] X.J. Jia, J. Wang, D.C. Zhong, J. Wu, B. Zhao, D. Den Engelsen, X.Z. Luo, A thermo-sensitive supramolecular hydrogel derived from an onium salt with solution-gel-crystal transition properties, RSC Adv (2016). https://doi.org/10.1039/c6ra23761d.

[151] A.P. Dos Santos Pereira, M.H.P. Da Silva, É.P. Lima, A. Dos Santos Paula, F.J. Tommasini, Processing and characterization of PET composites reinforced with geopolymer concrete waste, in: Materials Research, 2017. https://doi.org/10.1590/1980-5373-MR-2017-0734.

[152] G.Z. Kyzas, E.A. Deliyanni, K.A. Matis, Activated carbons produced by pyrolysis of waste potato peels: Cobaltions removal by adsorption, Colloids Surf A Physicochem Eng Asp (2016). https://doi.org/10.1016/j.colsurfa.2015.11.038.

[153] I.A.W. Tan, A.L. Ahmad, B.H. Hameed, Adsorption of basic dye using activated carbon prepared from oil palm shell: batch and fixed bed studies, Desalination (2008). https://doi.org/10.1016/j.desal.2007.07.005.

[154] E. V. Liakos, K. Rekos, D.A. Giannakoudakis, A.C. Mitropoulos, G.Z. Kyzas, Carbonaceous adsorbents derived from agricultural sources for the removal of pramipexole pharmaceutical model compound from synthetic aqueous solutions, Processes (2021). https://doi.org/10.3390/pr9020253.

[155] Y. Al-Degs, M.A.M. Khraisheh, S.J. Allen, M.N. Ahmad, Effect of carbon surface chemistry on the removal of reactive dyes from textile effluent, Water Res (2000). https://doi.org/10.1016/S0043-1354(99)00200-6.

[156] J.J. Salazar-Rabago, R. Leyva-Ramos, J. Rivera-Utrilla, R. Ocampo-Perez, F.J. Cerino-Cordova, Biosorption mechanism of Methylene Blue from aqueous solution onto White Pine (Pinus durangensis) sawdust: Effect of operating conditions, Sustainable Environment Research (2017). https://doi.org/10.1016/j.serj.2016.11.009.

[157] S. Cheng, Y. Liu, B. Xing, X. Qin, C. Zhang, H. Xia, Lead and cadmium clean removal from wastewater by sustainable biochar derived from poplar saw dust, J Clean Prod 314 (2021) 128074. https://doi.org/https://doi.org/10.1016/j.jclepro.2021.128074.

[158] J.H. Potgieter, Adsorption of methylene blue on activated carbon: An experiment illustrating both the Langmuir and Freundlich isotherms, J Chem Educ 68 (1991) 349. https://doi.org/10.1021/ed068p349.

[159] N. Kannan, M.M. Sundaram, Kinetics and mechanism of removal of methylene blue by adsorption on various carbons - A comparative study, Dyes and Pigments (2001). https://doi.org/10.1016/S0143-7208(01)00056-0.

[160] B.H. Hameed, A.L. Ahmad, K.N.A. Latiff, Adsorption of basic dye (methylene blue) onto activated carbon prepared from rattan sawdust, Dyes and Pigments (2007). https://doi.org/10.1016/j.dyepig.2006.05.039.

[161] A.A. Attia, B.S. Girgis, N.A. Fathy, Removal of methylene blue by carbons derived from peach stones by H3PO4 activation: Batch and column studies, Dyes and Pigments (2008). https://doi.org/10.1016/j.dyepig.2006.08.039.

[162] Y.R. Lin, H. Teng, Mesoporous carbons from waste tire char and their application in wastewater discoloration, Microporous and Mesoporous Materials (2002). https://doi.org/10.1016/S1387-1811(02)00380-3.

[163] B. Bestani, N. Benderdouche, B. Benstaali, M. Belhakem, A. Addou, Methylene blue and iodine adsorption onto an activated desert plant, Bioresour Technol (2008). https://doi.org/10.1016/j.biortech.2008.02.053.

[164] B.H. Hameed, F.B.M. Daud, Adsorption studies of basic dye on activated carbon derived from agricultural waste: Hevea brasiliensis seed coat, Chemical Engineering Journal (2008). https://doi.org/10.1016/j.cej.2007.07.089.

[165] P. Senthil Kumar, R. Gayathri, Adsorption of Pb2+ ions from aqueous solutions onto bael tree leaf powder: Isotherms, kinetics and thermodynamics study, Journal of Engineering Science and Technology (2009).

[166] X. Ma, L.M. Smith, L. Cai, S.Q. Shi, H. Li, B. Fei, Preparation of high-performance activated carbons using bamboo through one-step pyrolysis, Bioresources (2019). https://doi.org/10.15376/biores.14.1.688-699.

[167] B.K. Nandi, A. Goswami, M.K. Purkait, Removal of cationic dyes from aqueous solutions by kaolin: Kinetic and equilibrium studies, Appl Clay Sci (2009). https://doi.org/10.1016/j.clay.2008.03.015.

[168] C.V. Rao, A.S. Giri, V. V. Goud, A.K. Golder, Studies on pH-dependent color variation and decomposition mechanism of Brilliant Green dye in Fenton reaction, International Journal of Industrial Chemistry (2016). https://doi.org/10.1007/s40090-015-0060-x.

[169] S.-T. Ong, P. Keng, S. Lee, M.-H. Leong, Y.-T. Hung, Equilibrium Studies for the Removal of Basic Dye by Sunflower Seed Husk (Helianthus annuus), International Journal of Physical Sciences 5 (2010).

[170] N.B. Hartmann, T. Hüffer, R.C. Thompson, M. Hassellöv, A. Verschoor, A.E. Daugaard, S. Rist, T. Karlsson, N. Brennholt, M. Cole, M.P. Herrling, M.C. Hess, N.P. Ivleva, A.L. Lusher, M. Wagner, Are We Speaking the Same Language? Recommendations for a Definition and Categorization Framework for Plastic Debris, Environ Sci Technol 53 (2019) 1039–1047. https://doi.org/10.1021/acs.est.8b05297.

[171] E. Tiwari, N. Singh, N. Khandelwal, F.A. Monikh, G.K. Darbha, Application of Zn/Al layered double hydroxides for the removal of nano-scale plastic debris from aqueous systems, J Hazard Mater 397 (2020) 122769. https://doi.org/https://doi.org/10.1016/j.jhazmat.2020.122769.

[172] A.A. Koelmans, N.H. Mohamed Nor, E. Hermsen, M. Kooi, S.M. Mintenig, J. De France, Microplastics in freshwaters and drinking water: Critical review and assessment of data quality, Water Res 155 (2019) 410–422. https://doi.org/https://doi.org/10.1016/j.watres.2019.02.054.

[173] K. Shosaku, Distribution of Nanoparticles in the See-through Medaka (Oryzias latipes), Environ Health Perspect 114 (2006) 1697–1702. https://doi.org/10.1289/ehp.9209.

[174] K. Mattsson, M.T. Ekvall, L.-A. Hansson, S. Linse, A. Malmendal, T. Cedervall, Altered Behavior, Physiology, and Metabolism in Fish Exposed to Polystyrene Nanoparticles, Environ Sci Technol 49 (2015) 553–561. https://doi.org/10.1021/es5053655.

[175] S. Singh, M. Kalyanasundaram, V. Diwan, Removal of microplastics from wastewater: available techniques and way forward, Water Science and Technology 84 (2021) 3689–3704. https://doi.org/10.2166/wst.2021.472.

[176] J. Sun, X. Dai, Q. Wang, M.C.M. van Loosdrecht, B.-J. Ni, Microplastics in wastewater treatment plants: Detection, occurrence and removal, Water Research (Oxford) 152 (2019) 21–37. https://doi.org/10.1016/j.watres.2018.12.050.

[177] B. Ma, W. Xue, C. Hu, H. Liu, J. Qu, L. Li, c, Chemical Engineering Journal 359 (2019) 159–167. https://doi.org/https://doi.org/10.1016/j.cej.2018.11.155.

[178] W. Perren, A. Wojtasik, Q. Cai, Removal of Microbeads from Wastewater Using Electrocoagulation, ACS Omega 3 (2018) 3357–3364. https://doi.org/10.1021/acsomega.7b02037.

[179] Y. Zhang, A. Diehl, A. Lewandowski, K. Gopalakrishnan, T. Baker, Removal efficiency of micro- and nanoplastics (180 nm–125 μm) during drinking water treatment, Science of The Total Environment 720 (2020) 137383. https://doi.org/https://doi.org/10.1016/j.scitotenv.2020.137383.

[180] A. Villacorta, L. Rubio, M. Alaraby, M. López-Mesas, V. Fuentes-Cebrian, O.H. Moriones, R. Marcos, A. Hernández, A new source of representative secondary PET nanoplastics. Obtention, characterization, and hazard evaluation, J Hazard Mater 439 (2022) 129593. https://doi.org/https://doi.org/10.1016/j.jhazmat.2022.129593.

[181] N. Mishra, G. Das, A. Ansaldo, A. Genovese, M. Malerba, M. Povia, D. Ricci, E. Di Fabrizio, E. Di Zitti, M. Sharon, M. Sharon, Pyrolysis of waste polypropylene for the synthesis of carbon nanotubes, J Anal Appl Pyrolysis 94 (2012) 91–98. https://doi.org/10.1016/j.jaap.2011.11.012.

[182] W.M. Qiao, S.H. Yoon, Y. Korai, I. Mochida, S. Inoue, T. Sakurai, T. Shimohara, Preparation of activated carbon fibers from polyvinyl chloride, Carbon N Y 42 (2004) 1327–1331. https://doi.org/https://doi.org/10.1016/j.carbon.2004.01.035.

[183] Y.N. Kim, Y.-O. Kim, S.Y. Kim, M. Park, B. Yang, J. Kim, Y.C. Jung, Application of supercritical water for green recycling of epoxy-based carbon fiber reinforced plastic, Compos Sci Technol 173 (2019) 66–72. https://doi.org/https://doi.org/10.1016/j.compscitech.2019.01.026.

[184] X. Liu, F. Tian, X. Zhao, R. Du, S. Xu, Y.-Z. Wang, Recycling waste epoxy resin as hydrophobic coating of melamine foam for high-efficiency oil absorption, Appl Surf Sci 529 (2020) 147151. https://doi.org/https://doi.org/10.1016/j.apsusc.2020.147151.

[185] M. Calero, R.R. Solís, M.J. Muñoz-Batista, A. Pérez, G. Blázquez, M. Ángeles Martín-Lara, Oil and gas production from the pyrolytic transformation of recycled plastic waste: An integral study by polymer families, Chem Eng Sci 271 (2023) 118569. https://doi.org/https://doi.org/10.1016/j.ces.2023.118569.

[186] W. Chen, Y. Chen, Y. Shu, Y. He, J. Wei, Characterization of solid, liquid and gaseous products from waste printed circuit board pyrolysis, J Clean Prod 313 (2021) 127881. https://doi.org/https://doi.org/10.1016/j.jclepro.2021.127881.

[187] R. R. Solís, M. Martín-Lara, A. Ligero, J. Balbís, G. Blázquez, M. Calero, Revalorizing a Pyrolytic Char Residue from Post-Consumer Plastics into Activated Carbon for the Adsorption of Lead in Water, Applied Sciences 12 (2022) 8032. https://doi.org/10.3390/app12168032.

[188] A. Ligero, M. Calero, A. Pérez, R.R. Solís, M.J. Muñoz-Batista, M.Á. Martín-Lara, Low-cost activated carbon from the pyrolysis of post-consumer plastic waste and the application in CO2 capture, Process Safety and Environmental Protection 173 (2023) 558–566. https://doi.org/https://doi.org/10.1016/j.psep.2023.03.041.

[189] X. Zhao, Y. Long, S. Xu, X. Liu, L. Chen, Y.-Z. Wang, Recovery of epoxy thermosets and their composites, Materials Today 64 (2023) 72–97. https://doi.org/https://doi.org/10.1016/j.mattod.2022.12.005.

[190] Y. Kan, Q. Yue, B. Gao, Q. Li, Preparation of epoxy resin-based activated carbons from waste printed circuit boards by steam activation, Mater Lett 159 (2015) 443–446. https://doi.org/https://doi.org/10.1016/j.matlet.2015.07.053.

[191] Y. Kan, Q. Yue, S. Liu, B. Gao, Effects of Cu and CuO on the preparation of activated carbon from waste circuit boards by H3PO4 activation, Chemical Engineering Journal 331 (2018) 93–101. https://doi.org/https://doi.org/10.1016/j.cej.2017.08.113.

[192] Y. Kan, Q. Yue, B. Gao, Q. Li, Comparative study of dry-mixing and wet-mixing activated carbons prepared from waste printed circuit boards by NaOH activation, RSC Adv 5 (2015) 105943–105951. https://doi.org/10.1039/C5RA18840G.

[193] S. Ge, S.Y. Foong, N.L. Ma, R.K. Liew, W.A. Wan Mahari, C. Xia, P.N.Y. Yek, W. Peng, W.L. Nam, X.Y. Lim, C.M. Liew, C.C. Chong, C. Sonne, S.S. Lam, Vacuum pyrolysis incorporating microwave heating and base mixture modification: An integrated approach to transform biowaste into eco-friendly bioenergy products, Renewable and Sustainable Energy Reviews 127 (2020) 109871. https://doi.org/https://doi.org/10.1016/j.rser.2020.109871.

[194] T. Otowa, Y. Nojima, T. Miyazaki, Development of KOH activated high surface area carbon and its application to drinking water purification, Carbon N Y 35 (1997) 1315–1319. https://doi.org/10.1016/S0008-6223(97)00076-6.

[195] D.A. Khuong, K.T. Trinh, Y. Nakaoka, T. Tsubota, D. Tashima, H.N. Nguyen, D. Tanaka, The investigation of activated carbon by K2CO3 activation: Micropores- and macropores-dominated structure, Chemosphere 299 (2022) 134365. https://doi.org/https://doi.org/10.1016/j.chemosphere.2022.134365.

[196] Y. Xi, D. Yang, X. Qiu, H. Wang, J. Huang, Q. Li, Renewable lignin-based carbon with a remarkable electrochemical performance from potassium compound activation, Ind Crops Prod 124 (2018) 747–754. https://doi.org/10.1016/J.INDCROP.2018.08.018.

[197] J. Zhang, W. Zhang, H. Zhang, J. Pang, G. Cao, M. Han, Y. Yang, A novel synthesis of hierarchical porous carbons from resol by potassium acetate activation for high performance supercapacitor electrodes, J Alloys Compd 712 (2017) 76–81. https://doi.org/https://doi.org/10.1016/j.jallcom.2017.04.066.

[198] A.I. Osman, C. Farrell, A.H. Al-Muhtaseb, A.S. Al-Fatesh, J. Harrison, D.W. Rooney, Pyrolysis kinetic modelling of abundant plastic waste (PET) and in-situ emission monitoring, Environ Sci Eur 32 (2020) 112. https://doi.org/10.1186/s12302-020-00390-x.

[199] A.G. Rodríguez-Hernández, J.A. Muñoz-Tabares, J.C. Aguilar-Guzmán, R. Vazquez-Duhalt, A novel and simple method for polyethylene terephthalate (PET) nanoparticle production, Environ Sci Nano 6 (2019) 2031–2036. https://doi.org/10.1039/C9EN00365G.

[200] S. Brunauer, P.H. Emmett, E. Teller, Adsorption of Gases in Multimolecular Layers, J Am Chem Soc 60 (1938) 309–319. https://doi.org/10.1021/JA01269A023/ASSET/JA01269A023.FP.PNG_V03.

[201] A. Ebadi, J.S. Soltan Mohammadzadeh, A. Khudiev, What is the correct form of BET isotherm for modeling liquid phase adsorption?, Adsorption 15 (2009) 65–73. https://doi.org/10.1007/S10450-009-9151-3/METRICS.

[202] G.L. Aranovich, The theory of polymolecular adsorption, Langmuir 8 (1992) 736–739. https://doi.org/10.1021/la00038a071.

[203] G.L. Aranovich, M.D. Donohue, A New Approach to Analysis of Multilayer Adsorption, J Colloid Interface Sci 173 (1995) 515–520. https://doi.org/https://doi.org/10.1006/jcis.1995.1353.

[204] P. Zhang, L. Wang, Extended Langmuir equation for correlating multilayer adsorption equilibrium data, Sep Purif Technol 70 (2010) 367–371. https://doi.org/https://doi.org/10.1016/j.seppur.2009.10.007.

[205] M. Asadullah, M.A. Rahman, M.A. Motin, M.B. Sultan, Preparation and Adsorption Studies of High Specific Surface Area Activated Carbons Obtained from the Chemical Activation of Jute Stick, Adsorption Science & Technology 24 (2006) 761–770. https://doi.org/10.1260/026361706781388950.

[206] K.L. Erickson, Thermal decomposition mechanisms of epoxies and polyurethanes, International SAMPE Symposium and Exhibition (Proceedings) 51 (2006).

[207] F. Torres-Herrador, A. Eschenbacher, J. Blondeau, T.E. Magin, K.M. Van Geem, Study of the degradation of epoxy resins used in spacecraft components by thermogravimetry and fast pyrolysis, J Anal Appl Pyrolysis 161 (2022) 105397. https://doi.org/10.1016/j.jaap.2021.105397.

[208] J.H. Kim, G. Lee, J.E. Park, S.H. Kim, Limitation of K2CO3 as a Chemical Agent for Upgrading Activated Carbon, Processes 2021, Vol. 9, Page 1000 9 (2021) 1000. https://doi.org/10.3390/PR9061000.

[209] H. Teng, Y.-C. Lin, L.-Y. Hsu, Production of Activated Carbons from Pyrolysis of Waste Tires Impregnated with Potassium Hydroxide, J Air Waste Manage Assoc 50 (2000) 1940–1946. https://doi.org/10.1080/10473289.2000.10464221.

[210] L. Muniandy, F. Adam, A.R. Mohamed, E.-P. Ng, The synthesis and characterization of high purity mixed microporous/mesoporous activated carbon from rice husk using chemical activation with NaOH and KOH, Microporous and Mesoporous Materials 197 (2014) 316–323. https://doi.org/https://doi.org/10.1016/j.micromeso.2014.06.020.

[211] H.M. El-Bery, M. Saleh, R.A. El-Gendy, M.R. Saleh, S.M. Thabet, High adsorption capacity of phenol and methylene blue using activated carbon derived from lignocellulosic agriculture wastes, Sci Rep 12 (2022) 5499. https://doi.org/10.1038/s41598-022-09475-4.

[212] W. Shen, Z. Li, Y. Liu, Surface Chemical Functional Groups Modification of Porous Carbon, Recent Patents on Chemical Engineering 1 (2010) 27–40. https://doi.org/10.2174/1874478810801010027.

[213] B. Das, N.K. Mondal, Calcareous Soil as a New Adsorbent to Remove Lead from Aqueous Solution: Equilibrium, Kinetic and Thermodynamic Study., Universal Journal of Environmental Research & Technology 1 (2011).

[214] K. Ezeh, I. Ogbu, K. Akpomie, N. Ojukwu, J. Ibe, Utilizing the Sorption Capacity of Local Nigerian Sawdust for Attenuation of Heavy Metals from Solution: Isotherm,

Kinetic, and Thermodynamic Investigations, Pacific Journal of Science and Technology 18 (2017) 251–264.

[215] G.M. Burke, D.E. Wurster, M.J. Berg, P. Veng-Pedersen, D.D. Schottelius, Surface Characterization of Activated Charcoal by X-Ray Photoelectron Spectroscopy (XPS): Correlation with Phenobarbital Adsorption Data, Pharm Res 9 (1992) 126–130. https://doi.org/10.1023/A:1018900431661.

[216] J.S. Noh, J.A. Schwarz, Effect of HNO3 treatment on the surface acidity of activated carbons, Carbon N Y 28 (1990) 675–682. https://doi.org/10.1016/0008-6223(90)90069-B.

[217] V. Bernal, L. Giraldo, J.C. Moreno-Piraján, Physicochemical Properties of Activated Carbon: Their Effect on the Adsorption of Pharmaceutical Compounds and Adsorbate–Adsorbent Interactions, C (Basel) 4 (2018). https://doi.org/10.3390/c4040062.

[218] A. Rehman, M. Park, S.-J. Park, Current Progress on the Surface Chemical Modification of Carbonaceous Materials, Coatings (Basel) 9 (2019) 103. https://doi.org/10.3390/coatings9020103.

[219] M.A. Montes-Morán, D. Suárez, J.A. Menéndez, E. Fuente, On the nature of basic sites on carbon surfaces: an overview, Carbon N Y 42 (2004) 1219–1225. https://doi.org/https://doi.org/10.1016/j.carbon.2004.01.023.

[220] S. Cheng, S. Zhao, B. Xing, C. Shi, W. Meng, C. Zhang, Z. Bo, Facile one-pot green synthesis of magnetic separation photocatalyst-adsorbent and its application, Journal of Water Process Engineering 47 (2022) 102802. https://doi.org/https://doi.org/10.1016/j.jwpe.2022.102802.

[221] T.R. Sahoo, B. Prelot, Chapter 7 - Adsorption processes for the removal of contaminants from wastewater: the perspective role of nanomaterials and nanotechnology, in: B. Bonelli, F.S. Freyria, I. Rossetti, R.B.T.-N. for the D. and R. of W.P. Sethi (Eds.), Micro and Nano Technologies, Elsevier, 2020: pp. 161–222. https://doi.org/https://doi.org/10.1016/B978-0-12-818489-9.00007-4.

[222] S. Cheng, W. Meng, B. Xing, C. Shi, Q. Wang, D. Xia, Y. Nie, G. Yi, C. Zhang, H. Xia, Efficient removal of heavy metals from aqueous solutions by Mg/Fe bimetallic oxide-modified biochar: Experiments and DFT investigations, J Clean Prod 403 (2023) 136821. https://doi.org/https://doi.org/10.1016/j.jclepro.2023.136821.

[223] J. Ndi Nsami, J. Ketcha Mbadcam, The Adsorption Efficiency of Chemically Prepared Activated Carbon from Cola Nut Shells by on Methylene Blue, J Chem 2013 (2013) 1–7. https://doi.org/10.1155/2013/469170.

[224] X. Qin, X. Zeng, S. Cheng, B. Xing, C. Shi, G. Yi, Y. Nie, Q. Wang, C. Zhang, H. Xia, Preparation of double functional carbon-based ZnO derived from rape straw for dye wastewater treatment, Journal of Water Process Engineering 52 (2023) 103588. https://doi.org/https://doi.org/10.1016/j.jwpe.2023.103588.

APPENDIX

SUPPLEMENTARY INFORMATION

Chapter 3: Synchronous pyrolysis and activation of poly (ethylene terephthalate) for the generation of activated carbon for dye contaminated wastewater treatment

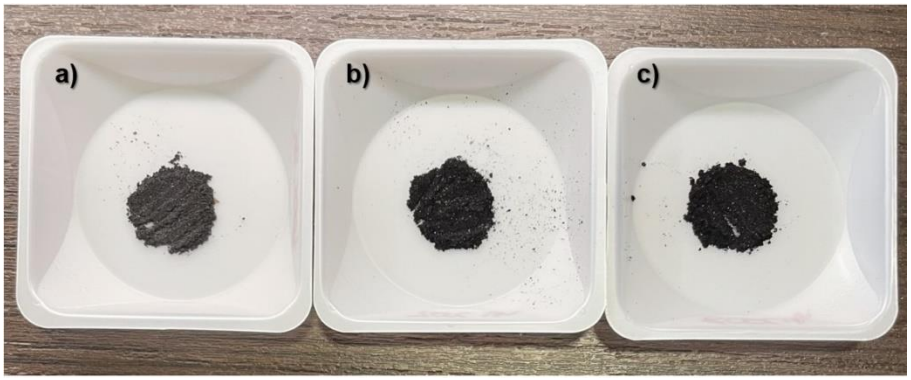

Figure 33: Images of PET activated carbon products a) AC-600C1h; b) AC-700C1h; and c) AC-800C1h.

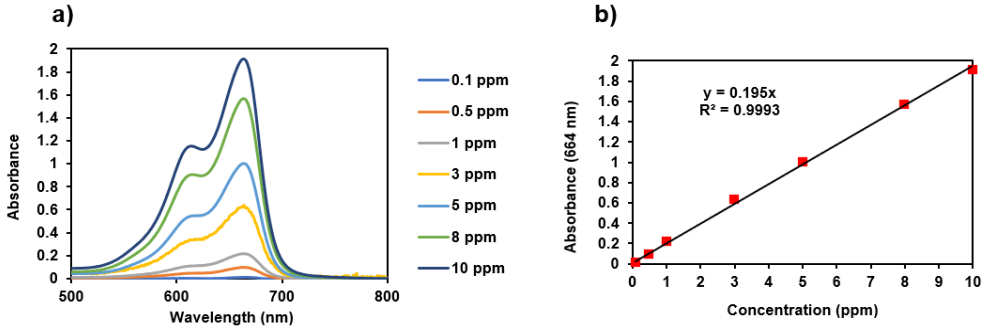

Figure 34: a) UV Vis spectra of methylene blue solutions at concentrations of 0.1-10 mg/L; and b) the corresponding calibration curve.

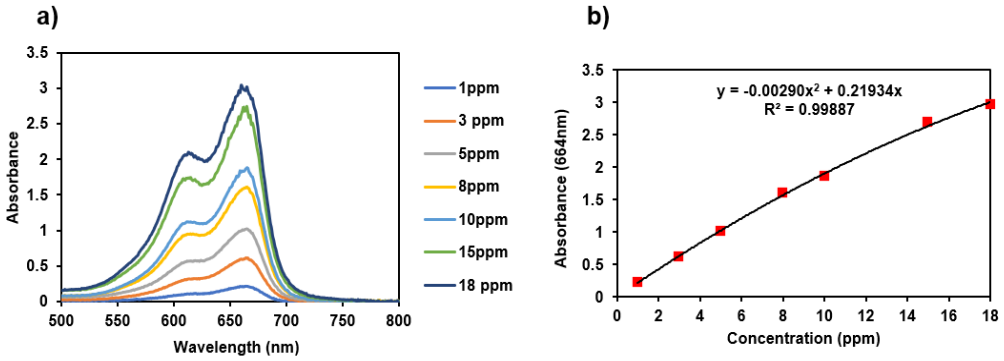

Figure 35: a) UV Vis spectra of methylene blue solutions at concentrations of 1-18 mg/L; and b) the corresponding calibration curve.

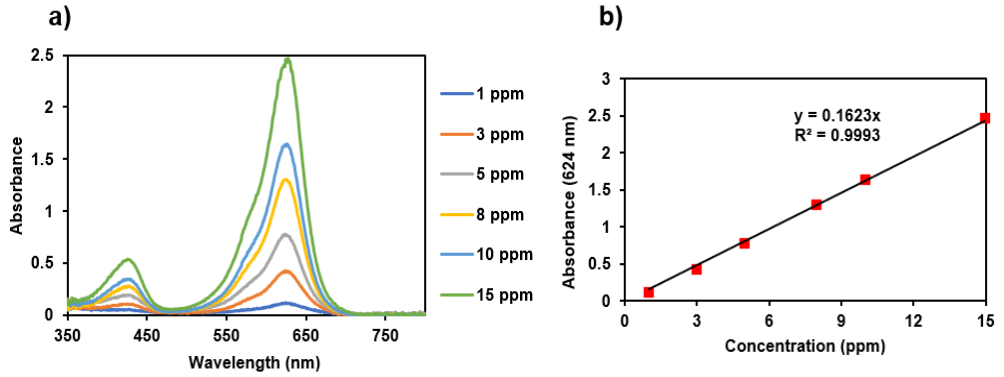

Figure 36: a) UV Vis spectra of brilliant green solutions at concentrations of 1-15 mg/L; and b) the corresponding calibration curve.

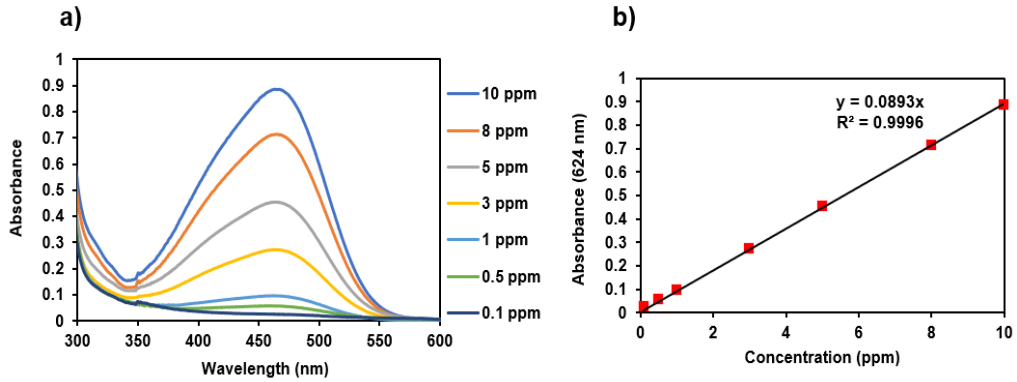

Figure 37: a) UV Vis spectra of methyl orange solutions at concentrations of 1-10 mg/L; and b) the corresponding calibration curve.

Chapter 4: Utilization of epoxy thermoset waste to produce activated carbon for the remediation of nano-plastic contaminated wastewater

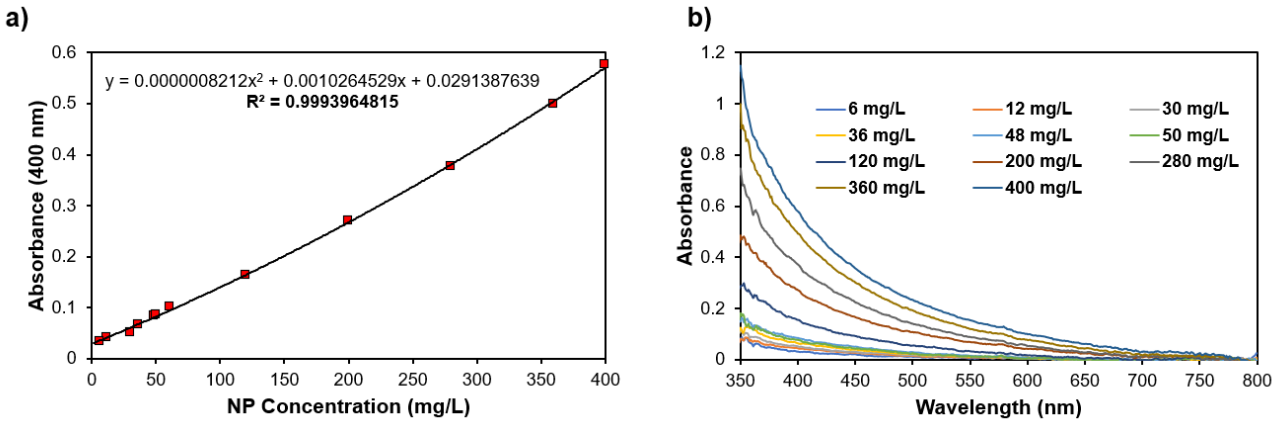

Figure 38: a) Calibration curve for the concentration of NPs in water based on UV-vis absorbance at 400 nm; and b) the corresponding UV-Vis spectra used to produce the calibration curve.

Table 18: Experimental design for the activation of cured epoxy.

Sample designation	Chemical Activator	Activator impregnation ratio (mass activator: mass cured epoxy)	Final treatment temperature
Control	N/A	N/A	600 ºC
AC-800C-1KOH	KOH	1:1	800 ºC
AC-800C-1K_2CO_3	K_2CO_3	1:1	800 ºC
AC-800C-1KOAc	KOAc	1:1	800 ºC
AC-600C-1KOH	KOH	1:1	600 ºC
AC-600C-2KOH	KOH	2:1	600 ºC
AC-800C-2KOH	KOH	2:1	800 ºC

Table 19: Comparison of BET surface area and yield of ACs produced using different K-containing activators.

Sample	Surface area (m^2/g)*	Yield (%)
Control	52.36 ±0.97	8.98 ± 0.62
AC-800C-1KOH	1728.54 ±6.81	23.3 ± 0.80
AC-800C-1K_2CO_3	1843.68 ±14.9	8.53 ± 1.35
AC-800C-1KOAc	1494.57 ±11.0	14.4 ± 2.18

*BET Surface area uncertainties are model related errors determined by the instrument.

Table 20: Comparison of BET surface area, yield and zeta potential of ACs produced by KOH activation at various conditions.

Sample	Surface Area (m^2/g)*	Yield (%)
Control	52.36 ±0.97	8.98 ± 0.62
AC-600C-1KOH	996.24 ±1.15	29.0 ± 2.71
AC-600C-2KOH	788.10 ±0.847	39.8 ± 3.72
AC-800C-1KOH	1728.54 ±6.81	23.3 ± 2.18
AC-800C-2KOH	1705.20 ±12.6	30.8 ± 2.88

*BET Surface area uncertainties are model related errors determined by the instrument.